Ink Jet Nozzle Test Station

by

Garth K. Grover

B.S., Mechanical Engineering
Princeton University, 1995

Submitted to the Department of Mechanical Engineering
in Partial Fulfillment of the Requirements for the Degree of
Master of Science in Mechanical Engineering

at the
Massachusetts Institute of Technology
June 1999

Signature of Author .....
Department of Mechanical Engineering

Certified by .....
Emanuel M. Sachs
Professor of Mechanical Engineering
Laboratory for Manufacturing and Productivity
Thesis Supervisor

Accepted by .....
Ain A. Sonin
Chairman, Department Committee on Graduate Students

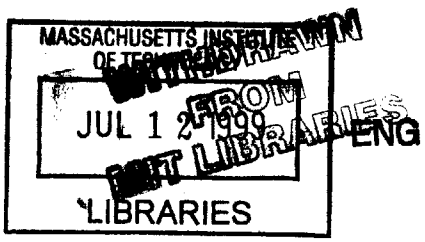

Ink Jet Nozzle Test Station

by

Garth K. Grover

Submitted to the Department of Mechanical Engineering

on May 21, in partial fulfillment of the requirements for the Degree of

Master of Science in Mechanical Engineering

Abstract

Three dimensional printing is a free form fabrication technique that uses inkjet technology to build parts directly from computer models. Binder is jetted into a powderbed, and the part is built up layer by layer. A major constraint on the rate of build and also on maximum part size is the number of nozzles in the printhead. In order to increase the number of nozzles in the printhead without increasing the failure rate of the printhead, the behavior of each nozzle must be characterized prior to installation.

The inkjet nozzle test station was designed and built to automatically characterize the performance of the inkjet nozzles used in the three-dimensional printing process. Video image analysis is used to detect and classify satellite droplets, and to measure jet velocity, droplet breakoff length, flowrate, and jet angle. Droplet velocity, droplet excitation signal frequency and droplet excitation signal amplitude are automatically varied in order to determine each nozzle's performance in the printhead operating region. Four motorized axes are used to control nozzle position, camera focus, and camera zoom level.

The test station has the capability to detect and classify satellite droplets to a minimum of 9 μm in diameter, which proved to be small enough to capture all significant satellites in the operating region of four different binders. The ability of the test station to automatically measure droplet velocity, jet angle, jet breakoff length, and jet flowrate was acceptable for use in testing nozzles for three dimensional printing. The test station was tested for repeatability and for robustness to variation in nozzle and binder type. This demonstrated capability meets the requirements of droplet screening for the three dimensional printing machine.

Thesis Supervisor: Emanuel M. Sachs
Title: Professor of Mechanical Engineering

Acknowledgements

This thesis is dedicated to my wife: Without your inspiration I could never have started this, and without your support I never could have finished it.

Mom and Dad - thank you for all the encouragement. Consider this my biggest OM project.

Mr. and Mrs. Fukuda - thank you for making me part of your family.

Dave and Jim - you both contributed much time and effort helping me complete this project. You were never too busy to lend a hand and I appreciate it.

Ely, thank you for giving me the opportunity to be a part of the 3DP community - I enjoyed working on this project and I hope that it shows in the final result.

Finally, thanks go out to my colleagues at General Electric Aircraft Engines in Lynn for all of their support.

TABLE OF FIGURES

1. Introduction

1.1 Three Dimensional Printing

Three Dimensional Printing (3DP) is a manufacturing process which can rapidly produce parts and tooling directly from computer models. Using ink jet printing technology binder is jetted into a bed of powder, printing a cross section of the desired part. The powder bed is lowered, a layer of powder is spread, and the next part cross section is printed into the powderbed. This process is repeated until the entire part has been printed, at which point the green part can be post processed as needed to produce the final part.

Figure 1 : 3 Dimensional Printing Process

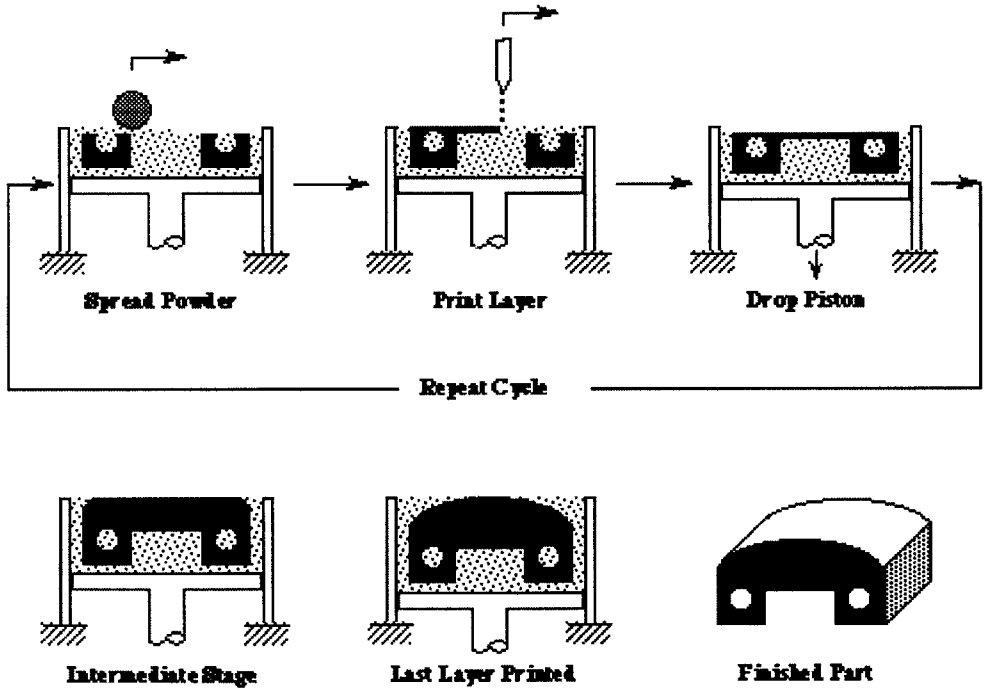

This manufacturing process is fast and also flexible, allowing the use of many different binders and material systems. One of the limitations of this process is the number of nozzles in the printhead. This impacts the size of the part that can be built and the time in which it can be built. Currently there are 8 nozzles on the 3DP Alpha printing machine, and the plan is to increase this number to around 96.

1.2 Printhead Overview

The printhead assembly contains a nozzle, a charging and deflection cell, and a catcher. The nozzle consists of a piezoelectric crystal attached to a ruby orifice by a length of tubing. The nozzle emits a stream of binder, which is broken up into droplets by the vibration of the piezoelectric crystal in the nozzle. The droplet breakoff occurs within the charging cell, where the droplets are given a certain electrical charge. The droplet then passes into an electric field generated by the deflection plates, which deflects the droplets a precise amount.

Figure 2 : Printhead Schematic

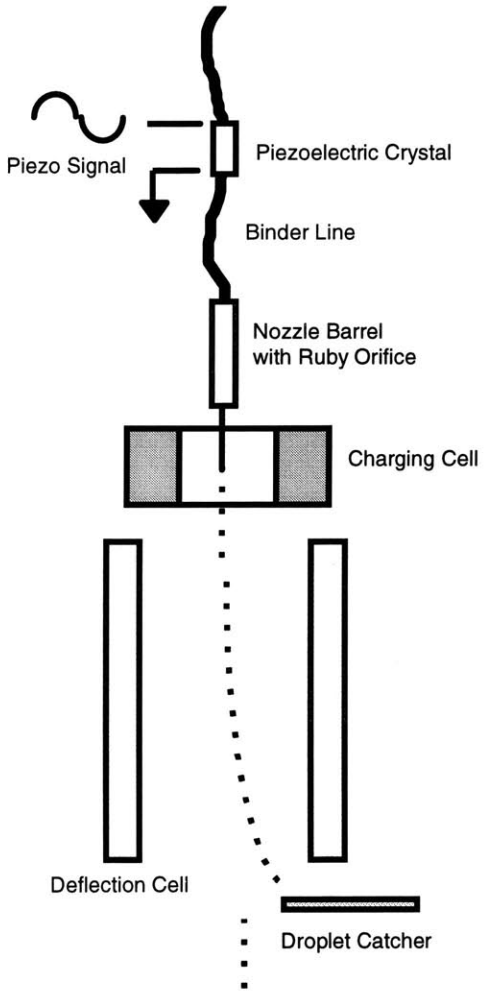

It is important that the breakoff of the droplet occur within the charging cell, in order for it receive the correct charge; this ensures that it will be deflected the appropriate amount in the deflection cell. The angle of the droplet stream must be small enough that it does not strike the walls of the charging cell in the X-Y

direction (also known as the machine's slow axis), and it must be small enough in the X-Z direction (machine's fast axis) that it causes a printing error of less than 0.001 inch. Finally, the nozzle must produce droplets in an acceptable manner, which means that rearward merging or infinite satellites are not permitted. These terms will be explained in depth in section 4.2.

In the multiple nozzle 3DP printhead, each nozzle is subject to the same piezo signal frequency and binder pressure, while the piezo signal amplitude is variable for each nozzle. The piezo amplitude is adjusted so that the jet's breakoff length occurs within the charging cell and so that rearward merging or infinite satellites are not produced.

1.3 Motivation for the Nozzle Test Station

By scaling up the printhead from 8 to 96 nozzles the problem of getting all of the nozzles to operate properly increases exponentially. One way to ensure that all of the jets will perform properly on the machine is to screen them beforehand in an environment simulating the printhead.

The nozzle test station automatically characterizes the performance of the nozzles so that those that might fail on the printhead are rejected. For a given binder pressure and piezo signal frequency, the test station sets the velocity to one of several levels and then varies piezo amplitude. At each piezo amplitude the satellite characteristics are determined and breakoff length is measured. The range of piezo amplitudes which produce acceptable nozzle performance is recorded at each jet velocity. This information, combined with automated jet angle measurements and flowrate measurements provides the information to decide if the nozzle is acceptable for use in the printhead.

1.4 Nozzle Test Station Overview

The nozzle test station uses image capture and analysis techniques combined with motion control technology to perform its characterization of the 3DP ink jet nozzles. These techniques allow the measurement of jet velocity, breakoff length, angle, and flowrate; most importantly satellite detection and analysis are also performed using these methods. All of this is done automatically. The operator loads the nozzle, selects the desired operating frequency, and the nozzle test station completes the rest itself.

1.5 Required Capability

In order to successfully characterize nozzle performance, the nozzle test station must meet the following requirements:

1. Properly detect and classify satellites which will affect the performance of the printhead
2. Identify nozzles which have an X-Y axis angle of magnitude greater than 1.15° (this keeps it from flooding charging cell)
3. Identify nozzles which have an X-Z axis angle of magnitude greater than 0.11° (produces a maximum printing error of .002 in. at 1.0 in. droplet flight distance)
4. Measure breakoff length of the jet and identify cases where breakoff length is less than 0.020 inches or greater than 0.100 inches (the dimensions of the charging cell)
5. Measure Jet Velocity to within +/- 0.1 m/s
6. Control jet velocity by varying binder pressure
7. Determine if the piezo amplitude is too high and the jet is overdriven
8. Focus on droplets automatically

2. Background

2.1 Piezoelectric Droplet Generation

In order to excite droplets to break off from the fluid jet in a stable, repeatable manner a piezoelectric crystal is attached to the fluid supply line of the nozzle. This crystal is excited by a sinusoidal electrical signal to produce mechanical vibrations in the fluid stream and the nozzle. The cylindrical fluid jet is inherently unstable due to surface tension, and so this disturbance grows rapidly causing the breakup of the jet into droplets. The Rayleigh velocity of the jet is the velocity at which this disturbance will grow the fastest for a given piezo excitation frequency, producing the minimum breakoff length in the jet.

$$V_R = f*4.51*d \qquad [4]$$

In this equation f is the piezo excitation frequency, v is the jet velocity, and d is the nozzle inner diameter. Because of this excitation the droplet generation cycle is very repeatable and also easily visualized.

2.2 Visualization of the Droplet Stream

Since the breakoff of the stream is very regular, the droplet stream can be visualized with a light emitting diode (LED) which is flashed at the same frequency that drives the piezoelectric crystal and excites droplet breakoff. The LED is consistently flashed at the same point in the droplet breakoff cycle and the resulting image appears to be a still picture of a specific instant. This works as long as the average illumination that reaches the CCD while the camera shutter is open is higher than the minimum required for the camera. This method has the advantage that it does not require a fast camera shutter to capture the image but rather relies on the repeatability of the droplet generation

and the synchronized, short duration LED pulse to generate a quality image. However, this method does not capture intermittent events, such as unsteady satellite generation.

In order to achieve the sharpest droplet image, the duration of the LED flash must be as short as possible while still providing adequate illumination to the CCD. This minimizes the amount of droplet movement during the illumination, which causes blurring of the image. To facilitate this, the LED can be driven with its maximum average current (remembering that it is only "on" for a small percentage of the time this can be much higher than its maximum steady state voltage). Also, the LED should be matched as closely as possible to the maximum spectral sensitivity of the CCD. Finally, the camera shutter should be open for as long as possible, in order to collect as many LED flashes as possible and increase the CCD illumination. For the apparatus used here the LED was driven with an "on" current of 300 mA, utilizing a transistor to switch the system on and off from a 5V source. The camera, a Pulnix TM200 had its maximum spectral sensitivity around a wavelength of 550 nm, while an LED with roughly 700 nm light was used.

With this setup, the LED delivered adequate illumination with a flash duration of 0.1 μs at a lens magnification of 2X to the CCD and a piezo drive frequency of 30 kHz. This 0.1 μs flash duration is the shortest that the Digital Input Output (DIO) card would allow without external electronics; this is limited due to the maximum oscillator frequency of the card, as explained in section 2.3. For a 10X magnification the duration was increased to 1 μs and the image suffered no noticeable blurring. At 20X the flash duration was increased to 2 μs and the image did begin to blur due to droplet movement but was still useable. The lens does not have a motorized iris, so the iris was held at a constant setting throughout. The iris was fully opened, in order to minimize the depth of field. This aided the autofocus routine in determining droplet Z-axis position using the focus distance. A motorized iris was not sourced with the lens because the

stepper motor controller board was already fully utilized controlling the X, Y, focus, and zoom axes.

2.2.1 Visualizing Intermittent Satellites

Visualizing a droplet stream by flashing a red LED once per droplet generation period has the disadvantage that objects which are not regular and repeatable appear blurred or get washed out on the CCD. In order to capture these objects the image can only be illuminated once, with enough light for the CCD to detect the event. A red LED flashing for 1 μs is not powerful enough - it can only illuminate the CCD adequately if it flashes at 35 kHz:

$$\text{duration} = 1\ \mu s * 35\ kHz\ \text{frequency} * 0.0167\ s\ \text{shutter} = 0.6\ ms$$

The LED adequately Illuminates the CCD if its cumulative duration is 0.6 ms during the time the CCD shutter is open. In order to adequately illuminate the CCD with one 1 μs flash the LED would have to be 0.6 ms / 1μs = 600 times as bright. This rules out a red LED as the light source to visualize intermittent objects. Infrared LED's have a higher intensity than visible LED's, but the spectral sensitivity of the Pulnix CCD camera used in the test stand is too low for these to be effective. A xenon strobe can produce the required light intensity, and it is better matched to the CCD camera's spectral response.

For the xenon strobe case, the strobe is fired at just below the camera shutter speed. The resulting image generally captures the flash, although occasionally a black image is returned if the strobe fires when the CCD isn't accepting light.

A complication with this approach is that the CCD camera is interlaced, which means that two images are actually taken and then combined, or interlaced, into one. Each independent image contains every other line of the combined image. If the CCD is illuminated only once, every other line in the image will be dark.

One solution to fix this problem is to remove the black lines utilizing software; this will produce an image with an incorrect aspect ratio. If the aspect ratio is important, the illuminated lines can be copied and used to replace the black lines.

In order to visualize a specific point during the droplet generation cycle utilizing only one xenon strobe flash the flash signal must be triggered by the piezo excitation signal, and then delayed before reaching the strobe. This is the same as was the case with the LED. The difference is that only one signal can be sent to the strobe each time the shutter is open, rather than once per droplet like the LED.

The decision was made to use the red LED for the bulk of the droplet visualization and analysis work, and use the xenon strobe in the simple mode discussed above, firing it once every 1/60 second independent of the shutter and piezo signal. In this way the strobe is used to manually check for intermittent satellites in regions where there is reason to suspect their presence, and there is no need to visualize specific instants in the droplet generation cycle.

2.3 LED Signal Delay Generation

The synchronization required to match the LED flash with the piezoelectric crystal excitation can be accomplished simply by using a function generator to drive the crystal and hooking the LED to the TTL output line. However this approach does not allow for a delay between the two signals. It is desirable to be able to put a delay between the droplet excitation signal and the LED signal so that the instant being visualized in the droplet generation cycle can be varied by the user or the analysis software.

In order to delay the LED signal, a digital input-output (DIO) card was used. The critical parameter for this card was its maximum oscillator frequency. The card uses the oscillator to begin counting when it is gated by the TTL signal; it then counts a specified number of oscillations and fires. Its output drives a transistor that switches the LED.

Inherent in this process is an uncertainty in the signal delay of twice the oscillator period. This uncertainty is due to a one period uncertainty in when the card begins counting and a one period uncertainty in the length of the delay. There is uncertainty in the beginning because after it is gated by the TTL signal the card starts counting on a rising edge of the oscillator signal, and it may have to wait up to one period for this event. There is uncertainty in the length of the delay once counting begins because the analog delay is being counted with an integral number of oscillator periods and there may be a mismatch of up to one oscillator period. This is shown in figure 3.

Figure 3 : Jitter in Delayed LED Signal

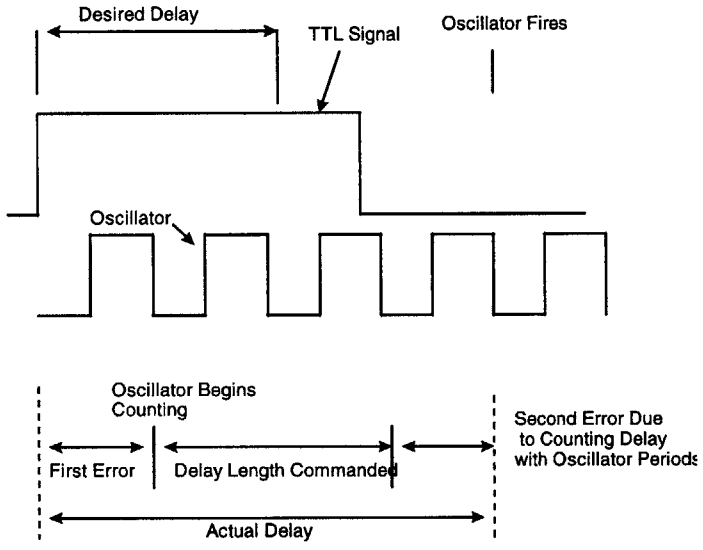

The uncertainty in the delayed pulse causes the LED to flash slightly out of phase with the droplet generation frequency, and the resulting image has an unsteady "jitter". The allowable "jitter" in the delay is 1% of the shortest droplet generation period expected. The highest piezo frequency anticipated is 50 kHz, and so the allowable jitter is .01*1/50kHz = 0.2 μs. This jitter is equal to two oscillator periods, and so the oscillator frequency is: fo = 2/0.2 μs = 10 MHz.

The National Instruments AT-AO-3 card was chosen for the test stand because it has a 20 MHz oscillator.

The minimum duration of the LED flash is also limited by the DIO card oscillator, as mentioned in section 2.2. The duration of the flash is subject to the same errors as the delay explained above, and so its minimum length is two oscillator periods, or 2*(1/20 MHz) = 1 X 10^{-7} = 0.1 μs. This was short enough to give a crisp image, without any blurring due to droplet motion.

2.4 Image Analysis

The images generated by the test station are captured by a video frame grabber board. This greyscale image is manipulated in National Instruments' LABView program, using the Image Acquisition (IMAQ) add-on package. The video image is converted into an array of pixel intensity values, varying from 0 - 260. This array is then analyzed to determine where particle edges are located. A particle is defined as any body (jet, droplet or satellite) represented in the image as a group of pixels of similar intensity. The array can also be filtered so that all pixels above a threshold intensity are assigned an intensity of zero (black), and all the pixels with intensities below the threshold are given an intensity of 1 (represented as red). This produces a binary black and red image.

2.4.1 Edge Detection

The edge of an object in the greyscale image is not a sharp, binary change in pixel intensity, but rather transition between different pixel intensities. In order to determine where the "true" edge of an object is, the edge detection routine examines the intensities of the pixels along a line in the image. When the slope of the intensity reaches a given value, the algorithm declares that point to be the location of an edge.

Figure 4 : Pixel Intensity Chart

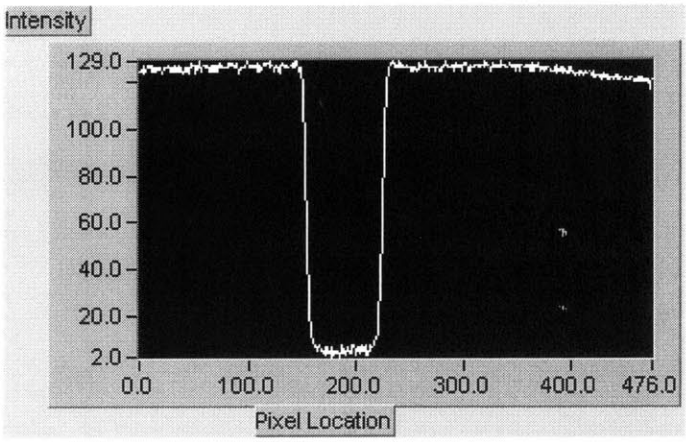

2.4.2 Using a Pixel Intensity Threshold to Filter an Image

The software can threshold the image making all pixels above a certain intensity threshold black, all the ones below red. In a binary image the edge of a particle is where the pixel intensity changes from 0 to 1. Once a greyscale image has been thresholded into a binary image it can then be used in LABView particle analysis routines. These routines calculate such characteristics as center of mass X-Y location in pixels, particle areas, the dimensions and locations of the rectangle which completely bounds each particle, circularity factors, and many more characteristics not used here.

In these LABView routines the connectivity of the pixels determines which pixels are considered connected to one another and part of a particle, and which are not. For a connectivity of 4 a pixel is considered attached to any pixels directly above, below, or beside it which have the same value of intensity, but not attached to any pixels diagonal from it. A connectivity of eight is the same as connectivity of four, except that pixels diagonally adjacent to the original pixel can

be considered as attached to it as well, if the intensities match. This is illustrated in figure 5.

Figure 5 : Connectivity of Particle Analysis Routine

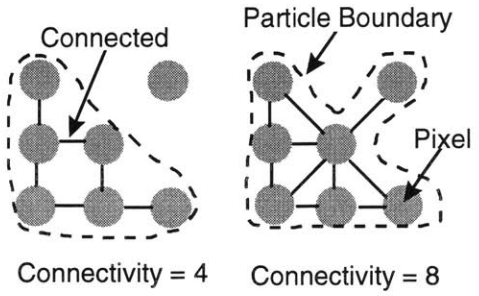

One unfortunate effect of using pixel intensity to threshold an image is distortion in the size of the resulting object in the binary image. The value of this threshold intensity affects the size of the thresholded object, as shown in the figure 6 where a chart showing the effect of thresholding on a droplet's diameter is presented.

Figure 6: Threshold Intensity Effect Chart

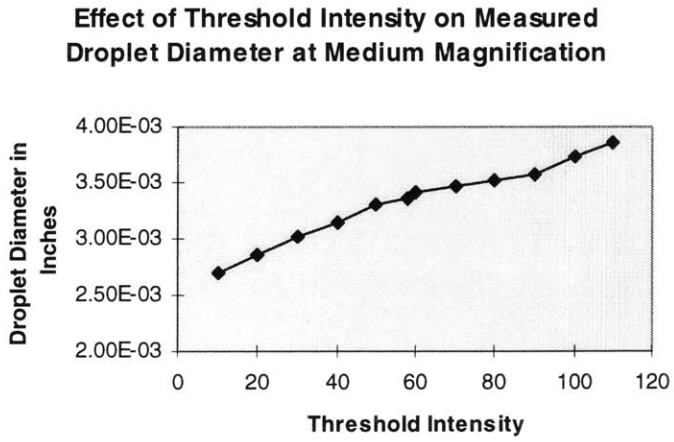

The intensity used to threshold the image can impact the droplet diameter by as much as 40%. In order to have an estimate of the true droplet diameter for comparison, the flowrate was measured by hand for this example, and the droplet diameter required by this flowrate at the piezo frequency of 35,000 Hz was calculated. This diameter was $3.34X10^{-3}$ inches. On the chart this corresponds to a threshold intensity of 58.

It would seem that 58 is the correct threshold intensity to use at medium zoom, except that satellites get filtered out with a threshold intensity this low. Adequate satellite imaging at medium magnification requires a threshold intensity above 70, with 85 the current benchmark. To solve this dilemma, the imaging is performed with a threshold of 85, and the diameters of the droplets used in the flowrate measurement are adjusted for distortion using an empirical "fudge factor" of 0.954. This produces surprisingly accurate flowrate measurements, as is shown in section 5.2.2.

3. Apparatus Setup

3.1 Overview

The nozzle test station consists of four component systems: fluid, motion, electronics, and video. The nozzle test station is laid out as shown in figure 7.

Figure 7: Nozzle Test Station Schematic

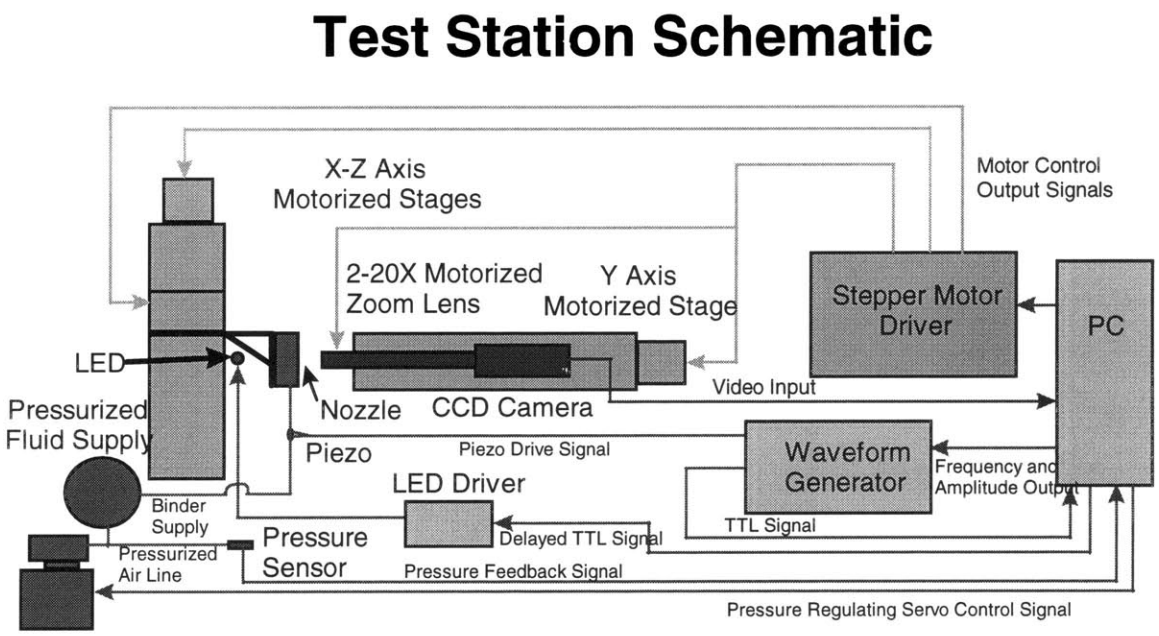

The coordinate system associated with the test station is illustrated in figure 8. The X-axis is located parallel to the axis of the vertical motion stage, the Z-axis is located parallel to the axis of the CCD camera and zoom lens, and the Y-axis is located along the horizontal motion stage which forms the base of the vertical stage holding the nozzle. This coordinate system is shown in the image in figure 9, where the X-axis points downstream, the Y-axis points vertically away from the stream, and the Z-axis points out of the page.

Figure 8: Coordinate System

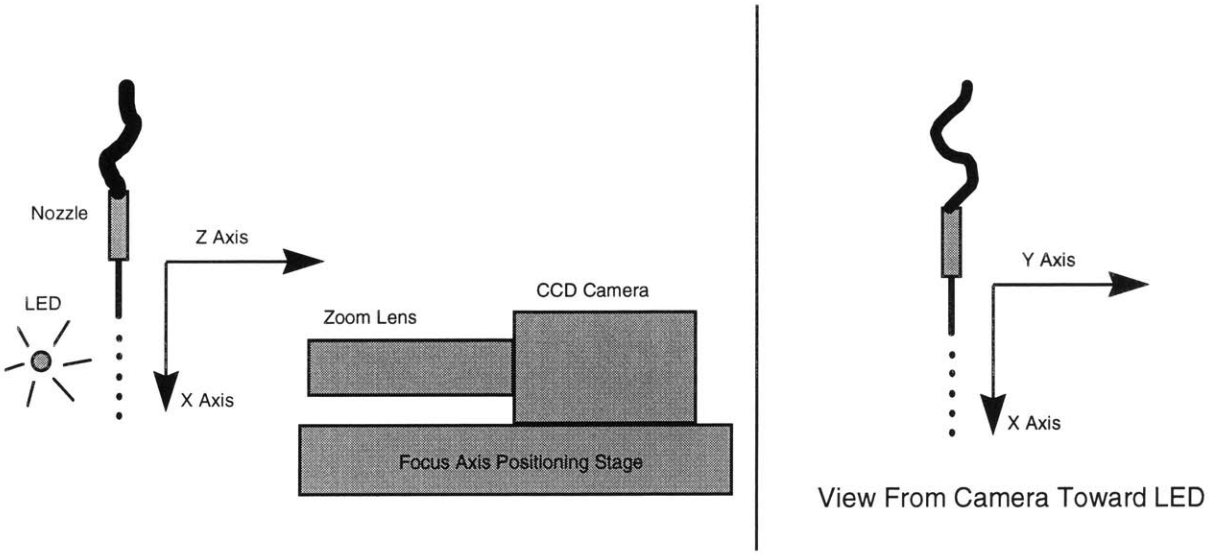

Figure 9 : Coordinate System Applied to Jet

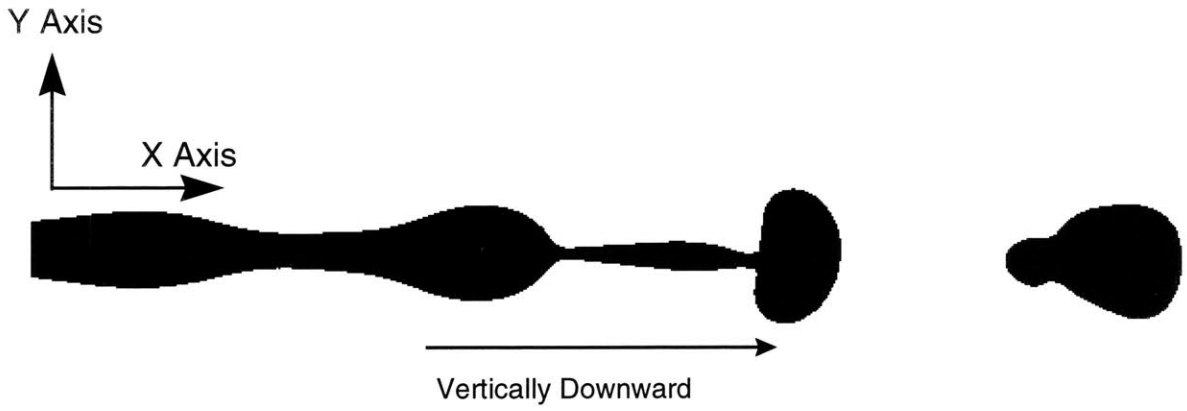

Figure 10 : Photo of Nozzle Test Station

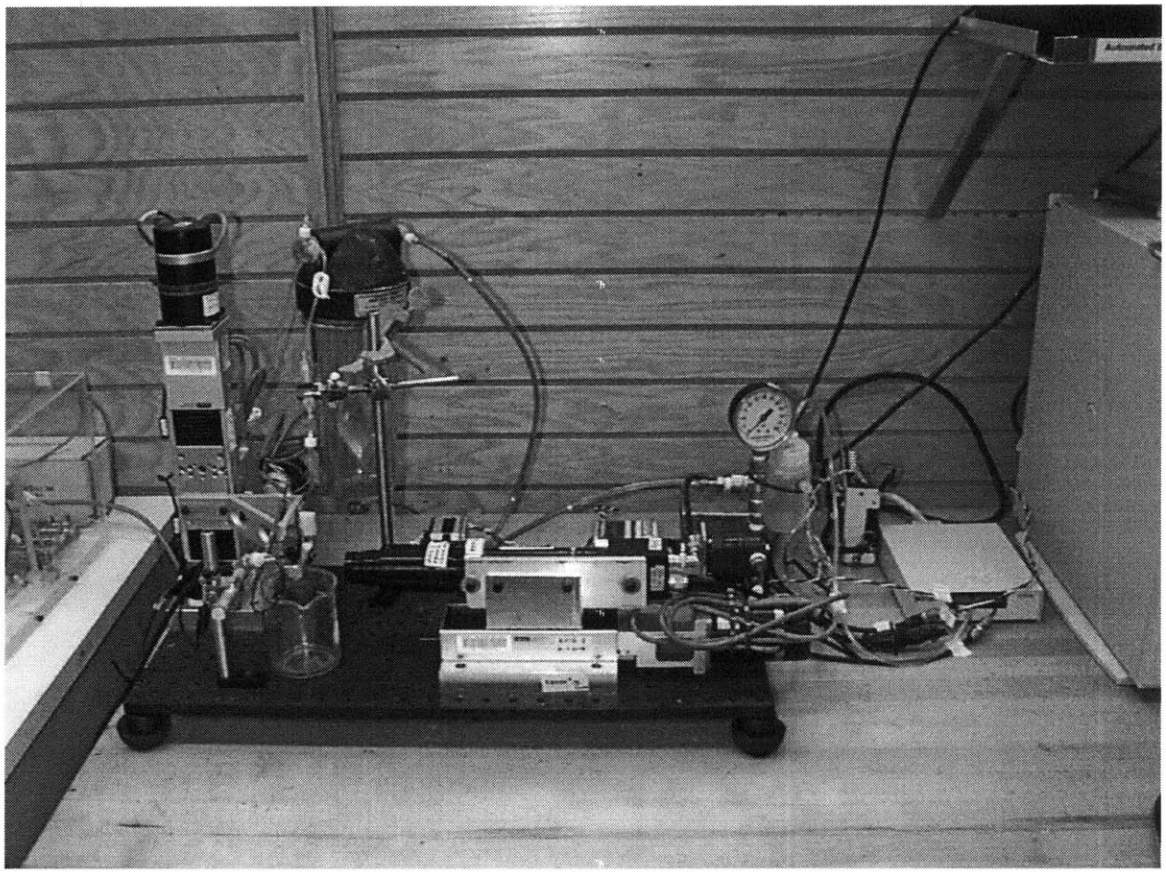

3.2 Components

3.2.1 Motion System

The motion system is composed of three leadscrew linear motion stages driven by stepper motors. Two of the stages are mounted in an X-Y configuration, with the nozzle holder and nozzle cantilevered off the platform of the vertical stage. The CCD camera and zoom lens are mounted to the third stage located as shown in figure 8. These stages are mounted on a 12 in. X24 in. optical breadboard plate. This plate is mounted on damping feet, to reduce the vibration transmitted to the system from the environment.

The motion stages have Hall effect limit switches, 5 mm pitch precision leadscrews, and 2000 count/revolution stepper motors mounted to the stage through bellows couplings. The stepper motors are equipped with rotary encoders, although these are not currently in use. The limit switches are used for two purposes - to prevent the positioning stages from reaching the end of the stage's travel, and also to position the nozzle during system initialization. These are highly repeatable, but are not used directly in any measurement routine.

The stepper motors are driven by a National Instruments NuDrive 4 axis stepper motor driver. This unit receives move commands from the motion control card in the PC, and returns information about the motor position and limit switch status.

3.2.2 Fluid System

The fluid system consists of a pressurized binder reservoir feeding a capillary line with a bayonet style nozzle attachment. A piezoelectric crystal is mounted on the fluid line to excite breakoff. A servomotor actuated pressure regulator pressurizes the binder reservoir, and is controlled from the digital input/output card of the PC through a relay circuit. There is a manual pressure regulator located upstream of the servo regulator to safeguard the system from accidental overpressure. Finally there is a pressure transducer located just downstream of the servo pressure regulator to provide pressure feedback to the PC.

The nozzle is attached to the bayonet, and snapped into the nozzle holder mounted to the vertical motion stage. This nozzle holder consists of a v-groove where the nozzle rests, with a steel spring used to retain it. This holder was designed to provide repeatable seating of the nozzle for the jet straightness measurement. There is a 5 micron filter located upstream of the piezo.

The piezoelectric crystal is driven by a sinusoidal electrical signal provided by the function generator and stepped up in voltage 10X by a transformer. The crystal is coupled to the nozzle through the tubing and fluid, and excites the droplets to break off.

3.2.3 Electronics

The electronics system begins with a 233 MHz Pentium PC which contains a video capture card, a digital input/output (DIO) card, and a motion control card.

The DIO card controls the pressure regulating servo by feeding a logical signal to a relay circuit. It also provides the delayed TTL signal for the LED to illuminate the droplet train. In addition, the card supports analog input so that it can read the output of the pressure transducer. This is a 12 bit ADC, which limits the pressure transducer resolution to 24 μV, or about .03 PSIG.

3.2.4 Video System

A 2-20X motorized zoom lens is attached to a black and white ½ in. CCD camera. This is mounted on the Z-axis (or Focus axis) motorized positioning stage. The output of the CCD camera is displayed on a black and white monitor, and also fed into the video capture card in the PC for use in LABView. The 2-20X zoom lens is actuated by a stepper motor, and the Z-axis stage is used to focus the lens.

4. Measurement Algorithms

4.1 Search Routine

4.1.1 Overview

The purpose of the nozzle test station is to qualify the performance of ink jet nozzles for a given binder before they are installed in the printhead. On the printhead the piezo excitation frequency and binder supply pressure will be the same for all the nozzles, but the piezo excitation amplitude will be tuned for each individual nozzle. The piezo excitation frequency of the machine is constant, and the pressure is set so that the average jet velocity is equal to the Rayleigh velocity (V_R), as defined earlier. Each nozzle that passes the nozzle test station will operate satisfactorily at V_R, V_R +/- 5% and V_R +/- 10%. It is assumed based on experience that in a population of "good" nozzles all run at the same binder pressure, the resulting spread in velocities will be less than +/- 10% of the mean V_R. Thus if all of the nozzles which pass the test stand run properly within +/- 10% of their individual V_R, then they should run properly on the printing machine where the mean V_R will be within +/- 10% of the individual jet's V_R.

4.1.2 Logic

The search routine begins by calculating V_R for the specific nozzle. Pressure is adjusted until the jet velocity is within a defined tolerance of V_R. The piezo signal amplitude is decreased to 1V, and the camera is moved 0.100 in. from the nozzle at medium magnification. At this point, the camera is looking at the jet at a distance from the nozzle equivalent to the exit of the charging cell on the printhead. Because the jet is being excited very weakly the droplet breakoff is much longer than the charging cell length. The piezo signal amplitude is increased until droplet breakoff is seen within the frame.

At this point the jet satisfies the maximum length criteria. The camera centers on breakoff, and determines if there are satellites present, and if there are it classifies them as forward merging, backward merging or infinite. The exact breakoff length is calculated as well.

The piezo amplitude is increased, and the satellite search and breakoff length measurements are performed again. When both an acceptable satellite and length condition is first encountered, the piezo amplitude, breakoff length, and breakoff phase are recorded. The software continues to step up in piezo signal amplitude until one of three limits is hit. The first limit is encountered if the type of satellites switches from none or forward merging to backward or infinite. The second potential limit is tripped if the breakoff length of the jet decreases to below the charging cell inlet length. Finally, if the breakoff length begins to increase with increasing piezo amplitude the jet is overdriven and out of its

Figure 11 : Definition of Overdriven Jet

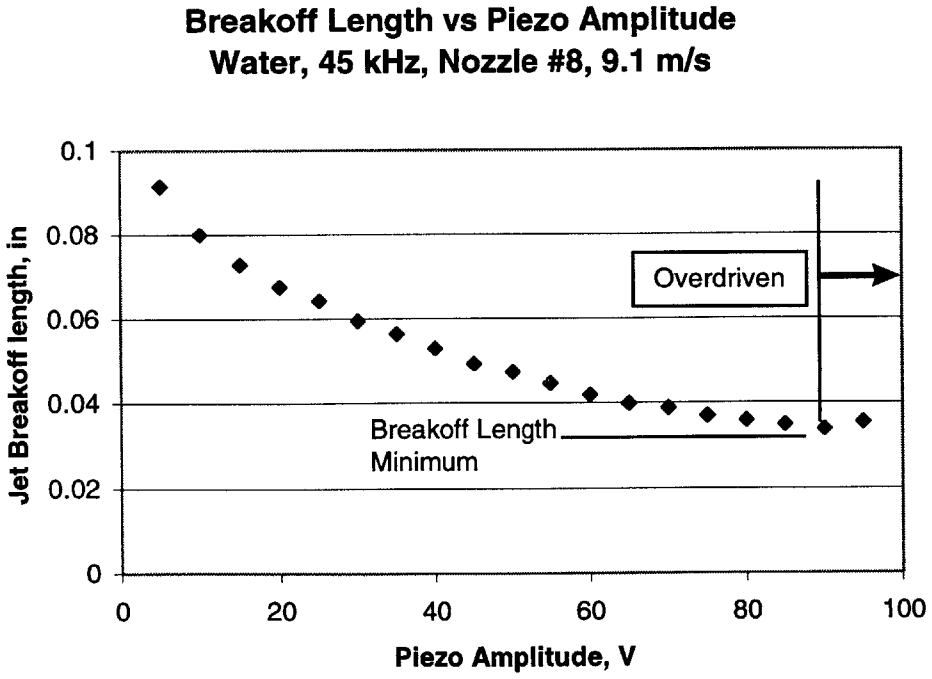

operating range. This is shown in figure 11. Once a limit is hit, the nozzle is no longer in its operating range and the search routine halts after recording piezo amplitude, breakoff length, and breakoff phase.

The nozzle's operation is characterized at the five velocities V_R, V_R +/- 5% and V_R +/- 10%, using the routine described above. If a given nozzle has a region of acceptable operation at all of these velocities, and if the binder pressure required to set V_R for the nozzle is within a given tolerance of a standard pressure, then the nozzle is acceptable for use in the printhead.

Figure 12 : Flowchart of Top Level Logic

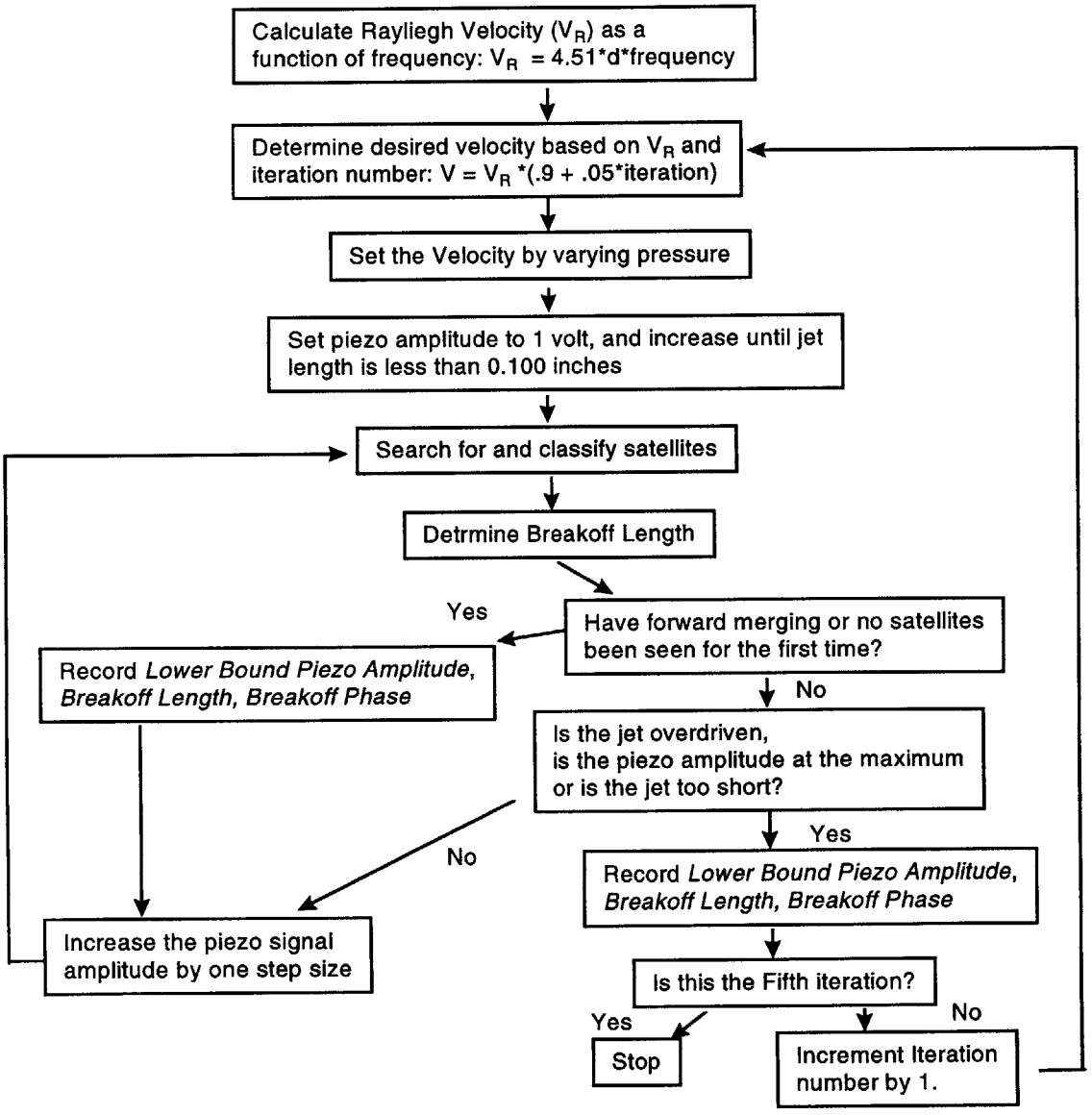

4.2 Satellite Detection and Classification

4.2.1 Satellite Overview

During droplet breakoff, the fluid connecting the droplet to the jet necks down into a ligament. Once the ligament snaps in one place, it can either be absorbed by the jet or new droplet, or it can detach in a second location and form its own much smaller droplet, called a satellite. These satellites can be of three kinds: forward merging, rearward merging, or infinite.

A forward merging satellite is formed when the ligament breaks off closest to the jet first and then near the droplet so that it has forward momentum relative to the droplet. It will have a higher velocity than the droplet, and will overtake the droplet and be absorbed by it. If this occurs relatively quickly, within one or two droplet generation periods, then it is fairly benign to the operation of the printhead. Figure 13 is an image of a forward merging satellite.

Figure 13 : Forward Merging Satellite

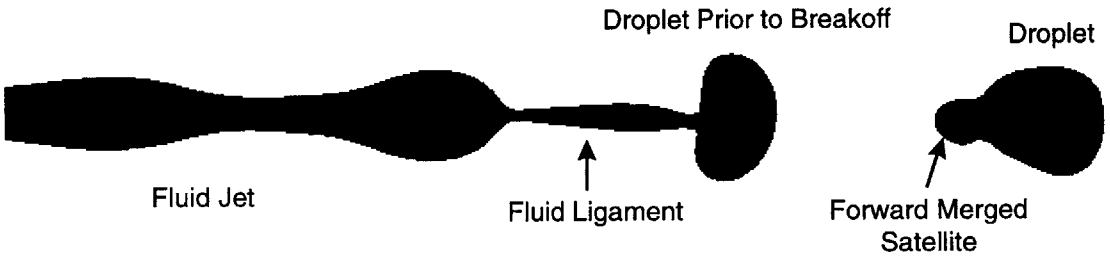

If the ligament snaps at both ends at nearly the same instant, it has very little momentum relative to the droplet, and will not be absorbed quickly, if at all. This hurts the printhead operability because the satellites have a much higher charge to mass ratio than the droplets and will be deflected either into the charging cell, flooding it, or else will be flung into the powder bed far from the intended location, causing a printing error. Figure 14 is an image of infinite satellites.

Figure 14 : Infinite Satellites

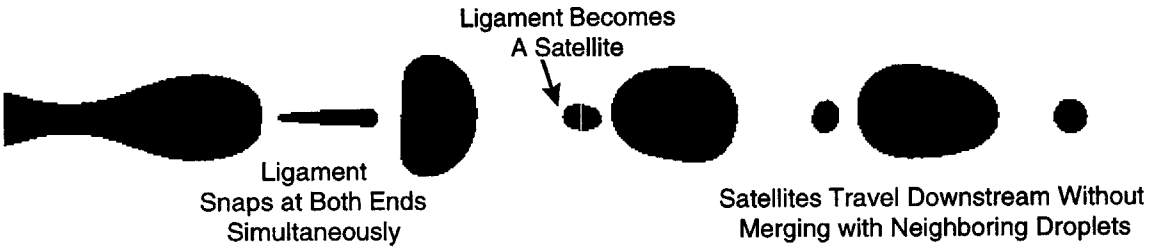

Finally, if the ligament snaps next to the droplet and then near the jet it will travel slower than the droplet and will merge either with the jet or with the droplet which forms behind it. This is also detrimental to printhead performance because the satellite will have a different charge than the next droplet formed and when it merges with it, the resulting droplet will have an error in its charge causing it to be deflected to an incorrect location on the powderbed. A rearward merging satellite is presented in figure 15.

Figure 15: Rearward Merging Satellite

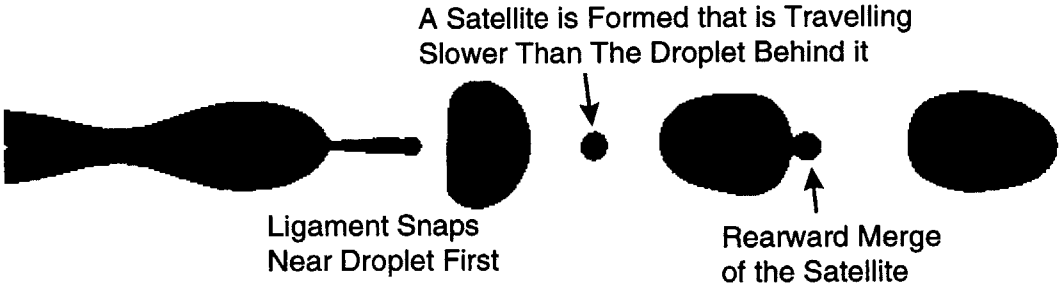

Therefore, it is important that the nozzle operate in either a satellite free mode, or with forward merging satellites. The satellite detection and classification algorithm uses video image analysis to determine if satellites are present, and if they are it then classifies them forward merging, rearward merging, or infinite.

4.2.2 Satellite Detection and Classification Algorithm

The algorithm zooms the camera in on the jet so that the end of the jet and two full droplets fill the image. The LED delay is set to zero, and an image is grabbed by the algorithm for processing. The image is converted into a binary image by thresholding the pixel intensities, and the LABView particle measurement routine is used to determine the two dimensional characteristics of the droplets and satellites in the image.

This LABView routine returns the center of mass (in 2-D space) for the particles, and also determines the location and size of the x-y rectangle required to fully bound the particle. The satellite detection routine then compares the y height of the box bounding the jet to the heights of the other bounding boxes in the image. Any particles whose height is less than 50% the maximum drop height in the frame is considered a satellite. This 50% factor is required because the dynamics of the drops can cause them to bulge and flex as they move, thus varying their height substantially. This factor was determined through experience.

Once the particles have been classified as droplets or satellites, the center of the satellite farthest downstream is tracked as the LED delay is increased from zero. By increasing the LED delay, the image steps through the droplet generation cycle. The delay is increased until the satellite either merges with a droplet or moves off the right edge of the screen. This is shown graphically in figure 16.

Figure 16: Satellite Classification Example

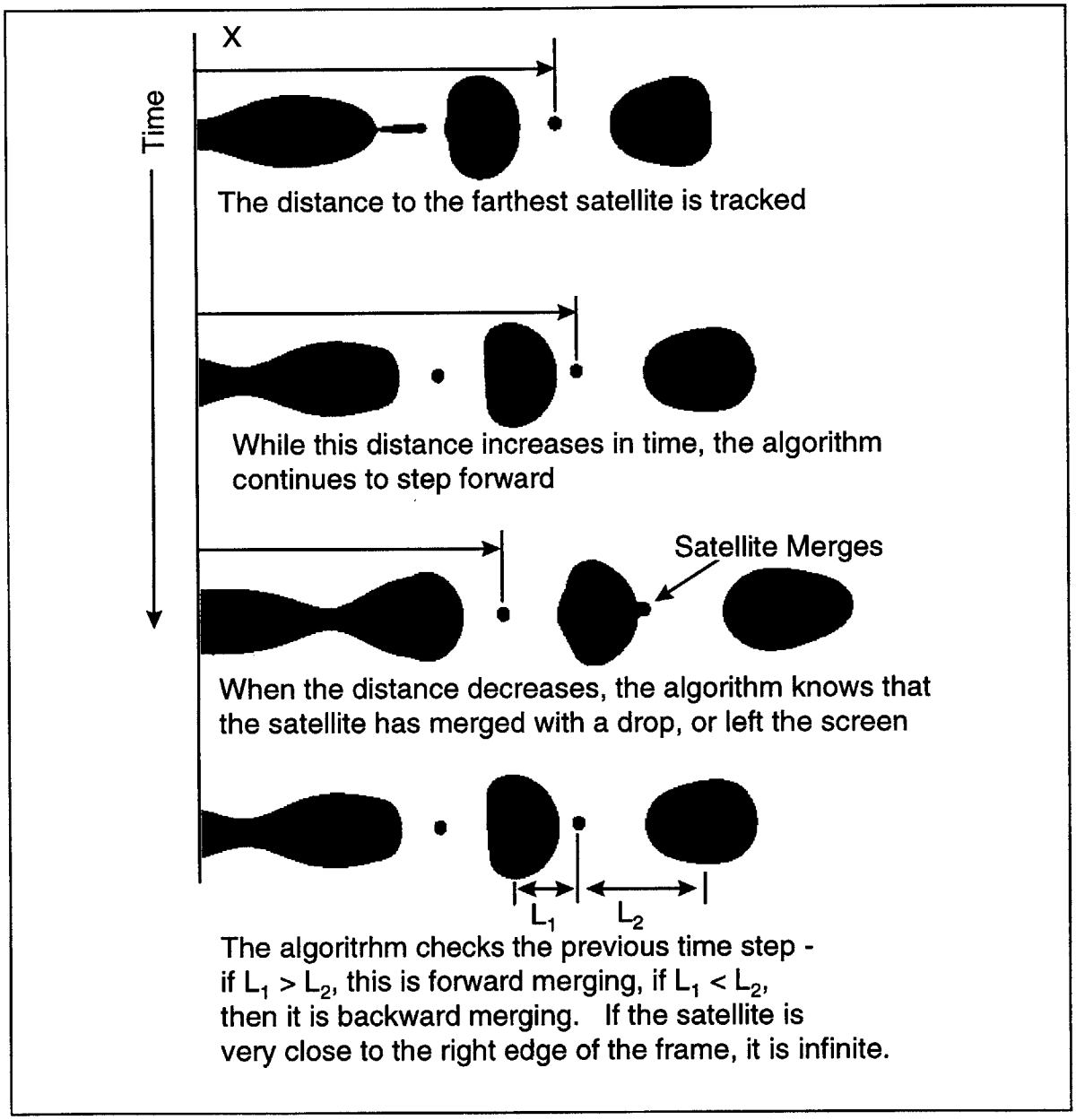

If the satellite was at the right hand edge of the image just before it disappeared, it is assumed to have left the image without merging and this case is classified as infinite satellites. Since two drops, in addition to the jet, are kept in the frame, this corresponds to a satellite which does not merge within two drop spacings of breakoff.

If the satellite is not infinite, then the algorithm measures the distance between the satellite and its neighboring droplets in the frame before it disappeared (by merging). If it is closer to the downstream droplet, then it is forward merging; otherwise it is rearward merging.

4.2.3 Minimum Detectable Satellite Size

The satellite detection routine can detect stable satellites larger than $5.0X10^{-4}$ in. (13 μm) in diameter at medium magnification (droplets are typically $3X10^{-3}$ in. or 80 μm in diameter). At high magnification satellites down to $3X10^{-4}$ in. (9 μm) in diameter can be detected. Figure 17 demonstrates the size of the smallest detectable satellites at medium and high zoom. The high zoom setting allows smaller satellites to be detected, but it is very difficult to distinguish between forward, backward, or infinite merging satellites with so little of the droplet train in view. In order for the software to characterize the satellites at high zoom, the camera will either have to move up and down the droplet stream constantly, or zoom in and out constantly. This would greatly increase the time for the algorithm to complete its work. A compromise between the needs of satellite detection and the need for a somewhat streamlined procedure resulted in the choice of medium zoom for satellite detection.

Figure 17: Minimum Detectable Satellite Size

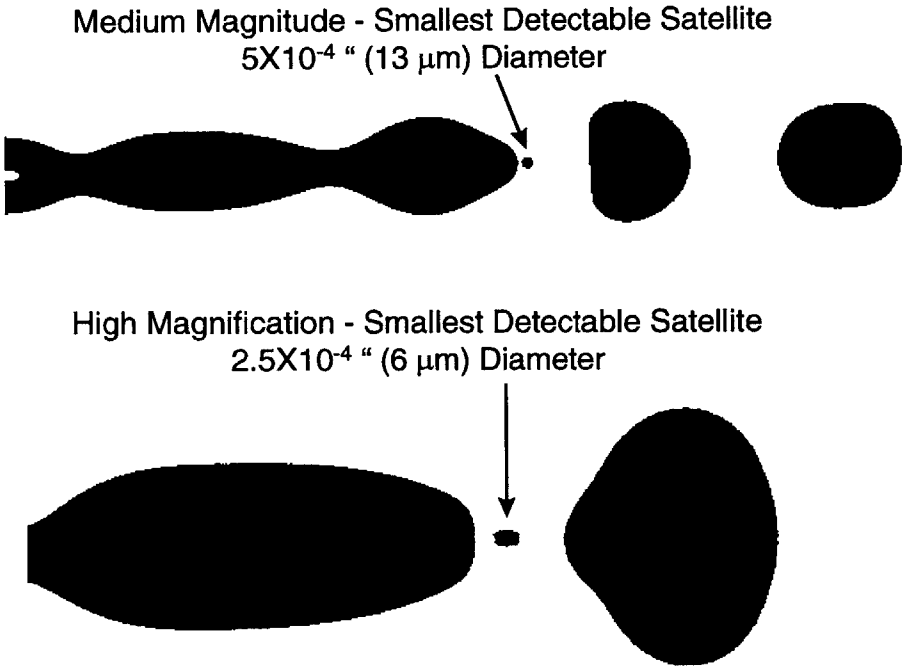

Earlier in section 2.4.2 the effect of threshold intensity on satellite detection was mentioned. As the threshold intensity increases, smaller satellites are detected. If the threshold is raised too high however, too much noise is transmitted, cluttering the image. A threshold of 85 at medium magnification is used here.

4.3 Jet Breakoff Length

Droplet breakoff from the jet occurs due to the excitation of the fluid jet by the vibrations of the piezo crystal. The crystal is driven be a sine wave input initiated by the arbitrary waveform generator (AWG) and boosted in amplitude by a transformer to its range of 0-100 volts. One of the test stand's main functions is to measure the length of the jet when the first droplet breaks off, as shown in figure 18.

The breakoff length is important because the droplets must break off from the jet while still within the charging cell in order to receive the correct charge. The charging cell extends from .020 in. to 0.100 in. below the nozzle.

Figure 18 : Jet Breakoff Length

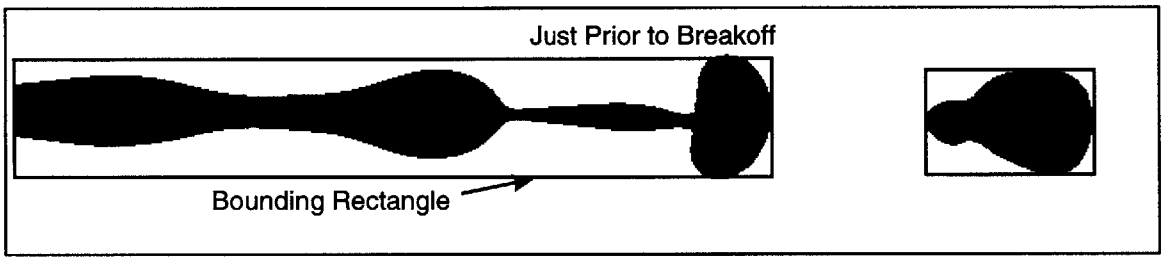

The breakoff length measurement must be taken at the moment in the period when the fluid ligament connecting the droplet to the jet initially snaps. To find this moment, the algorithm varies the LED delay, and at each delay point it measures the length of the jet. The end of the jet is defined as the right hand coordinate of the rectangle bounding the unbroken jet, shown in figure 18. The largest jet length is the breakoff length, which is measured from the right edge of the drop to the nozzle.

Since the camera is zoomed in on the breakoff, the nozzle is not visible in the frame. The location of the nozzle is known in motor counts, based on an earlier measurement. The distance between that point and the current motor position is then found (the current motor position represents the point at the center of the current frame). Finally, the distance in pixels between the location of the end of the jet at the instant of breakoff and the center of the current frame is measured, converted to motor counts, and added to the previous nozzle distance. When this is then converted to inches, it is the breakoff length.

Length = [(Center of Current frame - Nozzle Location) + (End of Jet Location - Center of Frame) / (pixels/count factor)] *inch/pixel factor

Figure 19: breakoff Length Calculation

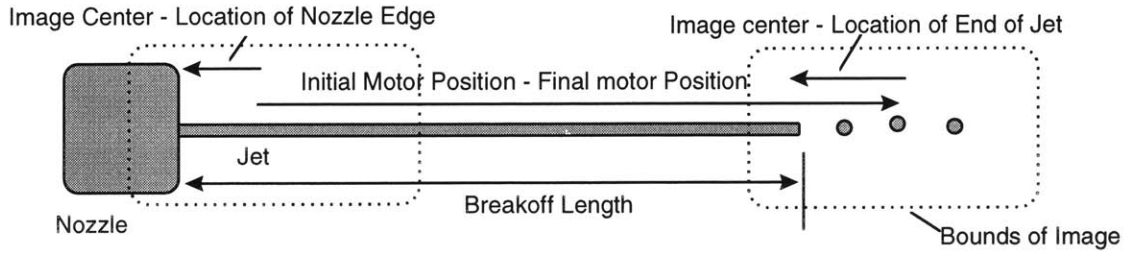

4.4 Jet Straightness

The nozzle test station determines the jet straightness in the X-Y plane and the X-Z plane, as shown in figure 21.

4.4.1 Centering on a Droplet

In order to be able to determine the X-Y angle to a high degree of accuracy, the target droplets being used in the calculation must be placed very precisely in the center of the camera frame. A routine was written for this purpose. The target droplet's center is determined by the LABView particle analysis routine, and the difference between that location and the center of the frame is determined in pixels. These offsets are then converted to motor counts, and the X and Y axis motors move the nozzle the specified amount.

The droplet is not in the exact center of the frame, due to random error in the pixel/count calibration factor. To correct for this, the droplet's center is again measured by the particle analysis routine, the offset from center is calculated in pixels, and the droplet is moved again. The effect of this "double centering" is to minimize the effect of the error in the pixel/count calibration factor. Figure 20 shows how this works.

Figure 20 : Double Centering to Reduce Droplet Position Error

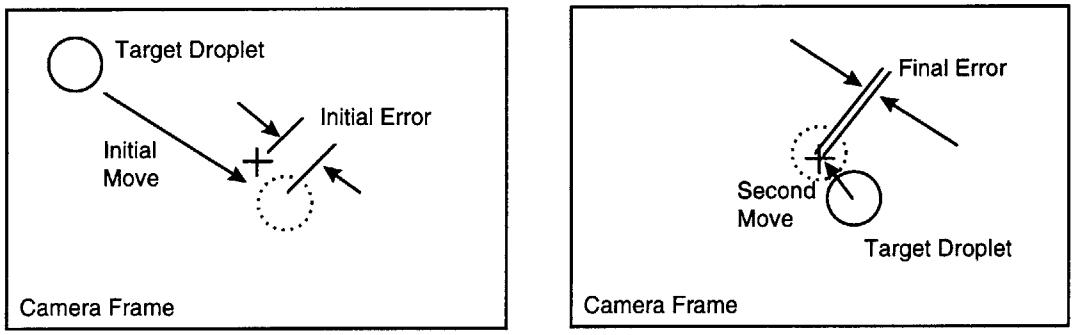

Initial Error = (Initial Move)*(percent calibration error)

Final Error = (Initial Error)*(percent calibration error)
= (Initial Move)*(percent calibration error)^2

Note that the expression for the final error in droplet position in figure 20 has as a factor the squared value of percent calibration error. Since this percent calibration error is 3.3% (or 0.033, see section 6.2.2 for the calculation of this quantity), squaring it reduces its effect on the final error to .0009 - a reduction of an order of magnitude.

4.4.2 Jet Straightness Measurement Logic

First a droplet near the jet breakoff is detected, and centered in the camera frame by the X-Y stepper motors on the motion stages. The X-Y center of the droplet is determined by the LABView IMAQ particle measurement routine which performs a two dimensional center of mass calculation on the droplet. The motorized lens then zooms in to high magnification, and the focal point of the droplet is found by the auto focus routine (this routine is explained in detail in appendix A). This point is the beginning of a line defining the jet's straightness.

The camera zooms out to low magnification, and the nozzle is raised to show droplets a specified distance downstream. The camera is zoomed out so that the droplet stream remains in the frame despite the jet angle. The nozzle is raised 0.800 inches - this is limited by the travel of the motion stage.

Once the move is complete the earlier process of selecting a droplet, centering on it, and zooming and focusing at high magnification is repeated. This droplet, focused and centered in the camera frame at high magnification, is the end of the line defining the jet's straightness.

The distances in the three axes from the beginning to the end of the line defining the jet's straightness is measured in motor counts, so that any length scale calibration issues are avoided. The angle in the X-Y plane is the arctangent of the Y axis distance divided by the X axis distance.

The X-Z coordinates are based on the Z axis motor position at the two droplets' focus points. Because of this, the accuracy of the focus algorithm limits the accuracy of the X-Z straightness measurement. This focus routine adjusts the Z axis motor position until it has reached a maximum edge contrast; this is discussed in appendix A. The minimum contrast difference which is detectable is +/- 0.085°.

The measurement is performed at high magnification, with the aperture fully open, giving the minimum depth of field and thus highest sensitivity to changes in focus axis camera position. A series of trials was conducted varying the aperture position. Having the aperture fully open yielded the most consistent focal position over repeated tests.

Figure 21 : Jet Straightness Measurement

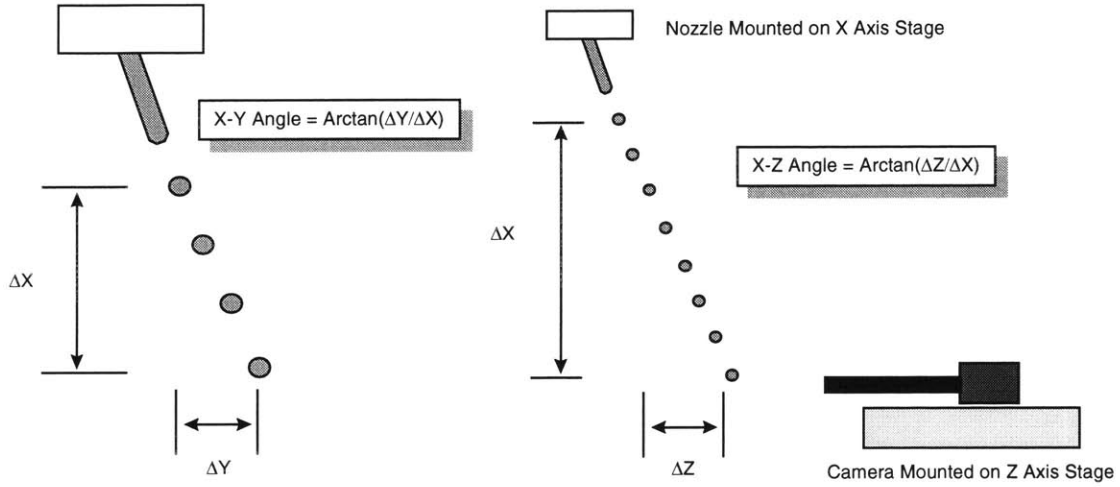

4.5 Droplet Velocity

The droplet velocity is measured by counting five droplets down from breakoff, centering the fifth droplet in the frame, moving a distance of ten droplets down the stream, finding another droplet, centering it in the frame, and measuring the distance in motor position. The velocity is then:

$$v_{drop} = \frac{\Delta_{motor} * \frac{inches}{count}}{(1 - \#drops) * (drop\_period)}$$

The X-Y center of the droplet is determined by the IMAQ particle measurement routine's center of mass calculation.

The distance over which the velocity is measured does not significantly affect the accuracy. The distance was varied from 5 droplets to 25 (approximately .050 in. to .250 in.) and the velocity measurement varied by less than 3%. The repeatability of the measurement also did not change appreciably - it was repeatable to +/- 1% at all distances from .050 in. to 0.250 in.. This 1 % repeatability is the 3σ value based on a 20 measurement trial.

The distance of the droplets from the nozzle when the measurement is taken does affect the measurement however. The velocity measurement is always started 5 droplets from breakoff, in order to improve its consistency. The velocity of the droplets varies along the droplet stream due to drag. Curodeau [3] predicted a change in velocity of 12 -13 % from breakoff to the powderbed for droplets after the lead droplet. The measured velocity changed approximately 10% when measured 1.0 in. downstream of the nozzle, compared to the velocity measured just downstream of the nozzle. This measurement was taken over a distance of 10 droplets (.006 in. approximately).

Since the average droplet velocity changes depending upon the distance from the nozzle and the distance over which the average is taken, the smallest number of droplets should be used for the average, without unduly increasing the error in the measurement. Also, a minimum number of droplets for the calculation speeds up the measurement routine, which is a key factor in the overall time to characterize a nozzle. Ten drops were used here, in order to keep the error less than 1% of the measurement.

4.6 Flowrate

The degree of droplet roundness is very important to the flowrate calculation, because it relies heavily on the measured radius of the drop to calculate volume. The routine moves 0.800 inches from breakoff, in order to ensure that the droplets which are being measured are round. It then measures the height and width of the bounding rectangles of all of the droplets visible in the frame, using the IMAQ particle measurement routine. This is done at medium magnification so that only 3-4 droplets are visible, and partial droplets cut off by the edge of the frame are not considered.

All of these heights and widths are averaged, to give the average droplet diameter, which is converted to inches from pixels through the calibration factor.

This average diameter is used to calculate the volume of the droplet. The droplet volume multiplied by the piezo frequency and binder density yields the mass flowrate.

$$m' = \frac{4}{3} * \pi * (\frac{D_{avg}}{2} * \frac{inches}{pixel})^3 * \rho_{binder} * f_{piezo} * (F_F)^3$$

Note that F_F is an empirical fudge factor which corrects the droplet diameter for distortion due to the thresholding process, as described in section 2.4.2.

5. Verification Testing

5.1 Overall Testing

5.1.1 Discussion of Output Plots

Figure 22 presents an example output plot. This plot presents the upper and lower piezo boundaries for each of the five velocities tested per jet. The Y axis is piezo amplitude in volts, and the X axis is jet velocity in meters per second. The symbol marking each piezo boundary point also conveys the manner in which the boundary was reached. The upper boundary can occur because the jet becomes overdriven by the piezo amplitude as explained in section 4.1.2, because the jets breakoff length decreases below the minimum, or because the piezo amplitude has reached the 100V maximum.

Figure 22 : Example Output Plot

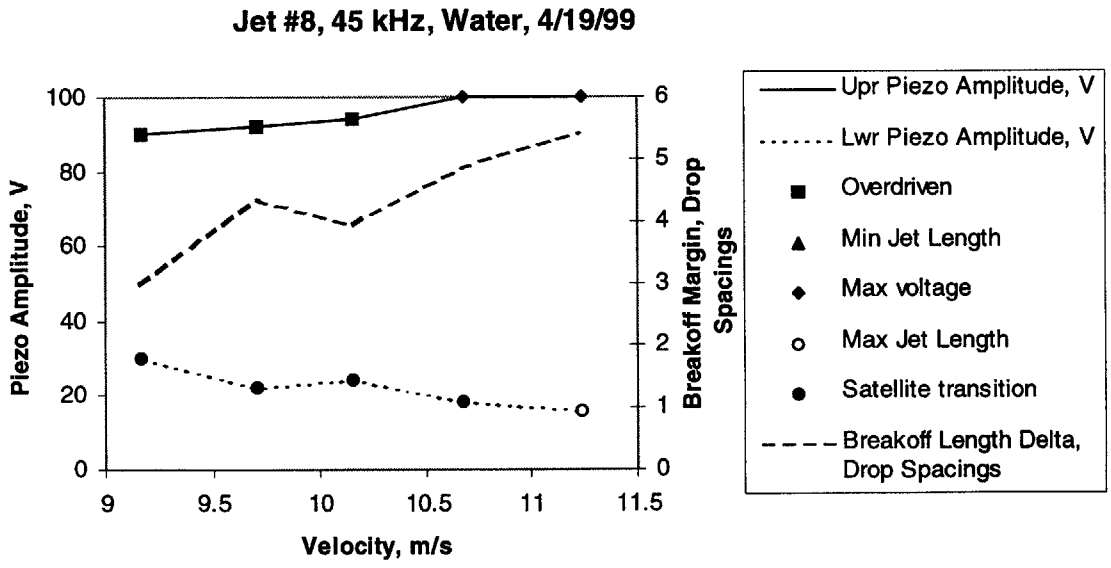

The lower boundary occurs when the jet breakoff length is less than the maximum 0.100 inches and no infinite or backward merging satellites are seen. The satellite transition mode shown above means that the transition from backward or infinite satellites to forward merging or no satellites occurred at a higher piezo amplitude than that required to make jet breakoff occur within 0.100 inches of the nozzle. The max jet length mode means the opposite: the piezo amplitude required to achieve an acceptable breakoff is greater than that required to get an acceptable satellite condition.

Finally, the breakoff margin plotted on the right hand Y axis is the difference between the breakoff length of the jet at the lower piezo boundary and the breakoff length at the upper piezo boundary, expressed in terms of drop spacing distance.

5.1.2 Testing for Repeatability

The first set of tests was conducted in order to establish the repeatability of the test stand results. The full test routine was run with a single nozzle jetting water at 35 kHz piezo signal frequency. This was repeated five times, on several different days. For the velocity measurements, the measurement started at the fifth drop from breakoff and used a 10 drop distance. A velocity tolerance of +/- 0.2 m/s was used in the subroutine which varies pressure to set velocity. Note that all testing referred to in this work was done with 50 μm diameter ruby orifice nozzles.

The resulting output plots are shown in figure 23. These charts show good consistency from test to test. All five charts have upper piezo boundaries around 70 V for all five test velocities, and lower bounds around 20 V for all five velocities. The upper boundary mode was predominantly the overdriven condition, although at lower velocities the minimum jet length mode also appeared.

Figure 23 : Nozzle Testing to Determine Consistency

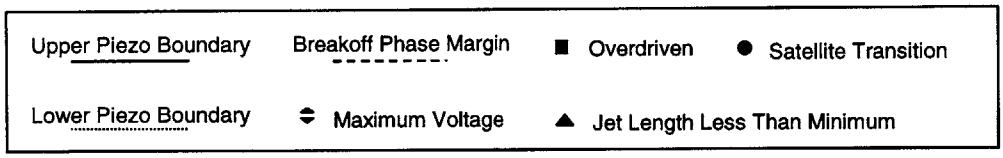

Piezo Boundaries vs Velocity
Jet # 3, 35 kHz, Water, 4/3/99

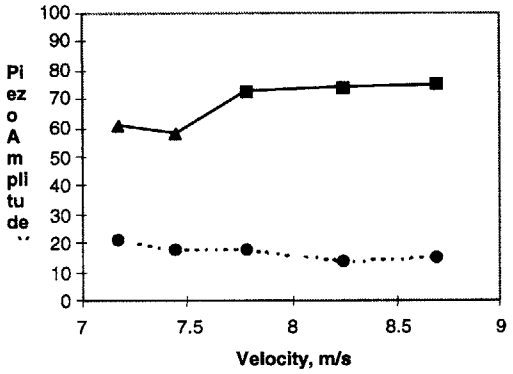

Piezo Boundaries vs Velocity
Jet # 3, 35 kHz, Water, 4/4/99

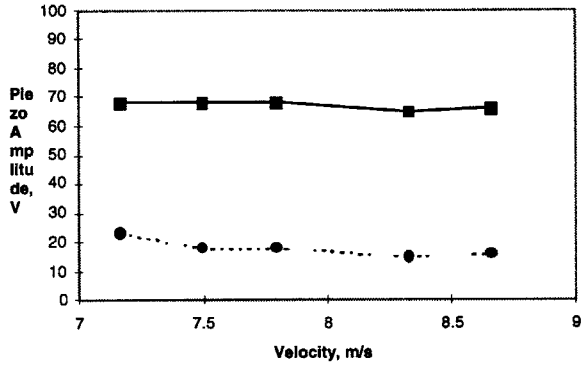

Piezo Boundaries vs Velocity
Jet # 3, 35 kHz, Water, 4/4/99a

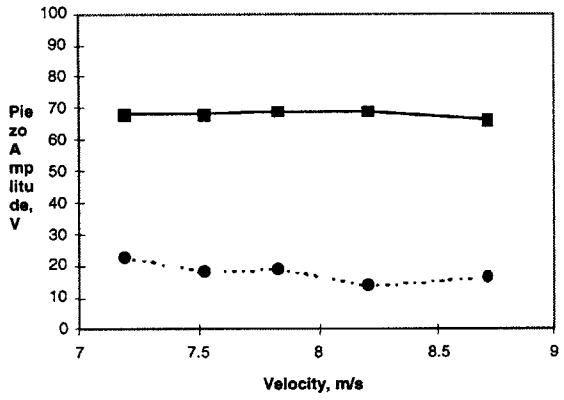

Piezo Boundaries vs Velocity
Jet # 3, 35 kHz, Water, 4/5/99

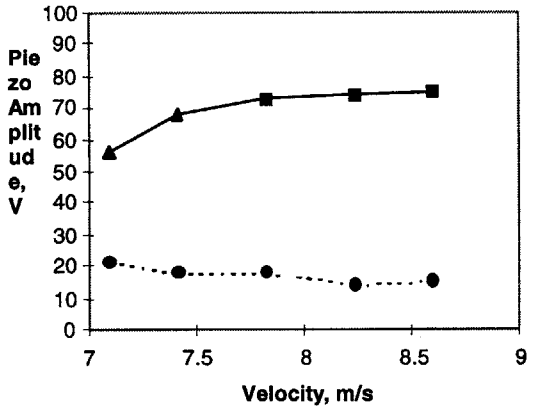

Piezo Boundaries vs Velocity
Jet # 3, 35 kHz, Water, 4/5/99a

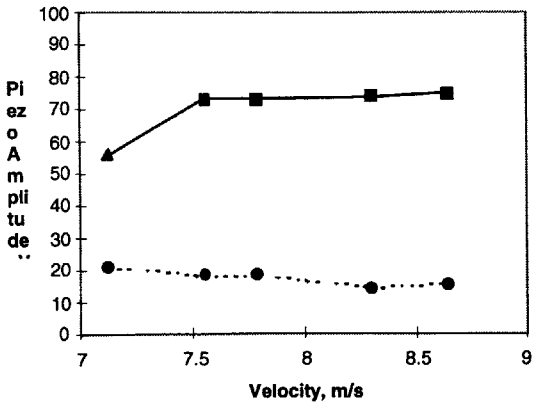

5.1.3 Testing Various Nozzles

In order to demonstrate the ability of the test stand to run reliably with a variety of different operating conditions several different types of nozzles were tested at 45 kHz jetting water. The nozzles, which are described in more detail in appendix C, had different tubing lengths connecting the piezo to the orifice and different methods for attaching the orifice to the tubing. Plots of the output are presented in figure 24. The different nozzles had somewhat different operating characteristics. Under the same testing conditions the upper piezo amplitude boundary varied up to 40 volts between nozzles. The upper piezo amplitude boundary modes also varied nozzle to nozzle, with all three modes being exhibited.

Figure 24 : Testing Various Nozzles

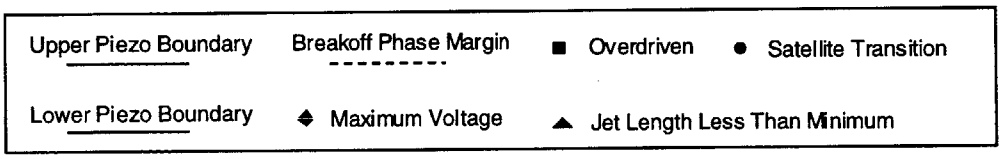

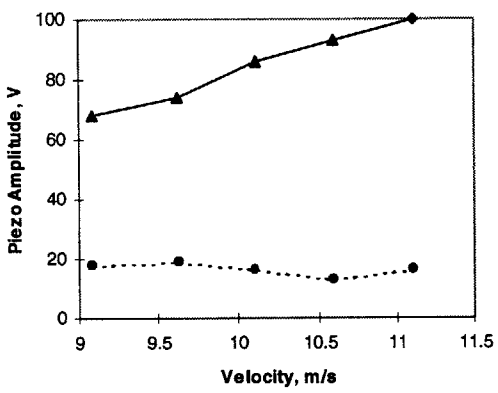

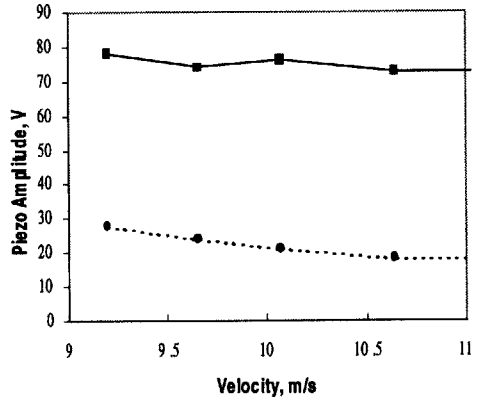

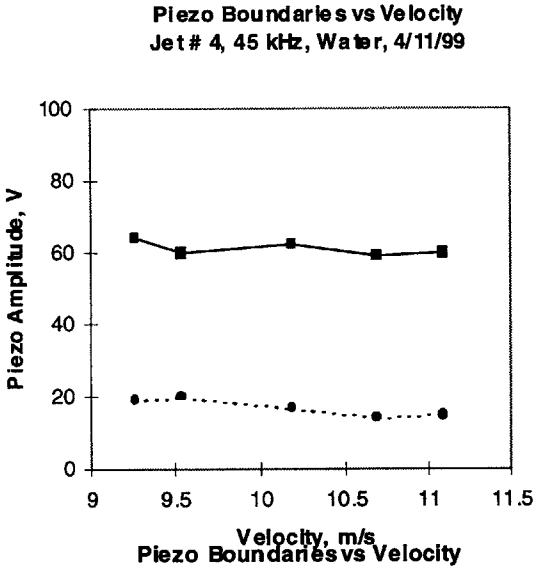

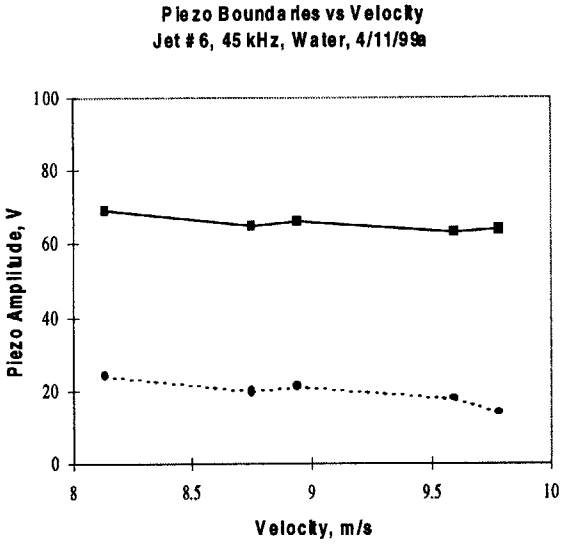

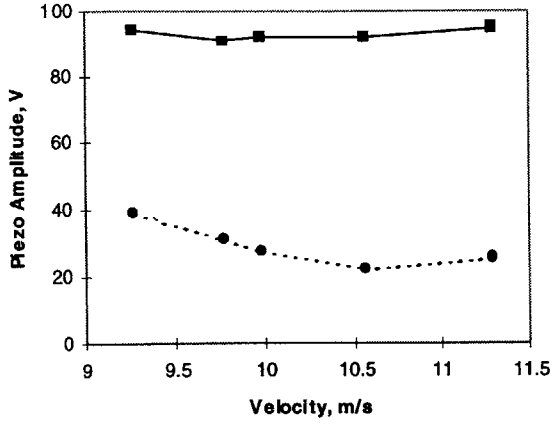

5.1.4 Testing Various Binders

Finally, three nominally identical nozzles taken from the 3DP alpha machine were tested with 4 different binders at two different piezo signal frequencies. The point of this testing was to demonstrate the ability of the test station to operate with different types of binders. The binders were water, acrysol, colloidal silica, and polyacrylic acid (PAA), and they were jetted at 40 and 45 kHz. The acrysol was 18% solids loading, the colloidal silica was 15% solids loading, and the PAA was a 3% by volume solution with water. The test station operated properly with the various binders, as is shown in the charts in appendix D.

The binder type definitely affected the performance of the nozzles. The acrysol test results are shown in figure 25. Acrysol tended to increase both the lower and upper piezo boundaries, with the upper boundary primarily determined by maximum allowable piezo voltage. This would seem to indicate a weaker piezo influence on the jet with this binder.

The water test results are shown in figure 26. Water tended to lower the piezo boundaries compared to acrysol, with the upper boundary set exclusively by the overdriven jet condition. The water apparently provides a good coupling between the piezo and the jet, as compared to the acrysol.

The trends in the results for PAA and colloidal silica were less clear than for water and acrysol. The colloidal silica results are presented in figure 27, the PAA in figure 28. Jet # 4 seemed to have consistently lower piezo boundaries than the other two jets, with its upper boundary set by the overdriven jet condition every time. Otherwise the performance of the nozzles jetting colloidal silica was similar to that of acrysol with high piezo boundaries. The PAA seemed to be

more sensitive to piezo signal frequency, as it tended to have lower piezo boundaries at 40 kHz compared to 45 kHz. The mode at 40 kHz was the overdriven jet condition, while at 45 kHz the maximum piezo voltage condition was dominant.

Finally, Jet #6 jetting colloidal silica at 45 kHz had a very small difference between its upper and lower piezo amplitude boundaries. Indeed, at a jet velocity 10% below the Rayleigh velocity the nozzle never crossed the lower piezo boundary; that is, the piezo amplitude was increased to 100 V and the nozzle was still producing backward merging or infinite satellites.

Figure 25 : Testing With Acrysol

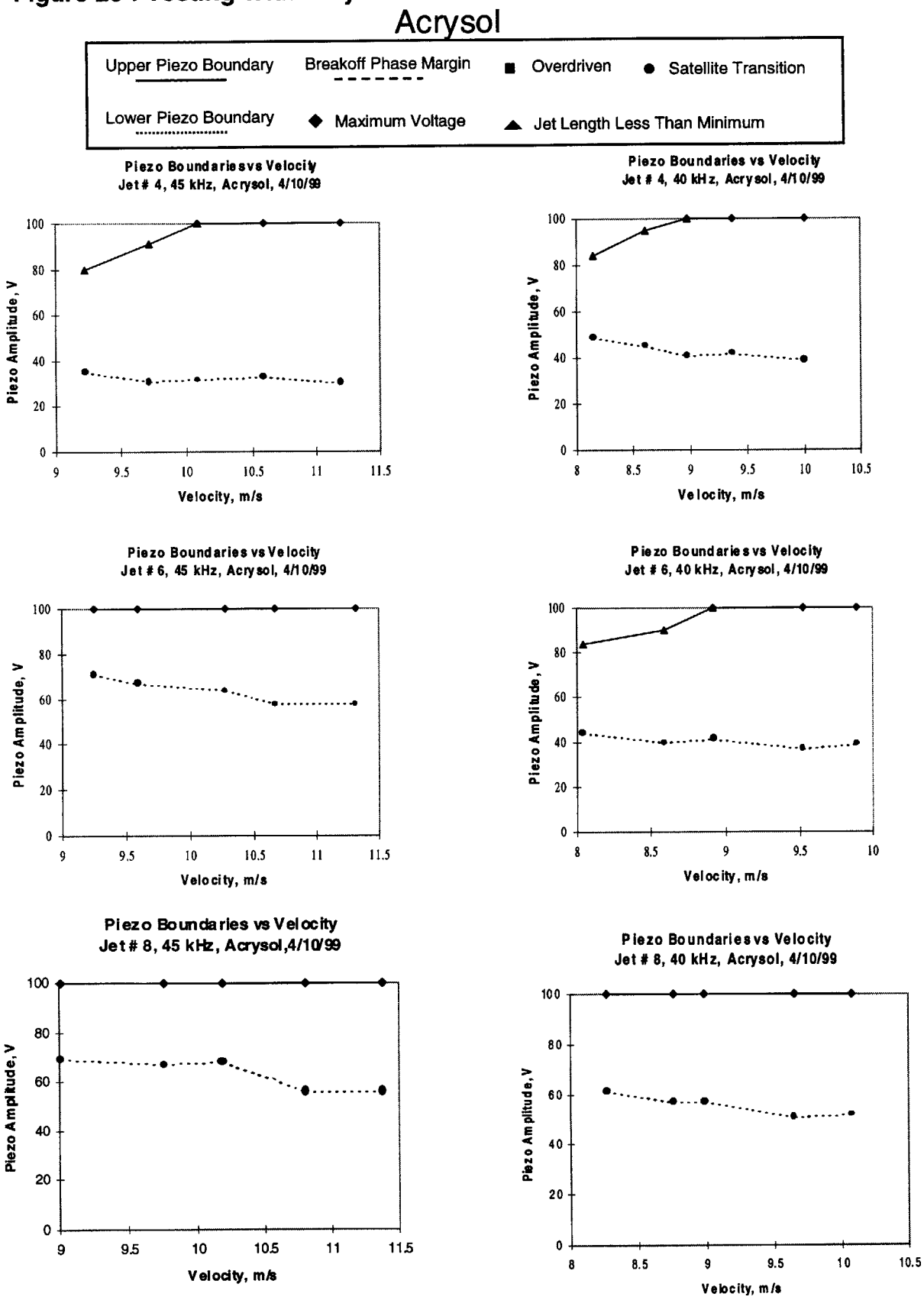

Figure 26 : Testing With Water

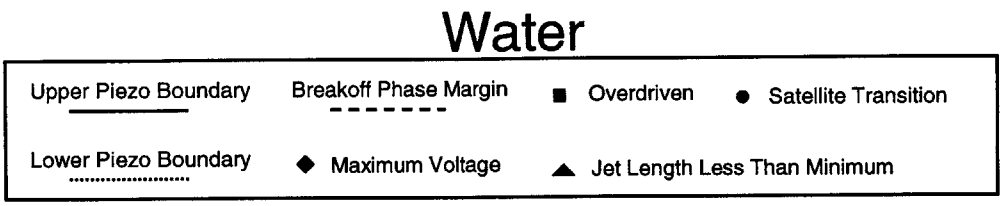

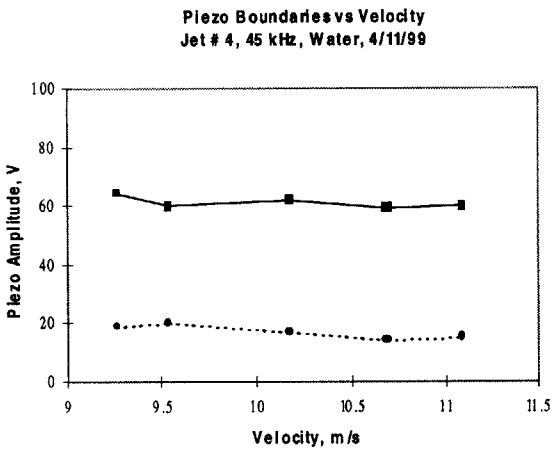

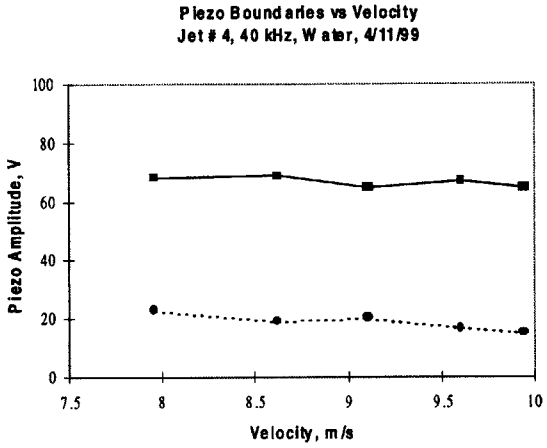

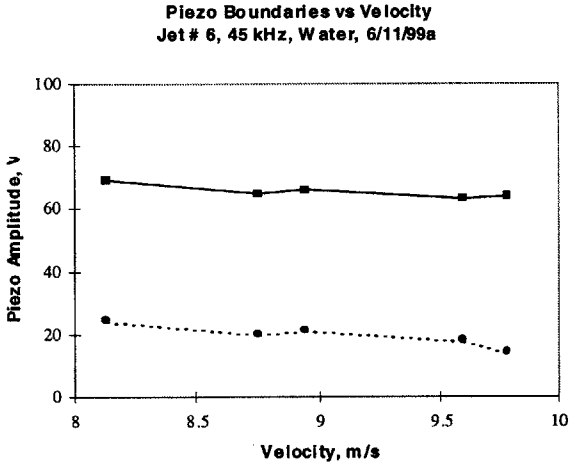

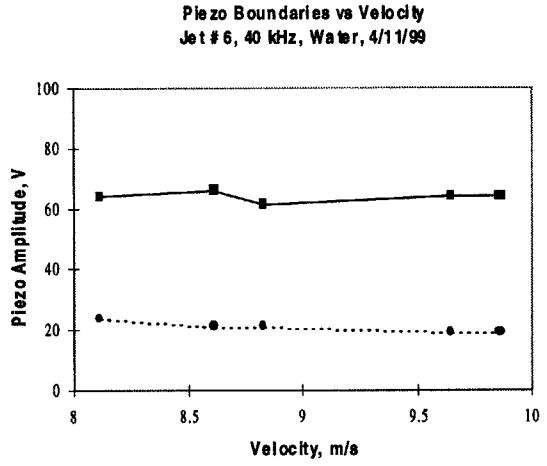

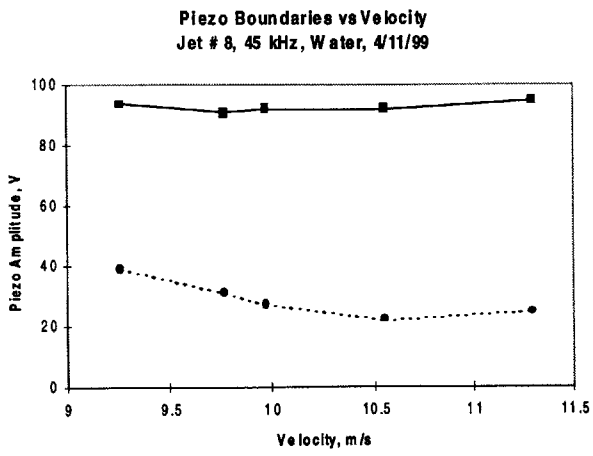

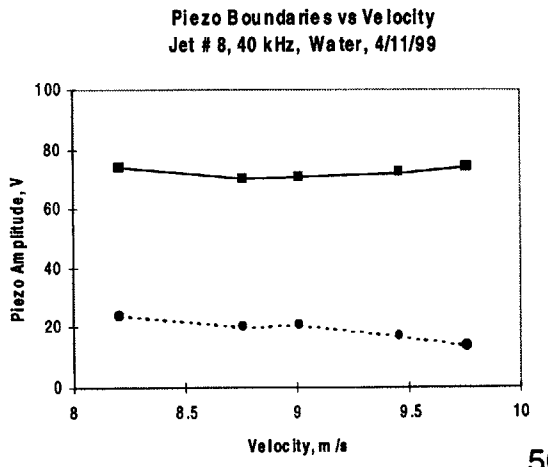

Figure 27 : Testing With Colloidal Silica

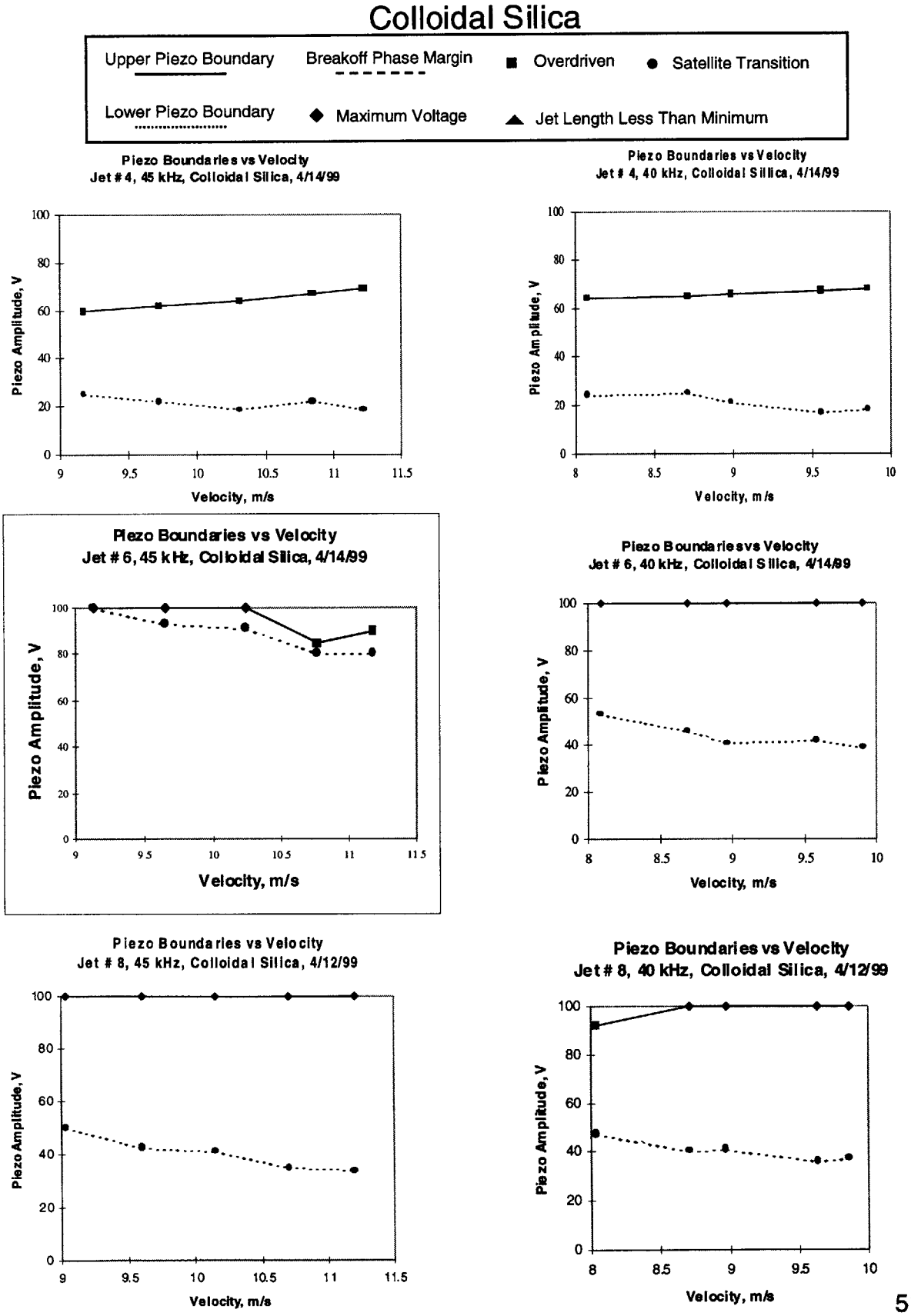

Figure 28 : Testing with Polyacrylic Acid

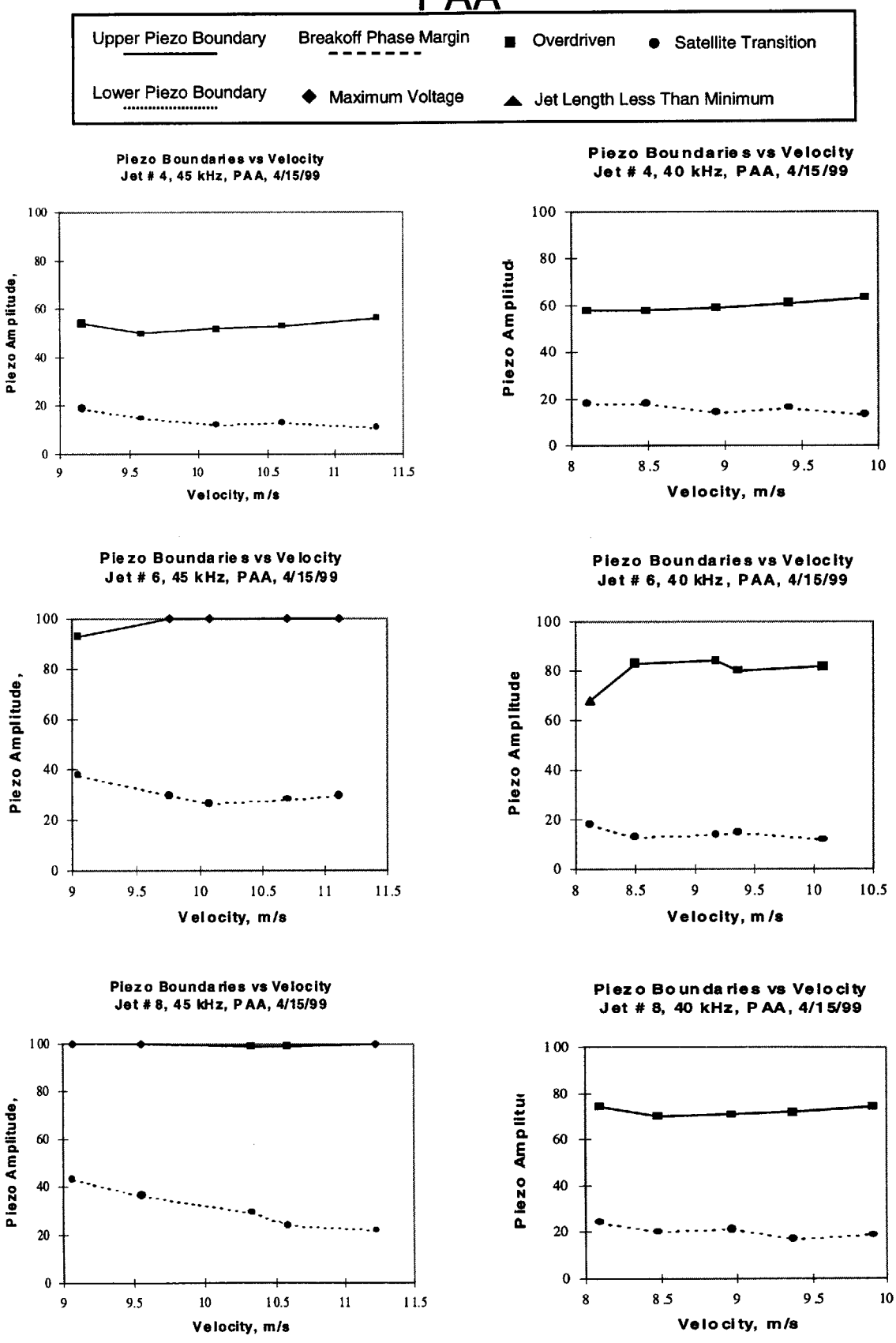

5.1.5 Observations from the Initial Testing

It was noticed that at high piezo amplitudes, very small (less than 6 μm diameter) forward merging satellites occasionally occurred, and these were not detected by the software. These were not detected due to their small size. However, these satellites were seen to merge very quickly (within one droplet spacing of breakoff) and so were considered benign to the printing process.

Finally, in all of the initial testing, a velocity tolerance of 0.2 m/s was used for the routine which sets velocity by varying pressure. This wide tolerance was necessary because the servo pressure regulator lacked the desired resolution. This resulted in poor spacing between test points in the output charts. This was addressed by the addition of a better servo regulator in the follow-on testing. The better servo regulator was able to set the velocity to within +/- 0.1 m/s.

5.2 Component Testing

The components of the test station routine were also tested individually, specifically the velocity calculation, the mass flow calculation, and the angle measurements.

5.2.1 Velocity Calculation

The test station velocity calculation was compared to the time of flight measurement performed by the 3DP Alpha machine. The Alpha machine calculation is based on charging the droplet stream with a sinusoidal signal with wavelength equal to the flight distance of the droplets. The location of the drop

at the powderbed is recorded by an optical sensor and converted to an electrical signal. The difference in the amplitude of the signal at breakoff and at the powderbed level is converted into a time of flight:

$$TOF = (1/freq)*(\varphi-\varphi_0)/2\pi \quad [5]$$

The Alpha Machine measurement is taken over a distance of 0.96 inches. The same jet was used in the Alpha machine and the nozzle test station. In both instances the flowrate was adjusted to 1.31 g/min.

In order to compare the nozzle test station velocity measurement to the Alpha machine time of flight measurement the velocity measurement was converted to an equivalent time of flight. This was done by converting from meters/second to inches/second, and then dividing the Alpha machine's flight distance by this velocity. The velocity was measured starting .025 in. from breakoff and was measured over 0.050 in. (ten drops, the same method used throughout the testing described here). The results were:

	Alpha Machine TOF(msec)	Nozzle Test Station TOF (msec)
Results:	2.50	2.60

This confirmed that the velocity measurement routine produces reasonable results.

5.2.2 Flowrate Calculation

The flowrate calculation of the test station was checked with manual measurements of the flowrate under a variety of conditions. Figure 29 shows the results of the testing. The difference between the test station flowrate and the hand measured flowrate was less than 3% for these six measurements.

Figure 29 : Flowrate Testing

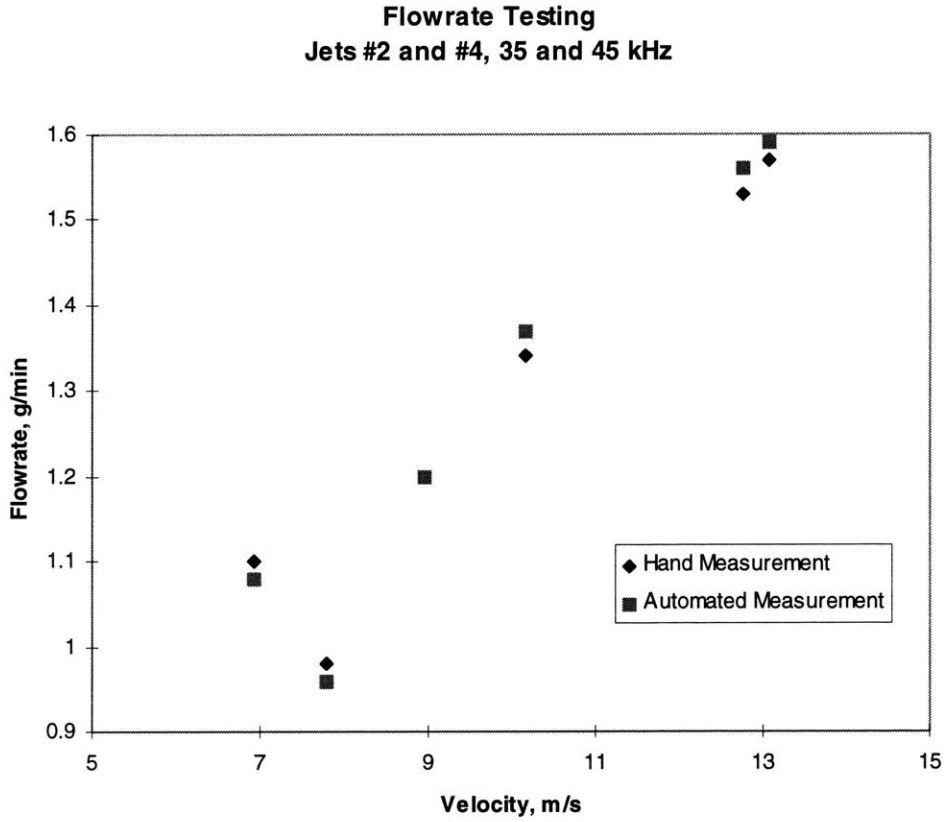

5.2.3 Angle Measurement

The angle measurements were tested three ways. First, the automated X-Y angle measurement was compared against a manual estimate of the angle based on the image output. This confirmed that the X-Y angle algorithm was functioning properly.

Next, the autofocus routine which provides the Z-axis data for the X-Z (or X-Focus) axis angle calculation was tested for repeatability. The routine was tested near breakoff and 0.8 in. from breakoff at high magnification with the iris

fully open, with 10 repetitions. This produced a repeatability of +/- 5 motor counts in focus position, which translates to +/- 0.04°.

Finally, the repeatability of the measurement was tested by taking the same angle measurement ten times. The X-Y angle measurement had a standard deviation of 0.03°, while the X-Focus angle measurement had a standard deviation of 0.04°. Note that this test was conducted with the same pixel/count calibration factor and LED delay for all datapoints, so it provides a measure of the random error associated with the measurement. Also, in order to minimize random droplet motion the ruby orifice of the nozzle was cleaned just prior to use. This is discussed in greater depth in section 6.6.1.

5.3 Testing Improvements

After the initial series of test were complete, several minor modifications were made to the software, primarily to correct inconsistency of the Breakoff Margin measurement. In order to verify that the measurement had been corrected, and also to prove that the changes did not adversely affect the original software, a series of four back to back test were done using nozzle #8 jetting water at 45 kHz.

Also, in the additional testing, a pressure regulating servo with a finer pressure resolution was used, and the velocity tolerance was reduced to +/- 0.1 m/s. This is evident in the output plots, because the five velocity points in each graph are much more consistently spaced than in the initial testing, where a velocity tolerance of 0.2 m/s was used.

6. Error Analysis

6.1 Overview

There are three major functions of the test stand: measurement of jet characteristics, detection and classification of satellites, and mapping of the nozzle operating boundary. This chapter presents the random and systematic error present in the measurements of breakoff length, droplet velocity, flowrate, and jet angle.

6.2 Calibrations

In order to measure a dimension of an object visually, there has to be some calibration between the image and a known length scale. In this test stand, there are two calibrations. The first is the calibration of motor position (in counts) to inches. The second is the calibration of image pixels to motor counts.

6.2.1 Inch/Count Conversion Factor

The number of inches per motor counts is a fixed quantity and remains constant regardless of the settings of the test stand. It changes only as the stepper motor and motion stages wear. This calibration factor can be determined theoretically and experimentally. Theoretically, the motor is stepping at 2000 counts per revolution and the lead screw in the motion table has a pitch of 5 mm. This yields a conversion factor of 9.8425×10^{-5} in/count. Assuming that the motor does not lose any counts even though it is driven in an open loop mode, then the only error would be in the lead screw and bearings of the table. This is a precision screw, and the table has a quoted straight line tolerances of $+/- 4.3 \times 10^{-4}$ in. over the 2 in. travel of the table, with repeatability of $+/- 7.8 \times 10^{-5}$ in.

In order to verify this conversion factor experimentally, the distance which the stage moved when the motor was advanced 10000 counts (approximately 1.0 in. linear motion) was measured with digital calipers. The measured conversion factor was calculated as $9.835X10^{-5}$ in/pix. The min caliper resolution is $5X10^{-5}$, and all of this leads to an error in the experimental measurement of:

calibration error = motion stage move tolerance + measurement tolerance =

$$2*4.3X10^{-4} + 5X10^{-5} = 9.1X10^{-4}$$

This measurement was taken over 1.0 in., so the effect on the conversion factor of inches/count is:

error in conversion factor = calibration error / measurement size =

$$9.1X10^{-4}/1.0 = 0.09\%$$

So, the experimental conversion factor is 9.84 +/- .01 $X10^{-5}$ in/pixel, which agrees with the theoretical value. Since the precision screws are more accurate than the calipers, the theoretical value is used in the software.

6.2.2 Pixel/Inch Conversion Factor

The other calibration, image pixels per count, varies depending upon the level of camera zoom. During the initialization of the motion stages at startup, this conversion factor is measured for three levels of zoom: low, medium , and high. Low is approximately 2X magnification at the CCD, and corresponds to 0 motor counts on the zoom motor. Medium is zoomed in 4000 counts on the zoom motor, about 10X at the CCD. High is 8000 counts on the zoom motor, around 20X at the CCD.

The pixel/in conversion factor calibration is determined by finding an edge in the image, determining its location in pixels, moving the stage a given number of

Figure 30: Pixel/Inch Calibration Illustration

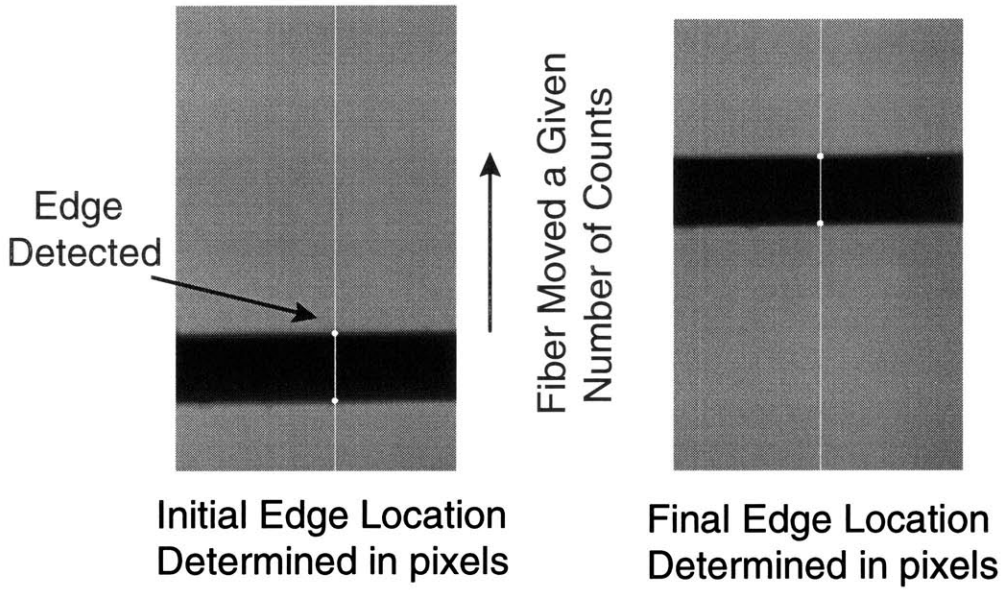

motor counts, and finding the location in pixels of the edge again. The difference in location in pixels divided by the size of the move in motor counts yields the conversion factor. This is shown in figure 30. As long as the motor does not "lose" a count as it moves, the error arises in the edge finding routine.

The calibration is done over a 60 count move (in the worst case), and the uncertainty in each edge detection is +/- 1 pixel. The error is:

pixel/count uncertainty = 2*1pixels/60 counts = +/- 3.3%.

Because this calibration factor is an order of magnitude worse than the in/count calibration for the motor, it is a major source of error in the following calculations.

6.2.3 Nozzle Zoom Recalibration

For the initial calibration of the pixel/inch factor, zoom level is set to zero manually, in response to a prompt from the software. The pixel/inch calibration is then carried out as described above. For long duration testing it is prudent to periodically recalibrate the inch/pixel factor by re-zeroing the zoom and running the calibration algorithm again.

The zoom axis has no limit switch. To ensure that the zoom axis has indeed been re-zeroed, the zoom stepper motor is commanded to return to zero zoom, and then move 20 motor counts beyond zero zoom. This will cause the zoom axis to find the end of its travel.

6.2.4 Nozzle Holder Angle

One of the functions of the nozzle test station is to measure the angle of the jet. In order for this to be accurate the angle of the nozzle holder to the base plate must be measured. This angle can then be used to offset the measured jet angle to arrive at the true jet angle:

$$\text{Jet Angle} = \text{Measured Jet Angle} - \text{Holder Angle}$$

This angle was measured by placing a straight .062 in. diameter rod into the holder, and focusing on an edge of the rod at high magnification. The nozzle holder was then moved up to the end of the vertical stage's travel, and the edge of the rod was again focused on. The arctangent of the Y- and Z-axis moves divided by the X-axis move gave the holder angle in the Y-axis and Z-axis directions. These were 0.06° in the Y-axis and -1.05° in the Z-axis. Note that if the structure supporting the nozzle holder is altered in any way this calibration must to be repeated.

6.3 Measurement of Breakoff Length

The breakoff measurement, as described in section 4.3, uses both the pixels/count and in/count conversion factors to determine breakoff length. The pixels/count conversion is used to track the distance of the nozzle from the center of the image, and the distance of the jet breakoff from the center of the image. In the worst case, the pixel/count conversion factor would be applied over the entire jet breakoff length, which is 0.030 in. at a minimum. Note that generally the majority of the measurement involves only the in/count conversion factor and so has a much higher accuracy than this. This would yield a percentage error on the measurement equal to the percentage error on the pixel/count calibration factor that was found above, 6.6%. There is an additional complication to this, however.

During the operation of the software, an algorithm in the software adjusts the zoom level of the camera to ensure that the jet breakoff and two droplets are kept in the image. This is described in appendix B. By changing the zoom level, the pixel/count calibration is also changed. Rather than re-measure this every time the camera zoom is changed a small amount, a derivative of pixel/count calibration as a function of zoom is used to adjust the calibration:

new pixel/count calibration factor = old factor + (derivative of pixel/count factor with zoom level)*(zoom change in counts)

The derivative was taken from a plot of pixel/count calibration factor vs zoom level in motor counts presented in appendix C. This introduces additional error into the calibration factor, the level of which depends upon how much the zoom is changed from the original level. Also presented in the appendix is an estimate of the maximum error introduced by this process. The addition error introduced by this process is 1.5% of the value of the pixel/count calibration factor. This

combines with the previously discussed calibration factor error by the root sum of squares method to yield the overall breakoff measurement error:

Overall breakoff length error^2 = (pixel/count calibration error)^2 + (error due to zoom change)^2

Overall breakoff length error = $(.066^2 + .015^2)^{0.5}$ = 6.8%

For a jet to be acceptable it must breakoff within the charging cell which extends from 0.020 in. to 0.100 in. below the nozzle. This software declares any jet between 0.030 in. and 0.090 in. in length at breakoff to be acceptable. Thus, this calculation needs to be accurate to at least +/- 10%; the +/- 6.8% error on breakoff length calculated above achieves this. Note again that this is a very conservative estimate of the error.

6.4 Velocity Measurement

This also relies on both conversion factors; the pix/count factor is used to center the drops and the in/count factor is used to measure the distance from the first drop to the tenth drop. However, the effect of the pix/count factor is reduced because once the droplet has been centered initially, the process is repeated to reduce the error in the drop centering (as explained in section 4.4.2). The maximum error that the pix/count factor could contribute is:

droplet centering error = move size*(pixel/count calibration error in percent)^2

= 0.018 inch*$(0.033)^2$ = 0.00002 inches

The exponent of 2 on the pixel/count calibration error is due to the recentering of the droplet. The error introduced by the in/count calibration is (for an estimate of 10 drop spacings = 0.100 inches):

in/count error = measurement distance * in/count factor error in percent
= 0.100 in*0.001 = 0.0001 in

The total error is:

Velocity Error (%) = [2*(droplet centering error) + in/count error) / distance
= [2*(.00002 in) + 0.0001 in]/ 0.100 in = 0.0014 = 0.14%

Note that the coefficient of 2 before the droplet centering error is required because the error applies to the droplet centering done at each end of the measurement. A mentioned in section 4.5, the droplet velocity depends upon the distance from the nozzle where the measurement is taken. This is due to the effects of drag on the droplet as it travels away from the nozzle. This effect produced up to a 5% difference over the travel of the motion stage (1.5 inches). Since the velocity routine counts down five droplets from breakoff before it begins its measurement, there is no guarantee that the measurement is always starting at the same distance from the nozzle as the breakoff distance varies. However, experience indicates that at most this effect is limited to 1-2% of the measurement.

Finally, near breakoff the droplets tend to have fairly non-round shapes for a few droplet spacings, before becoming spherical. The effect of this on the velocity measurement was investigated by varying the LED phase delay and repeatedly running the velocity measurement. The standard deviation of the ten sample test with a varied LED phase delay was 0.022 m/s, compared to 0.0084 m/s with a constant LED phase delay. While this indicates that there is an effect due to the droplet shape, it is not large enough to impact the accuracy of the results.

6.5 Flowrate Measurement

This calculation relies completely on the pixel/count and inch/pixel conversion factors, and is impacted by distortion of the droplet's diameter in the processing software.

First, the 3.3 % uncertainty of the pixel/count and the 0.1% uncertainty of the in/pixel factor combine by the root sum of squares method to give an uncertainty of 3.3 % on the measurement of the droplet diameters. Since the diameter measurement is cubed to get the volume, the volume has an uncertainty due to the calibrations of +/- 10%.

The measurement suffers from distortion of the droplet size in the processing software. Since the droplet is an image it does not have an absolute edge, but rather a sharp increase in pixel intensities, as was shown in section 2.4.1. Section 2.4.2 presented the result that varying the threshold intensity of the image can change the droplet diameter by as much as 40%. This error due to threshold intensity value is fairly consistent, allowing the use of an adjustment factor (the "Fudge Factor") of 0.955 on the measured droplet diameter to account for the distortion. This reduces the calculated mass flow rate by 13%. Despite these issues, this measurement has shown good agreement with hand measured flow rates, as shown in section 5.2.2.

6.6 Measurement of Jet Angle

This measurement is composed of two pieces - the X-Y angle calculation, and the X-Z (focus) angle calculation. The calculation is done over 0.8 inches in the X axis direction.

The Y-axis measurement is affected by the pixel/count calibration in the same manner as the velocity measurement, because the same repeated centering routine is used (see section 4.4.2 for an explanation of this routine and its impact on droplet centering error). This yields the following error:

$$\text{Y-axis error} = \tan^{-1}[2*\text{drop move size}*(\text{pixel/count calibration error in percent})^2/\text{measurement distance}]$$

$$\text{Y-axis error} = \tan^{-1}[2*0.018 \text{ in} * (0.033)^2 / 0.8 \text{ in}]$$
$$= +/- 0.003°$$

This seems a bit on the optimistic side, given the standard deviation in the measurement of 0.03° for a ten measurement sample as described in section 5.2.3. This is due to random droplet motion, which will be discussed in section 6.6.1.

The Z-axis (focus) measurement error is driven by the accuracy of the autofocus routine. This is accurate to +/- 0.0006 inches at high magnification; this is multiplied by two since each end of the stream must be focused for the measurement.

$$\text{Z-axis error} = \tan^{-1}[2*\text{focus error /measurement distance}]$$

$$\text{Y-axis error} = \tan^{-1}[2*0.0006 \text{ inches} / 0.8 \text{ in}]$$
$$= +/- 0.086°$$

This is in good agreement with the results of section 5.3 which showed a standard deviation of this measurement to be .04° over a ten measurement sample.

6.6.1 Random Droplet Motion

The accuracy and repeatability of the angle measurements, especially the X-Y angle measurement are hindered by the fact that far from the nozzle (in the case

of this testing 0.8 in.), the droplets are not stable in space. Random droplet motion was observed at high magnification, with motion up to .002 inches normal to the stream; this corresponds to an angle of 0.1º

The worst droplet motion was seen with a nozzle which had acrysol buildup around the orifice. This jet was also running at fairly low flowrate – 1.15 g/min of water. This was observed under a microscope. The nozzle was cleaned, and the binder pressure was increased to produce a flowrate of 2.1 g/min. This reduced the random droplet motion to less than .001 inches at 0.8 inches from the nozzle, or less than .07º. The series of ten angle measurements was repeated, and the X-Y standard deviation was 0.03º, while the X-Focus angle was 0.04º . This indicates that the random droplet motion is really driving the error in the angle measurements, and that every effort must be made to minimize this phenomenon.

7. Discussion

7.1 Results

The nozzle test station has been proven accurate and reliable over a variety of nozzles, binders, and operating conditions. The demonstrated level of accuracy of the various measurements is adequate for the purpose of characterizing nozzles for the 3DP printhead.

The point of the nozzle test station's characterization of nozzles is to enable the construction of printheads with up to 96 nozzles. This will dramatically increase the part build rate, bringing Three Dimensional Printing closer to being a production process. In this 96 nozzle printhead the binder pressure would be constant for all of the nozzles, and would be set to produce an average V_R for all of the nozzles. Each nozzle would be driven with the same piezo signal frequency, but with a variable piezo signal amplitude.

It is assumed that for a given pressure any nominally identical nozzle would produce a velocity within 10% of the population mean. That is why the nozzle test station tests each nozzle at +/- 10% V_R. If the nozzle passes the test station then it will run acceptably on the printhead with the common nozzle binder pressure set to produce the average V_R.

The nozzle test station also provides information about how much margin in breakoff distance exists between the piezo amplitude boundaries. This margin can be used to change the breakoff phase so that all jets are running at the same relative breakoff phase angle, to simplify the electronics of the system.

The fact that small satellites appeared near the overdriven jet condition and were not detected by the test station is interesting, but did not prove to be a problem.

The satellites were not detected by the test station because their pixel intensity is below the threshold intensity used to turn the greyscale image into a binary image. That threshold could be lowered to capture these satellites, but this would risk capturing background noise in the image as well.

These satellites were seen at the onset of the overdriven jet condition, and forward merged within a drop spacing of breakoff. It is not felt that these satellites are a problem because they will not impact the operation of the printhead.

The PAA binder used in the nozzle testing for this work was of the same concentration as binder successfully used for printing in the 3DP Alpha machine. Earlier testing with a higher concentration PAA binder produced intermittent satellites, which cannot be detected by the test station. These intermittent satellites appeared as a faint streak between the end of the fluid stream and the first droplet, and were only detected by the buildup they produced during printing. If the PAA concentration is increased, or another binder with intermittent satellites is introduced, then the check described in section 2.2.1 is relied upon to detect the satellites.

The result presented in section 6.6.1, that droplets can wander as much as .002 inch perpendicular to the stream at 1.0 inch from the nozzle is important. This results in an angle change of 0.1°. On the alpha machine droplet motion perpendicular to the jet is an order of magnitude less than this. The reason is the condition of the individual nozzle's ruby orifice. The nozzle which produced the large droplet lateral motion had been used with all four binder, and there was considerable buildup on the face of the ruby around the orifice. When this debris was removed, the droplet motion was reduced by roughly 50%.

In addition, a nozzle was taken directly from the alpha machine and was set up in the nozzle test station and observed; the lateral droplet motion from this nozzle

was .0002 in., or 0.01°, an order of magnitude better than the previous nozzle. It points out that attempting to measure the jet angle to +/- 0.1° is not possible unless the ruby orifice is in a good condition.

7.2 Possible Improvements

7.2.1 Time Per Test

Each time the nozzle test station is used to characterize a nozzle at a given frequency, it takes approximately 25 minutes to complete the testing. For an eight nozzle printhead segment, this would mean a 4 hour test . While the testing is automated, this is still a significant amount of time. The time per test is roughly split between setting the desired velocity and performing measurements. In order to reduce the amount of time per test the number of velocity points used could be reduced from five to three, at V_R, V_R +/- 10%. This is supported by the testing already completed, because the piezo boundaries were all fairly monotonic in nature. This would reduce the time per test by about 8 minutes.

8. References

[1] Brancazio, David, "Development of a Robust Electrostatically Deflecting Printhead for Three Dimensional Printing", MIT, Master's Thesis, May 1991

[2] Chijioke, Akobuije, "The Design and Construction of an Observation-Oriented Three Dimensional Printing Machine", MIT, Master's Thesis, June 1998

[3] Curodeau, Alain, "Three Dimensional Printing of Ceramic Molds with Accurate Surface Macro-Textures for Investment Casting of Orthopaedic Implants", MIT, PHD Thesis, September, 1995

[4] Heinzl, J., and Hertz, C.H., "Ink Jet Printing", Advances in Electronics and Electron Physics, vol. 65, pp 133-135

[5] Sachs, E., Brancazio, D., Milner, J., Serdy, J., Curodeau, A., Bredt, J., "High Rate, High Quality 3D Printing through Machine Design, On-line Measurement, and Control", Internal Journal of Machine Tools & Manufacturing

[6] Shutts, Christopher, "Development of a Reliable Electrostatic Multijet Printhead for Three Dimensional Printing", MIT, Master's Thesis, May 1995

Appendix A: Autofocus Routine

The autofocus routine uses the LABView image processing routines and the focus axis stage to focus the CCD lens on an object in the image. This is needed because the jet can be angled toward or away from the camera, and as the nozzle is moved up or down the droplets in the image go out of focus. In fact, comparing these focus points at extreme ends of the jet is used as a way to measure jet straightness.

First, the image is analyzed and a droplet is chosen for the routine to focus on. The maximum contrast at the edge of the droplet is measured (as described in section 2.4.1), and the camera position on the focus axis is varied by a specific step size. The edge contrast of the droplet is again measured, and if it has increased the camera takes another step in that direction. If the contrast has decreased, then the camera takes a step in the opposite direction. From this point on whenever the contrast decreases the camera steps backward 70% of the previous step size. This continues until the step becomes smaller than a specified size. At this point the image is considered focused.

Figure 31 : Focus Algorithm Figure

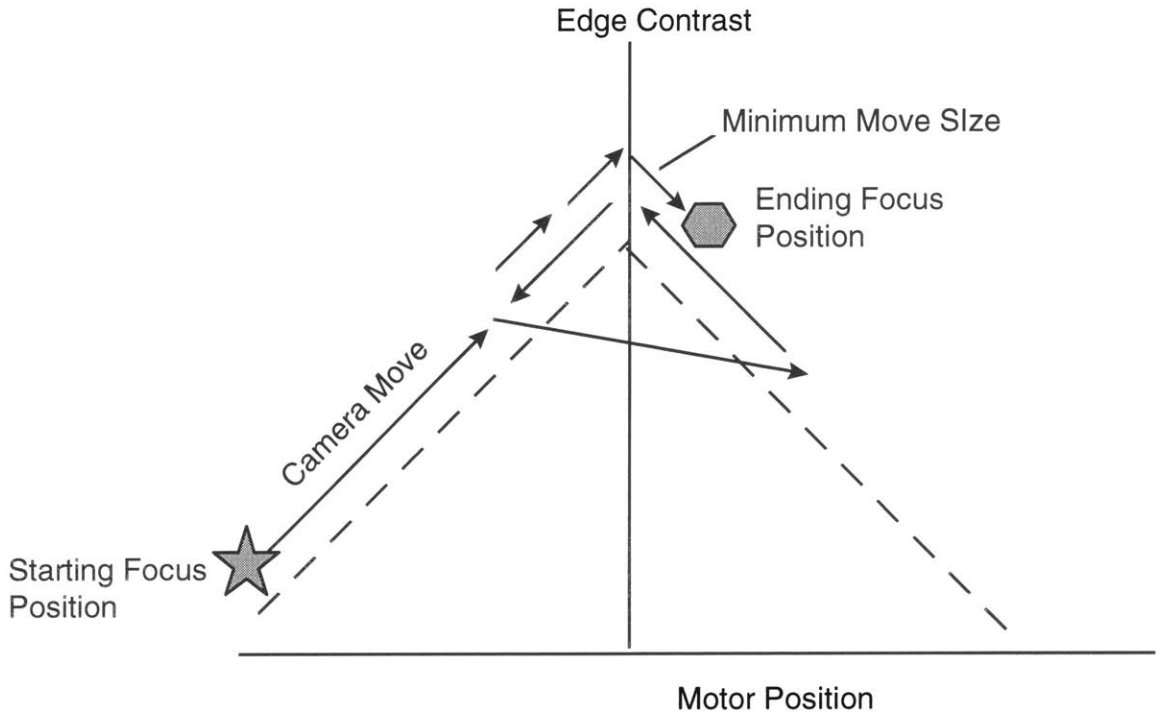

This routine does not rely on any absolute contrast levels or previous knowledge of the rate of change of contrast with step size in order to focus. All it requires is an initial step size and a minimum step size, and that there be an object in its view. This flexibility allows it to focus over a wider range of magnifications. The maximum edge contrast of an object varies with magnification and lighting, so that a routine which was calibrated to contrast would have to be recalibrated at each different zoom setting.

There are two subtleties in this routine. The first is that if an object is too far out of focus then its edge contrast is too low to be detected and the autofocus routine will not function properly. This is avoided by never letting an image get too far out of focus. For instance, when increasing magnification from low to high the zoom should be halted at medium magnification to allow refocusing before

zooming to high magnification and focusing again. If the lens is simply zoomed all the way in one step, the image may be too blurry to focus automatically.

The second subtlety involves how the autofocus routine finds the maximum edge contrast of the droplet. The software draws a line through the droplet and examines the intensity of the pixels along the line. The maximum derivative of intensity along the line is called the contrast. The location on the droplet where this line is drawn is important. Ideally, the line would be drawn directly through the center of the drop, where it would be perpendicular to the droplet edges and get the sharpest pixel intensity derivative. However, light is transmitted through the center of the drop, creating two bogus edges at the edges of the transmitted light at the center of the drop. These bogus edges would not be a problem, except that they have a different contrast than the true edge of the drop, and may confuse the focusing algorithm. Therefore, it is important that the pixel intensity line be drawn so that it avoids this transmitted light.

Figure 32 : Strategy to Optimize Edge Contrast Measurement

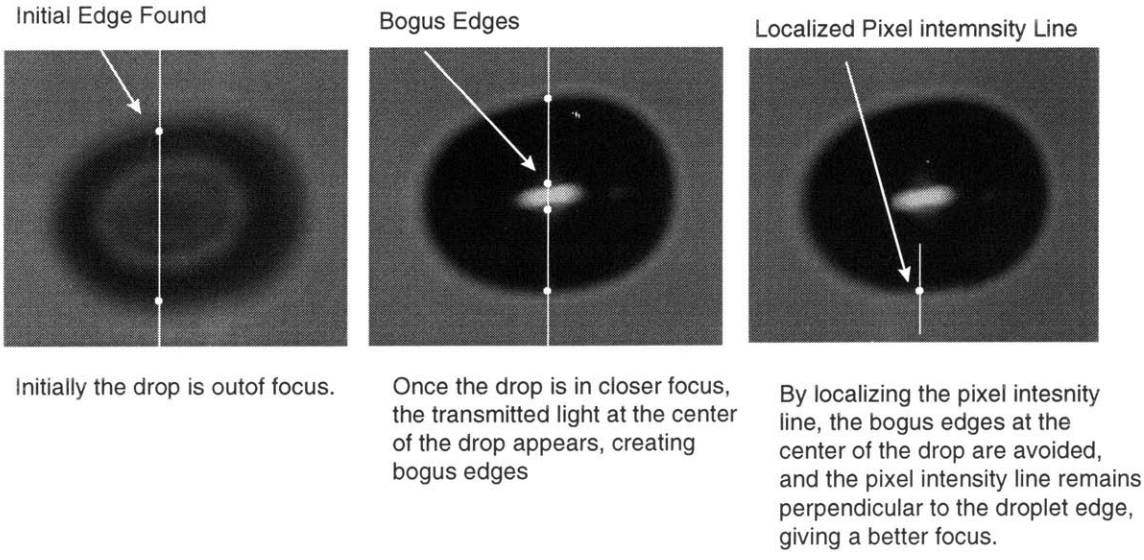

If the pixel intensity line is drawn just at the edge of the droplet, it can still be located perpendicular to the droplet edge and avoid the transmitted light, as

shown in figure 32. It is important that the pixel intensity line be perpendicular to the droplet edge, in order for it capture the sharpest change in pixel intensity at the droplet edge.

These details increased the accuracy of the autofocus routine at high magnification from +/- 20 motor counts (0.002 in.) in the Focus axis direction to +/- 6 motor counts (0.0006 in.). This reduced the uncertainty in the jet angle measurement from +/- 0.2° to +/- 0.086°.

Additionally, the autofocus routine was written so that it was robust to droplet motion in the frame during focusing. The angle measurement requires the largest separation in the X axis between the two droplets being used for the calculation. Droplets far downstream from the nozzle tend to exhibit a good deal of random motion (up to 0.002 in.), and so they move around the frame quite a bit. An enclosure was built to hold the test station and minimize the impact of external air currents, but the droplets are still very dynamic in nature. To minimize the impact of this on the autofocus measurement, the routine grabs a single image and performs all of its contrast measurements on that frame before moving the camera in the Z-axis during each iteration. Thus it doesn't really matter that the droplet bounces around. The routine is also robust to the cases where the droplet is partially off the screen - it can still find an edge and determine the optimum focal position.

Appendix B: Effect of Zoom Level on Pixel/Count Calibration

As the test station varies piezo amplitude and binder pressure, the size of the drops created and the distance between drops varies. In order to be able to maintain the same number of drops in the frame for the analysis, the system must vary the level of the camera's zoom. The relationship between the size of the nozzle movement which results from one motor count move and the size of a pixel in the frame is dependent upon zoom level. Therefore, if the zoom level is changed in order to track a given number of drops, then the calibration factor between pixels and motor counts will vary. A chart showing how the pixel/count calibration factor varies with zoom level is presented as figure 33 :

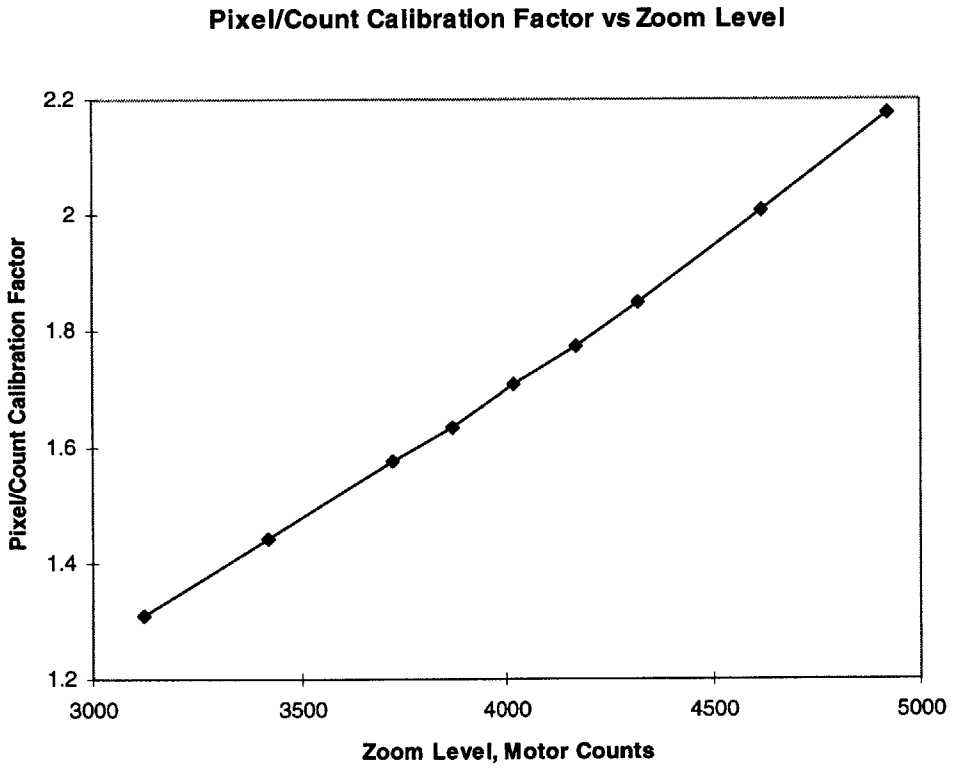

Figure 33 : Effect of Zoom Level on Pixel/Count Calibration Factor

Note that in figure 33 zero motor counts corresponds to zero zoom, 4000 motor counts corresponds to medium zoom, and 8000 motor counts corresponds to high magnification zoom.

There are three options to deal with this problem. The first is to do nothing, and to live with the error. If the zoom is adjusted as much as 900 counts (which was seen during testing) then this would lead to an error in the calibration factor of 30%, and in breakoff length of around 15% (depending upon the absolute length of the jet). This is not an acceptable error level.

Alternatively, the system could recalibrate at each new zoom level. This would eliminate the error, but would also increase the processing time per jet dramatically. Finally, a local derivative of the calibration factor with respect to zoom level could be used to estimate the change in calibration factor based on the change in zoom level. The fact that the curve of calibration factor vs zoom level is fairly straight makes this a viable alternative.

Change in calibration level = derivative * (zoom level change, in motor counts)

Based on the data presented in the above chart, the derivative was measured to be 0.00047 pixel/count/count. The maximum cumulative zoom move due to this process is 900 motor counts. Applying the derivative to this zoom move, an estimate of the maximum error possible in the calibration factor can be obtained:

Maximum zoom calibration change = maximum zoom move * derivative
= -900 motor counts * .00047 pixel/count/count = -0.42

Maximum error = original factor + calculated factor change - actual new value
= 1.71 - 0.42 - 1.31 = .02 pixel/count = 1.5%

Maximum error due to the estimation of the change in the pixel/count calibration factor is +/- 1.5%.

Another option to deal with this would be to have a look-up table containing the information in figure 33, rather than using a derivative to estimate the change in the pixel/count factor. In this case the only additional error in the pixel/count factor would arise from interpolation between datapoints. If increased accuracy becomes necessary in the breakoff measurement, look-up table method could be adopted.

Appendix C: BOA Nozzle Description

In order to demonstrate the robustness of the test stand, several different nozzles were tested under the same operating conditions. A nozzle consists of a piezoelectric crystal connected to a ruby orifice through a length of tubing. Standard nozzles have the piezo five inches from the ruby, which is swaged into a steel cylinder, as shown in the following figure. The steel cylinder is directly connected to the tubing. A bayonet style nozzle has the ruby swaged into a steel cylinder which fits onto a bayonet attached to the tubing. Both standard and bayonet style nozzles were used during the testing.

The length of tubing coupling the piezo to the ruby orifice was varied for the bayonet nozzles, with one nozzle set to five inches, the other to one inch. The type of piezo used in the testing was also varied. A bayonet nozzle with a wrap around piezo was also tested.

Figure 34: Boa Nozzle Schematic

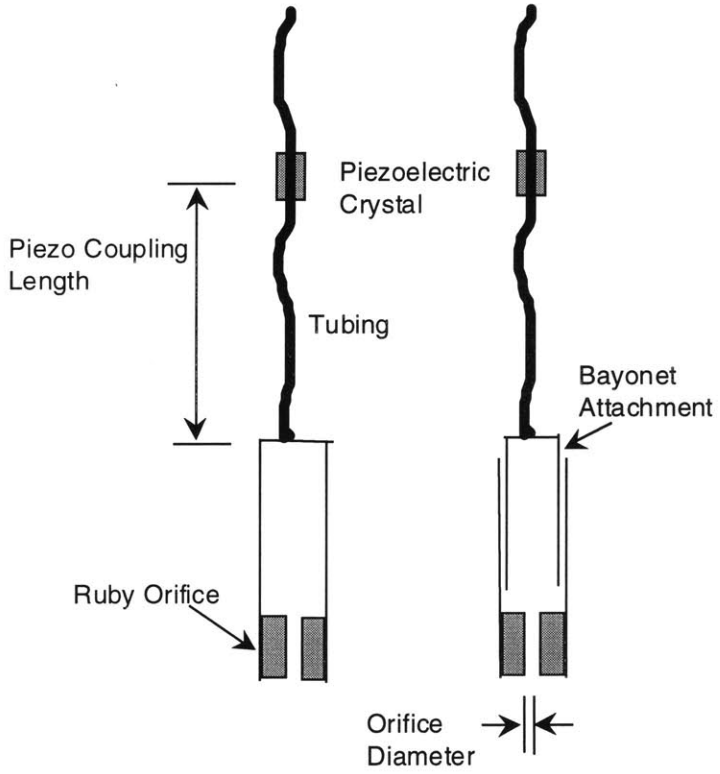

Appendix D: Software Flowcharts

Auto Focus Overview

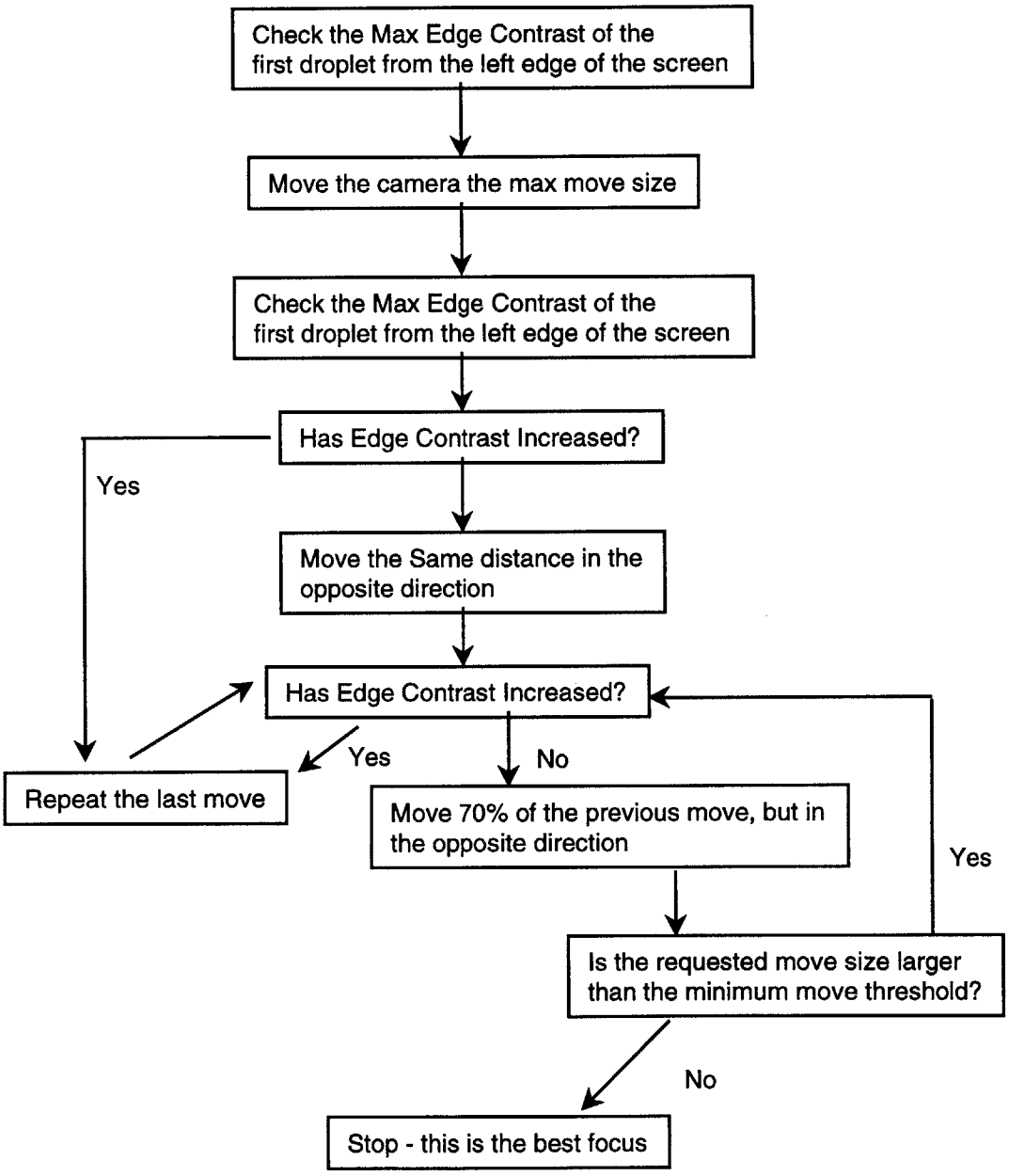

AWG CTL 2

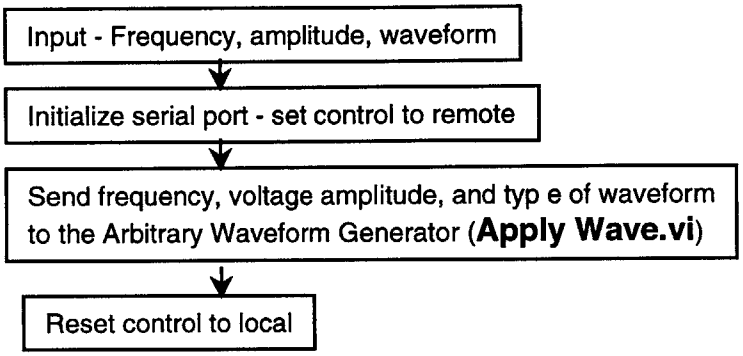

B/O Finder

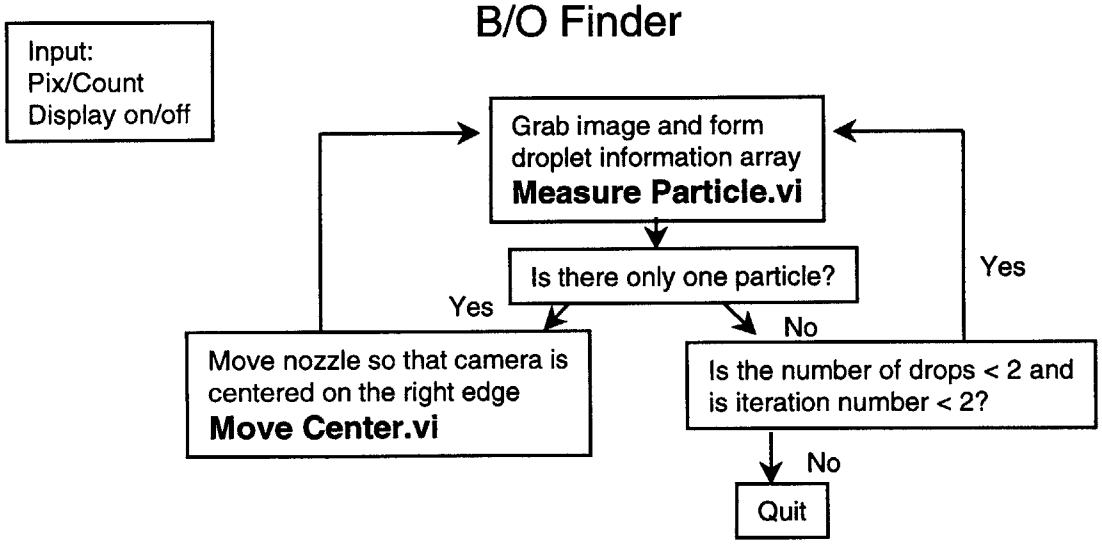

B/O Finder

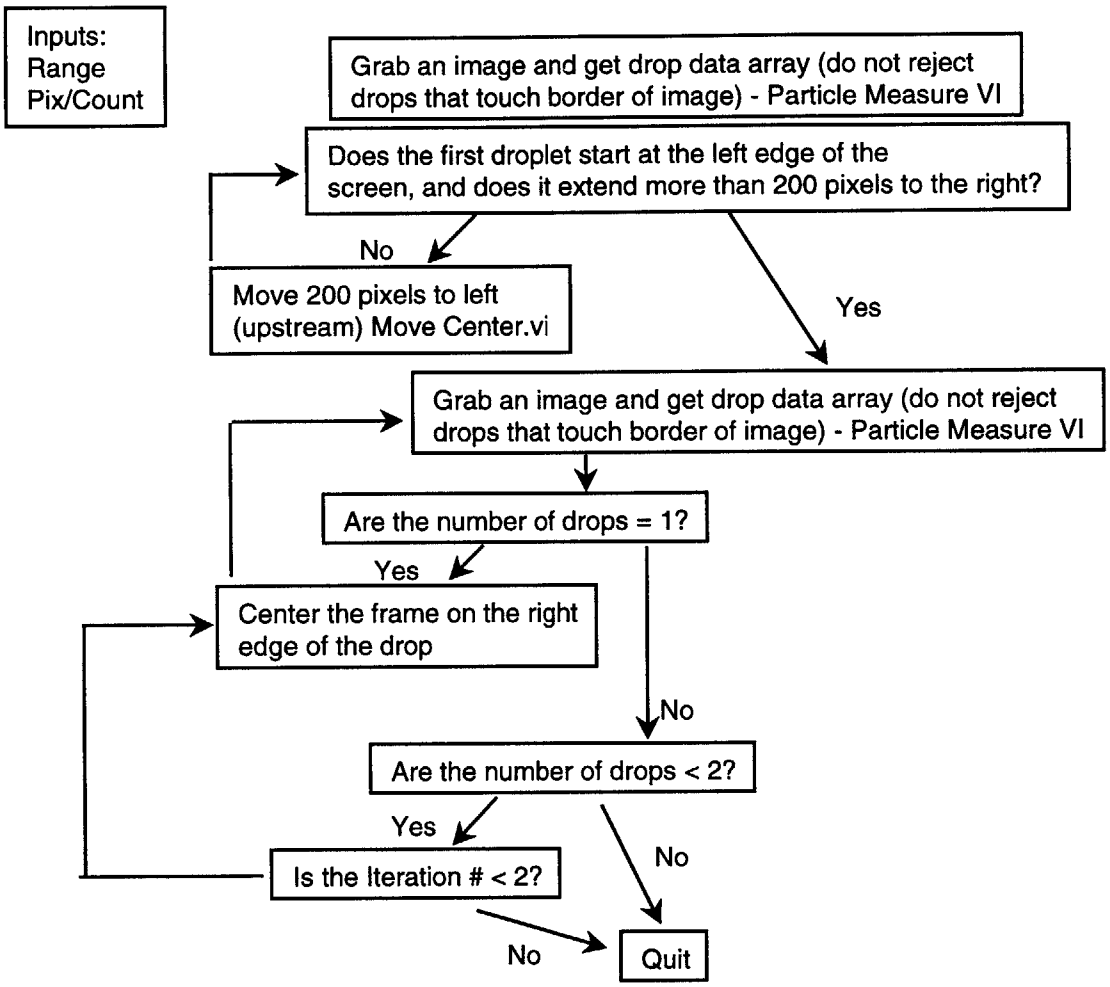
Inputs:
Range
Pix/Count
Grab an image and get drop data array (do not reject drops that touch border of image) - Particle Measure VI
Does the first droplet start at the left edge of the screen, and does it extend more than 200 pixels to the right?
No
Move 200 pixels to left (upstream) Move Center.vi
Yes
Grab an image and get drop data array (do not reject drops that touch border of image) - Particle Measure VI
Are the number of drops = 1?
Yes
Center the frame on the right edge of the drop
No
Are the number of drops < 2?
Yes
Is the Iteration # < 2?
No
No
Quit

B/O Subvi 3

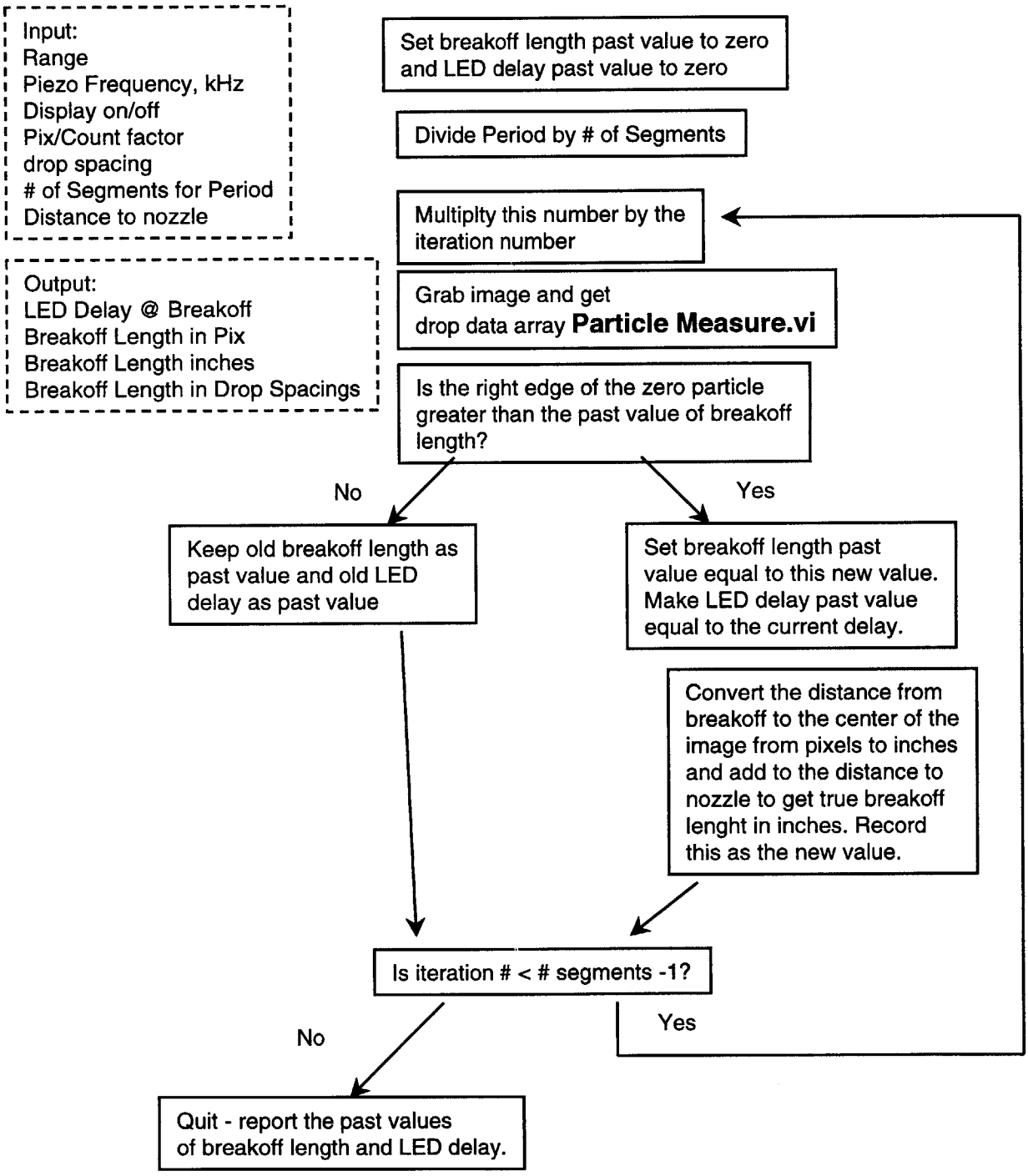
Input:
Range
Piezo Frequency, kHz
Display on/off
Pix/Count factor
drop spacing
# of Segments for Period
Distance to nozzle
Output:
LED Delay @ Breakoff
Breakoff Length in Pix
Breakoff Length inches
Breakoff Length in Drop Spacings
Set breakoff length past value to zero and LED delay past value to zero
Divide Period by # of Segments
Multiplty this number by the iteration number
Grab image and get drop data array Particle Measure.vi
Is the right edge of the zero particle greater than the past value of breakoff length?
No
Yes
Keep old breakoff length as past value and old LED delay as past value
Set breakoff length past value equal to this new value. Make LED delay past value equal to the current delay.
Convert the distance from breakoff to the center of the image from pixels to inches and add to the distance to nozzle to get true breakoff lenght in inches. Record this as the new value.
Is iteration # < # segments -1?
No
Yes
Quit - report the past values of breakoff length and LED delay.

B_O Tracker 2

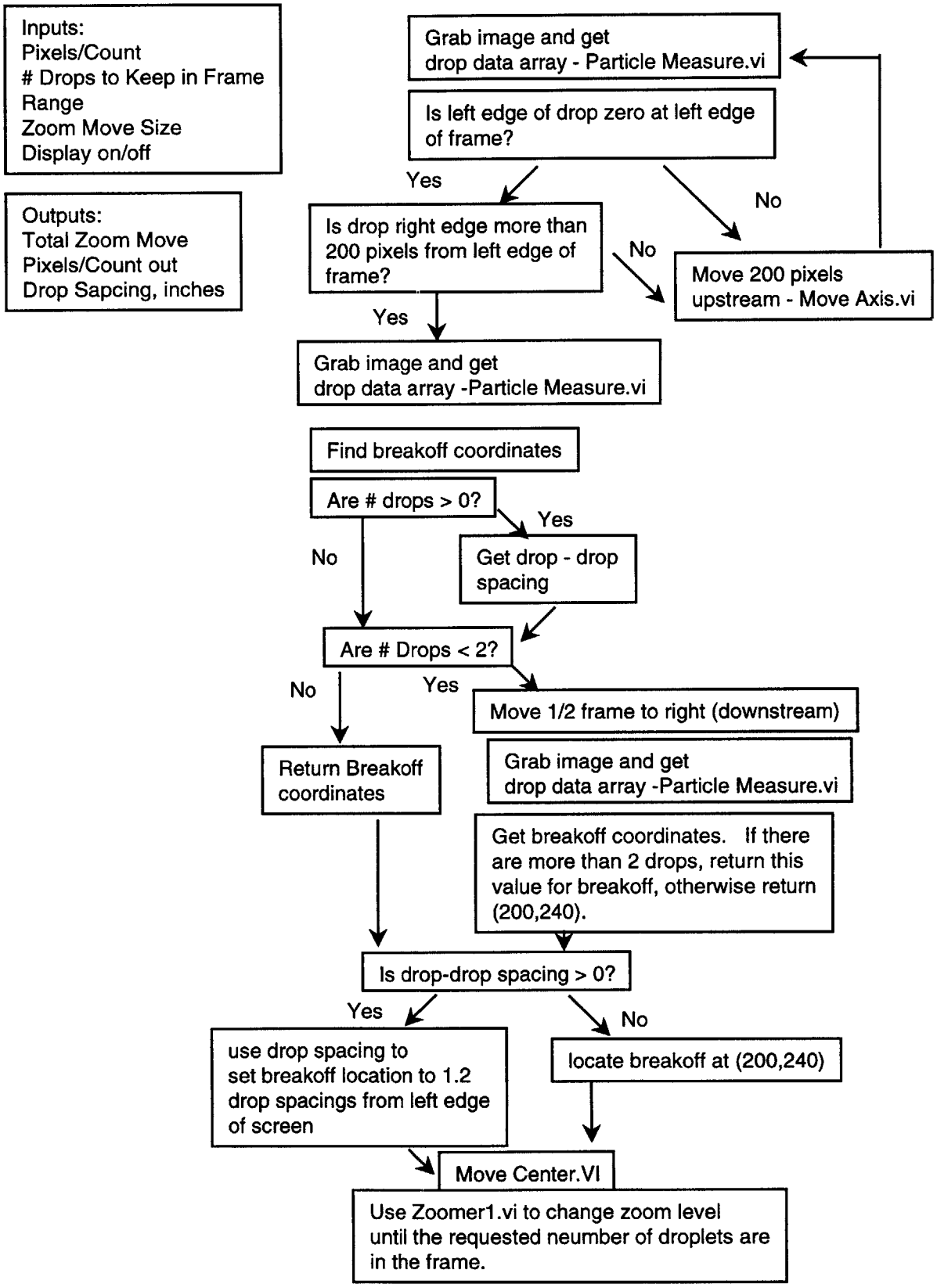
Inputs:
Pixels/Count
Drops to Keep in Frame Range
Zoom Move Size
Display on/off
Outputs:
Total Zoom Move Pixels/Count out
Drop Sapcing, inches
Grab image and get drop data array - Particle Measure.vi
Is left edge of drop zero at left edge of frame?
Yes
No
Is drop right edge more than 200 pixels from left edge of frame?
No
Move 200 pixels upstream - Move Axis.vi
Yes
Grab image and get drop data array -Particle Measure.vi
Find breakoff coordinates
Are # drops > 0?
Yes
No
Get drop - drop spacing
Are # Drops < 2?
No
Yes
Move 1/2 frame to right (downstream)
Return Breakoff coordinates
Grab image and get drop data array -Particle Measure.vi
Get breakoff coordinates. If there are more than 2 drops, return this value for breakoff, otherwise return (200,240).
Is drop-drop spacing > 0?
Yes
No
use drop spacing to set breakoff location to 1.2 drop spacings from left edge of screen
locate breakoff at (200,240)
Move Center.VI
Use Zoomer1.vi to change zoom level until the requested neumber of droplets are in the frame.

Boundary Finder

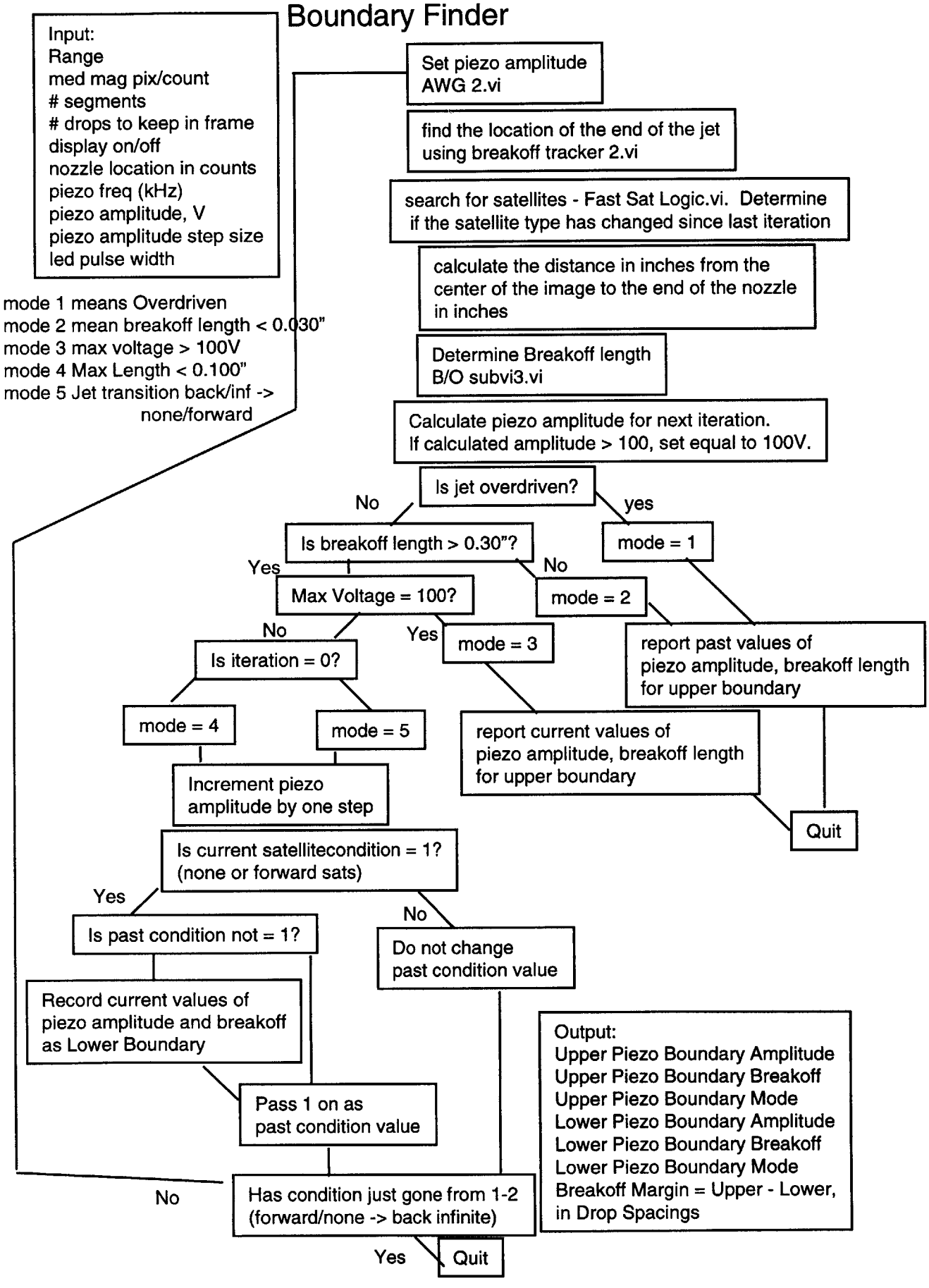

CD (Center Detect)

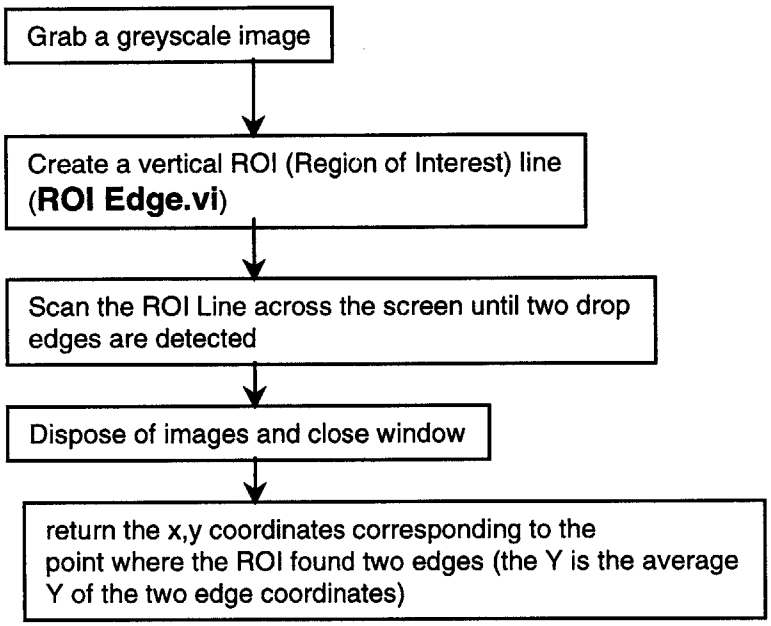

Drop Mover

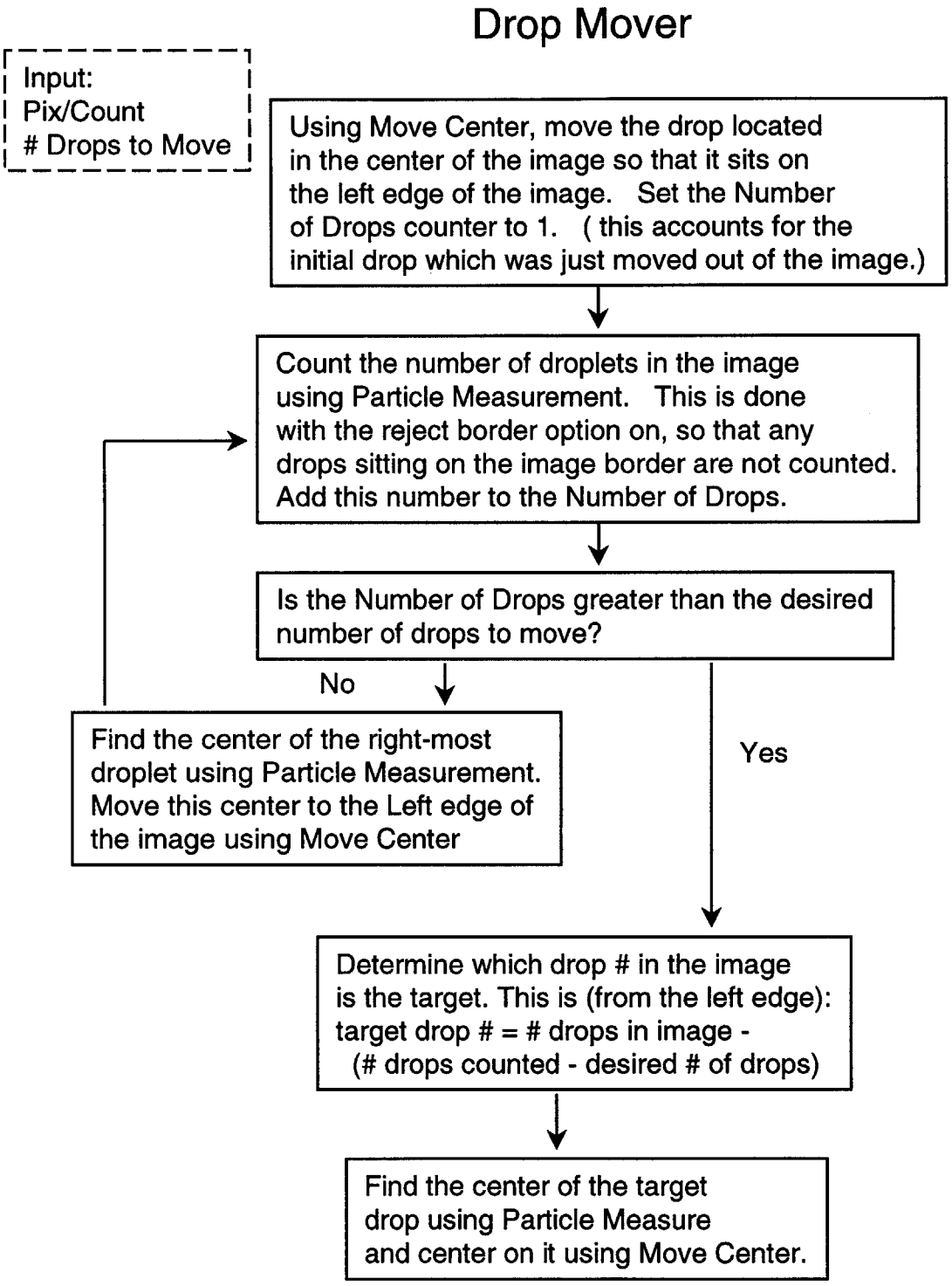
Input:
Pix/Count
Drops to Move
Using Move Center, move the drop located in the center of the image so that it sits on the left edge of the image. Set the Number of Drops counter to 1. (this accounts for the initial drop which was just moved out of the image.)
Count the number of droplets in the image using Particle Measurement. This is done with the reject border option on, so that any drops sitting on the image border are not counted. Add this number to the Number of Drops.
Is the Number of Drops greater than the desired number of drops to move?
No
Yes
Find the center of the right-most droplet using Particle Measurement. Move this center to the Left edge of the image using Move Center
Determine which drop # in the image is the target. This is (from the left edge):
target drop # = # drops in image -
(# drops counted - desired # of drops)
Find the center of the target drop using Particle Measure and center on it using Move Center.

Fast Focus 4

input:
Max move size
Min contrast to start focusing
Min contrast to stop focusing
display on/off
Threshold Move size
High sensitivity on/off

Grab droplet image and form droplet information array (**Particle Measure.vi**). Reject drops that touch the edge of the image.

Number of drops > 0?

No

Is high sensitivity on?

No

Draw vertical ROI thru center of 1st droplet

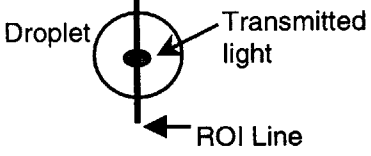

Yes

Is high sensitivity on?

Yes

Grab droplet image and form droplet information array (**Particle Measure.vi**). Include drops that touch the edge of the image.

Is the center of the first drop below the center of the screen? (Y-coord > 240?)

No

Draw ROI beginning .3*diameter below drop center, extending to 0.7*d below droplet center

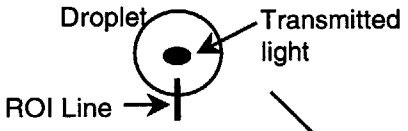

Yes

Draw ROI beginning .3*diameter above drop center, extending to 0.7*d above droplet center

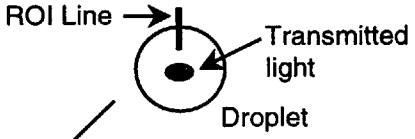

Yes

Draw vertical ROI thru center of 1st droplet

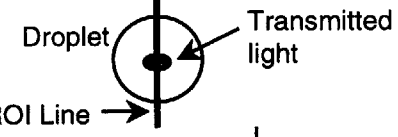

Find Droplet Edge Contrast
Find Thrsh.vi

Is contrast > min contrast to focus?

Yes

Quit

No

step size = Max move size

Move camera one step

Choose ROI placement as done above

Find Droplet Edge Contrast

Focus Move.vi

CONTINUED ON NEXT PAGE

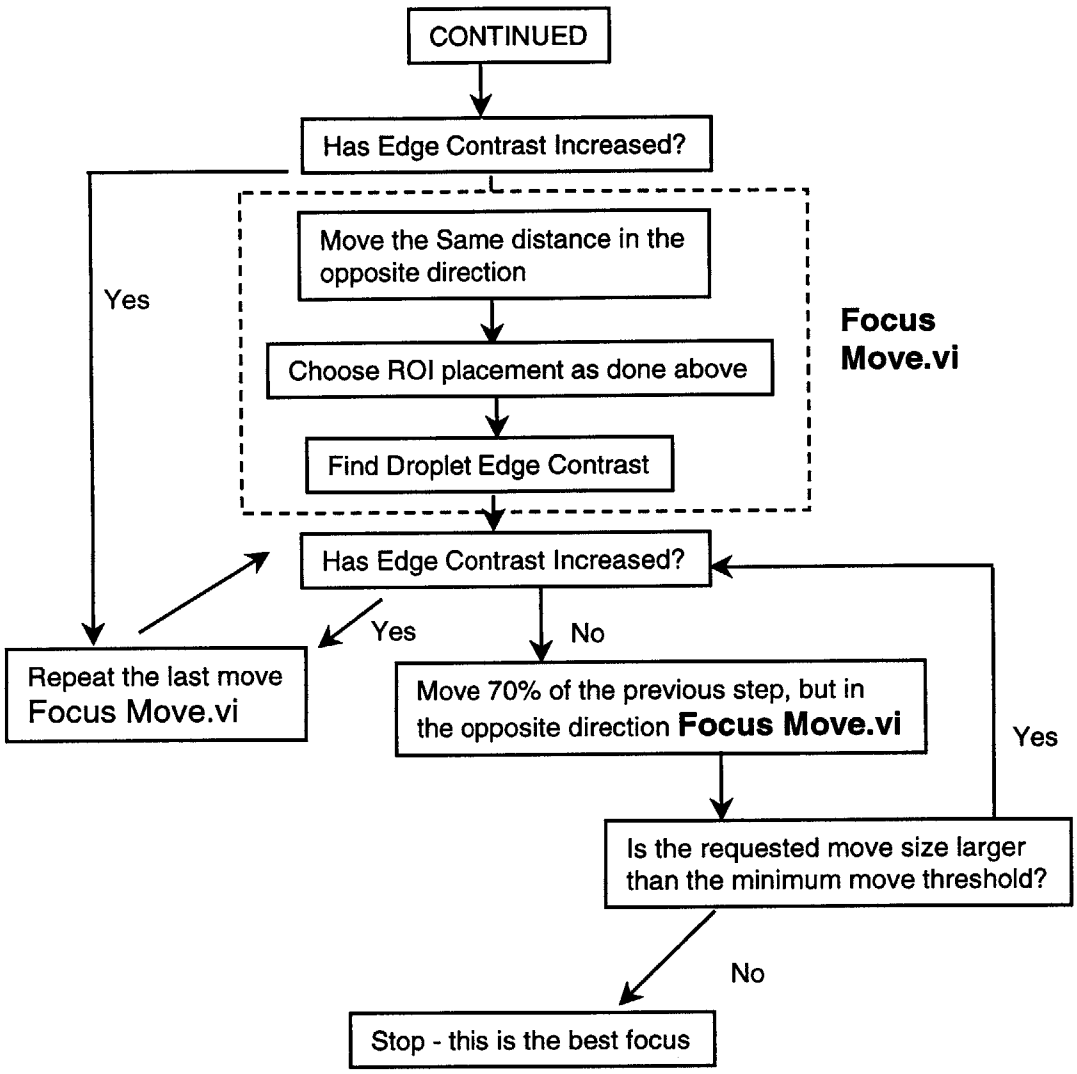
CONTINUED
Has Edge Contrast Increased?
Yes
Move the Same distance in the opposite direction
Choose ROI placement as done above
Find Droplet Edge Contrast
Focus Move.vi
Has Edge Contrast Increased?
Yes
No
Repeat the last move Focus Move.vi
Move 70% of the previous step, but in the opposite direction Focus Move.vi
Yes
Is the requested move size larger than the minimum move threshold?
No
Stop - this is the best focus

Fast Satellite Logic

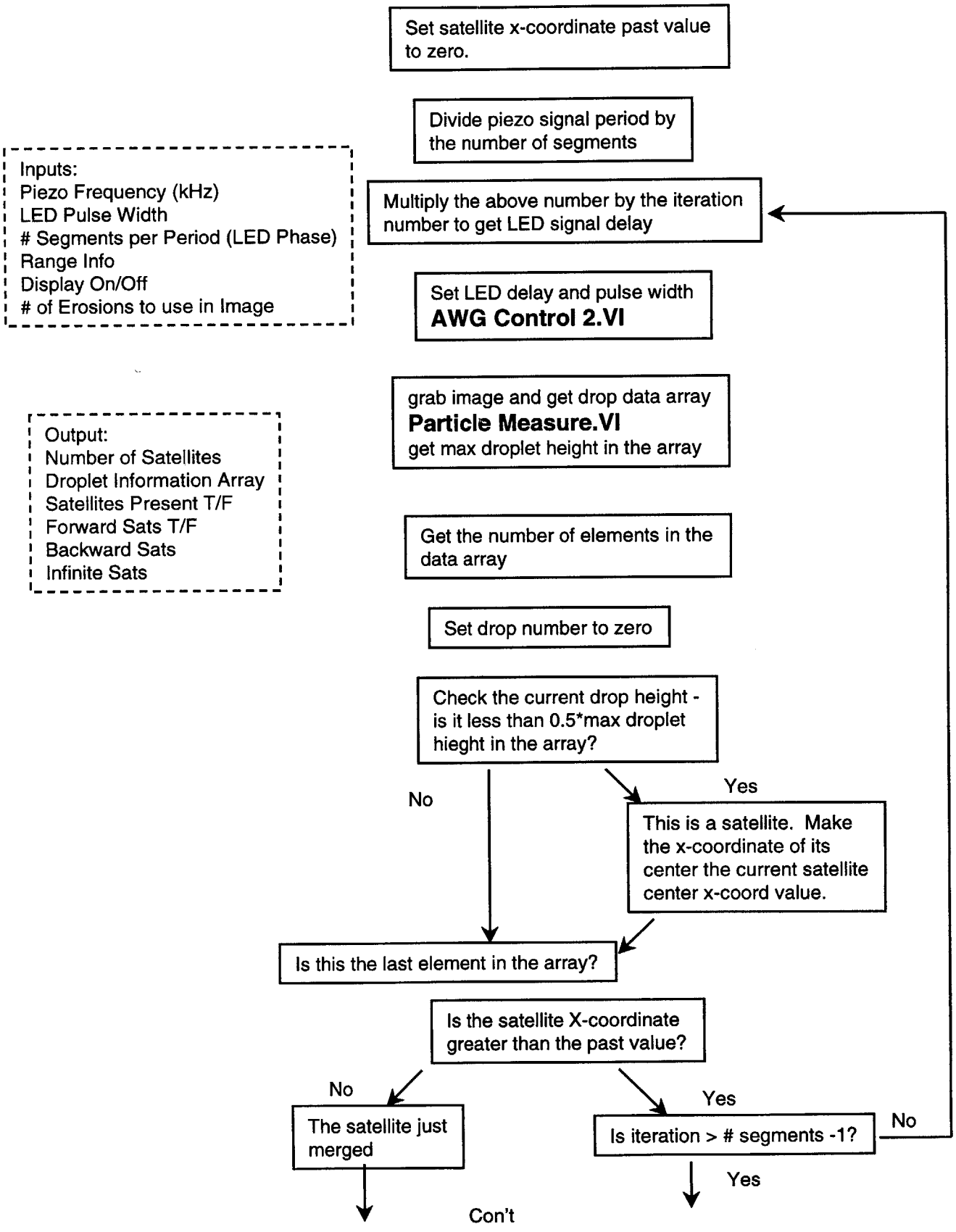

Con't

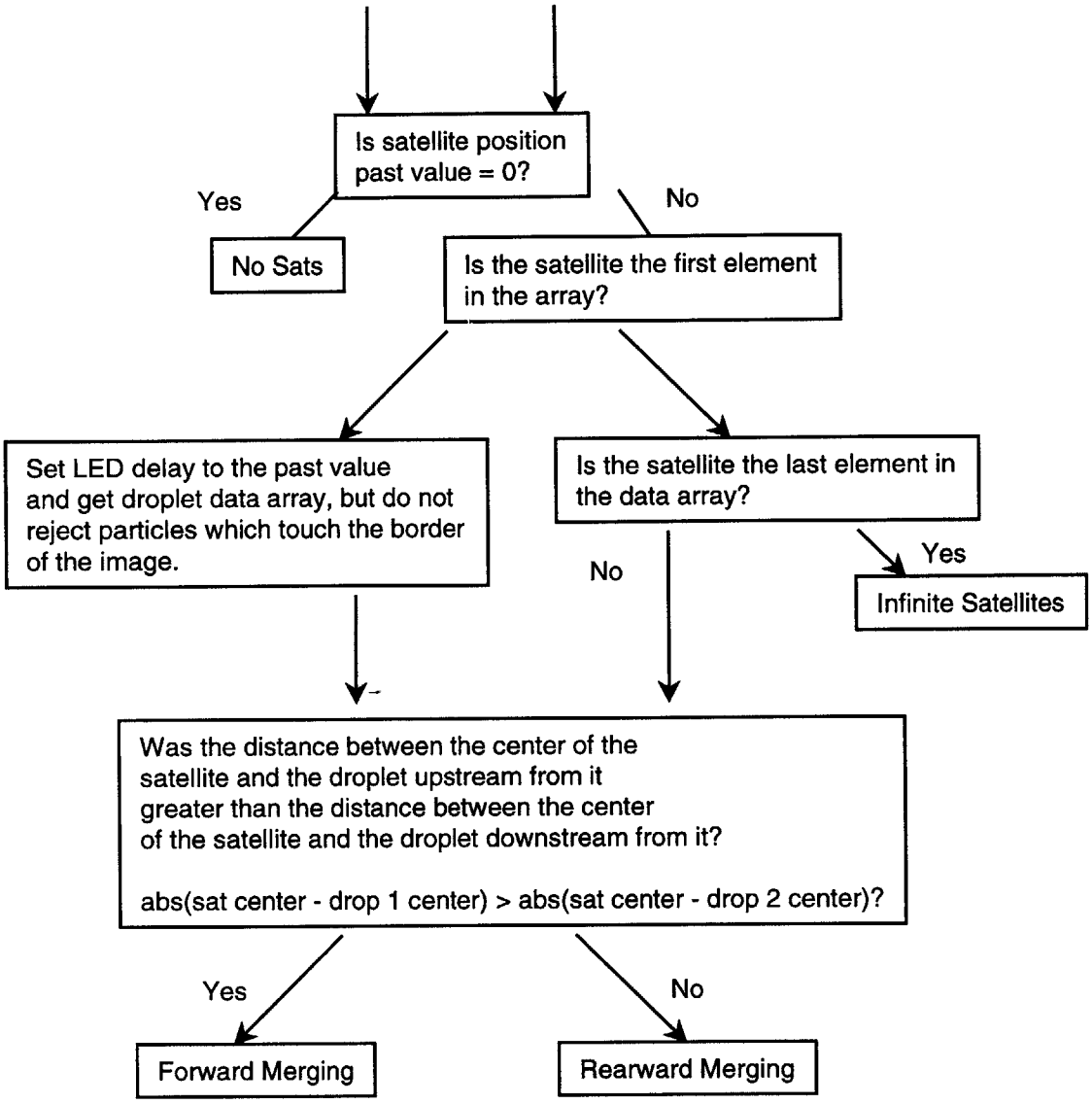
Is satellite position past value = 0?
Yes
No
No Sats
Is the satellite the first element in the array?
Set LED delay to the past value and get droplet data array, but do not reject particles which touch the border of the image.
Is the satellite the last element in the data array?
Yes
Infinite Satellites
No
Was the distance between the center of the satellite and the droplet upstream from it greater than the distance between the center of the satellite and the droplet downstream from it?
abs(sat center - drop 1 center) > abs(sat center - drop 2 center)?
Yes
No
Forward Merging
Rearward Merging

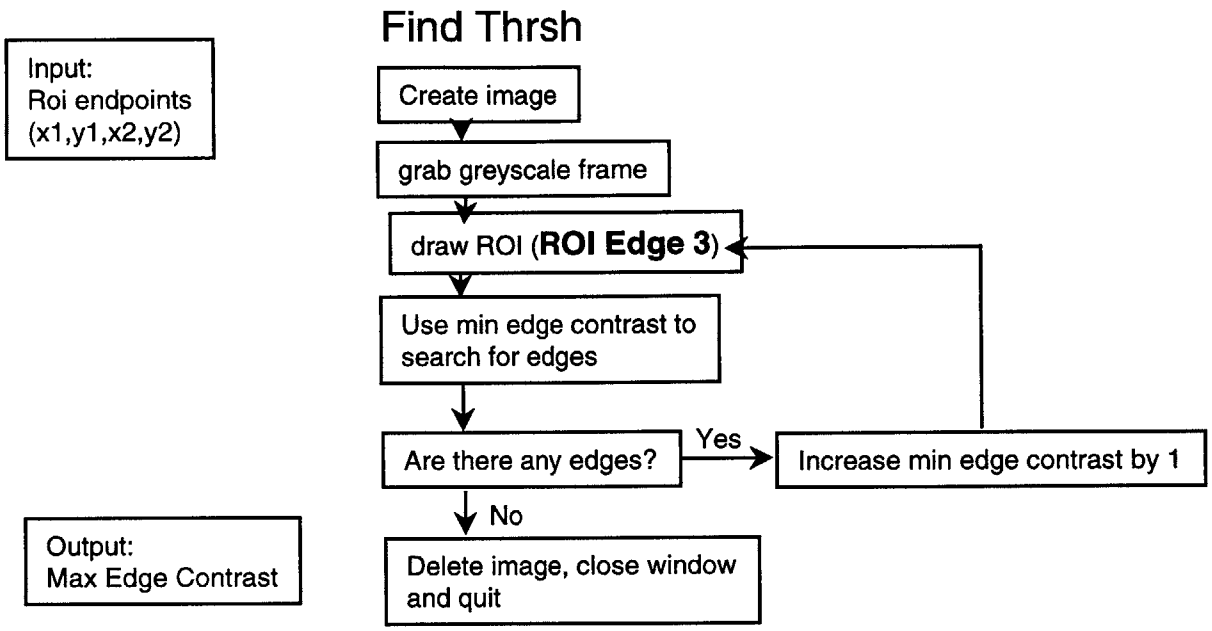
Find Thrsh
Input:
Roi endpoints
(x1,y1,x2,y2)
Create image
grab greyscale frame
draw ROI (ROI Edge 3)
Use min edge contrast to search for edges
Are there any edges?
Yes
Increase min edge contrast by 1
No
Delete image, close window and quit
Output:
Max Edge Contrast

Flow and Angle 2

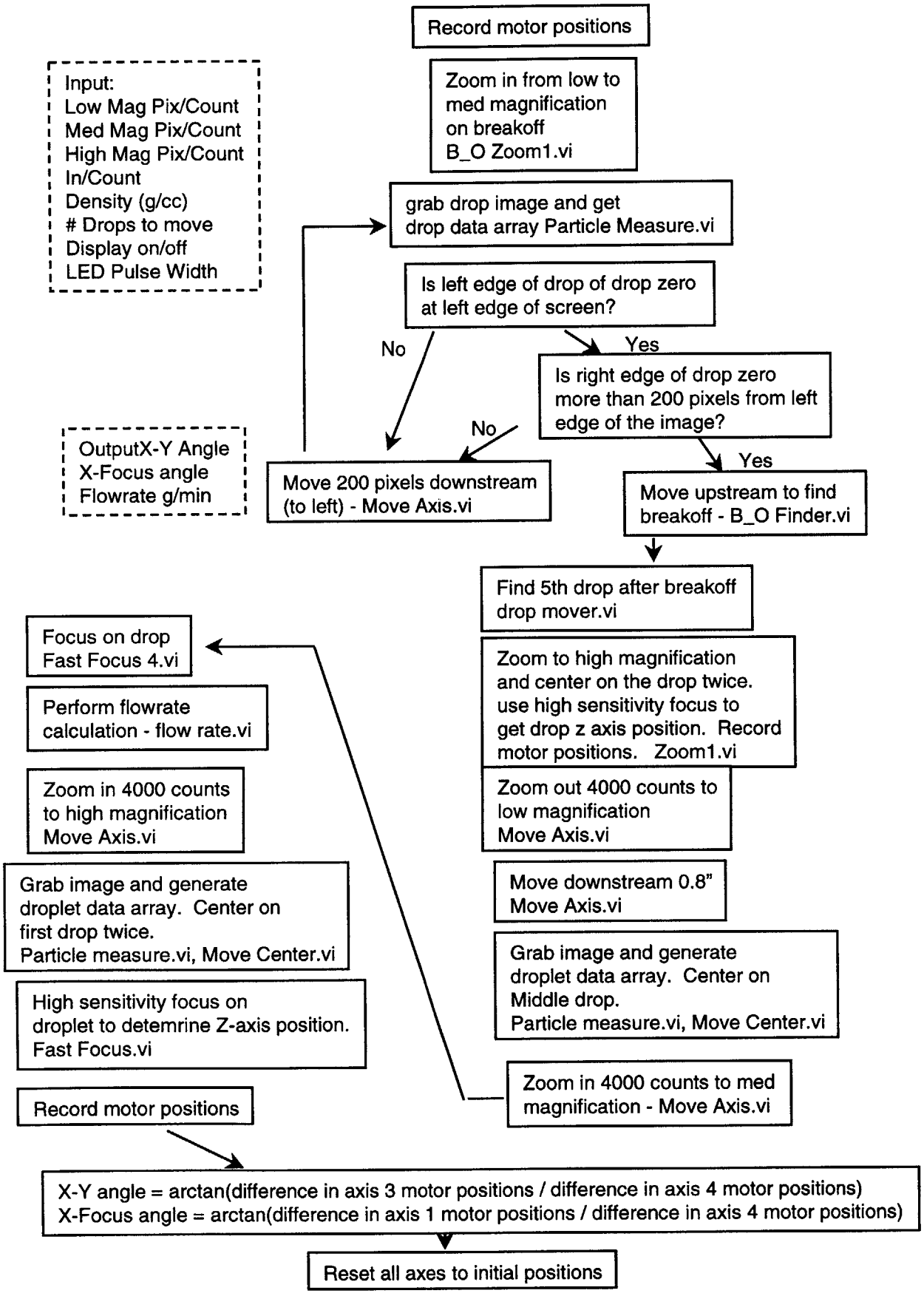

Move Axis

Inputs:
Move Target/Size
Type of move
(absoute vs relative)

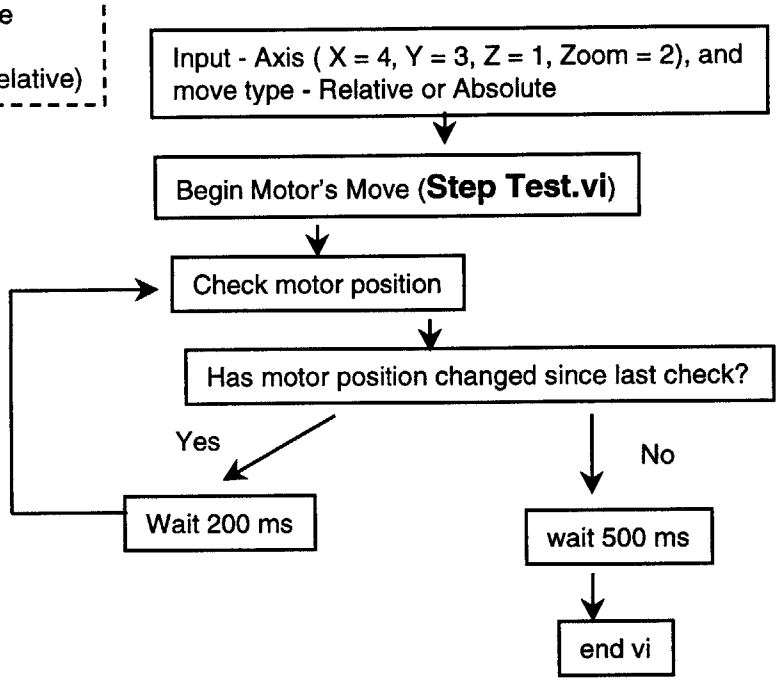

Move Center

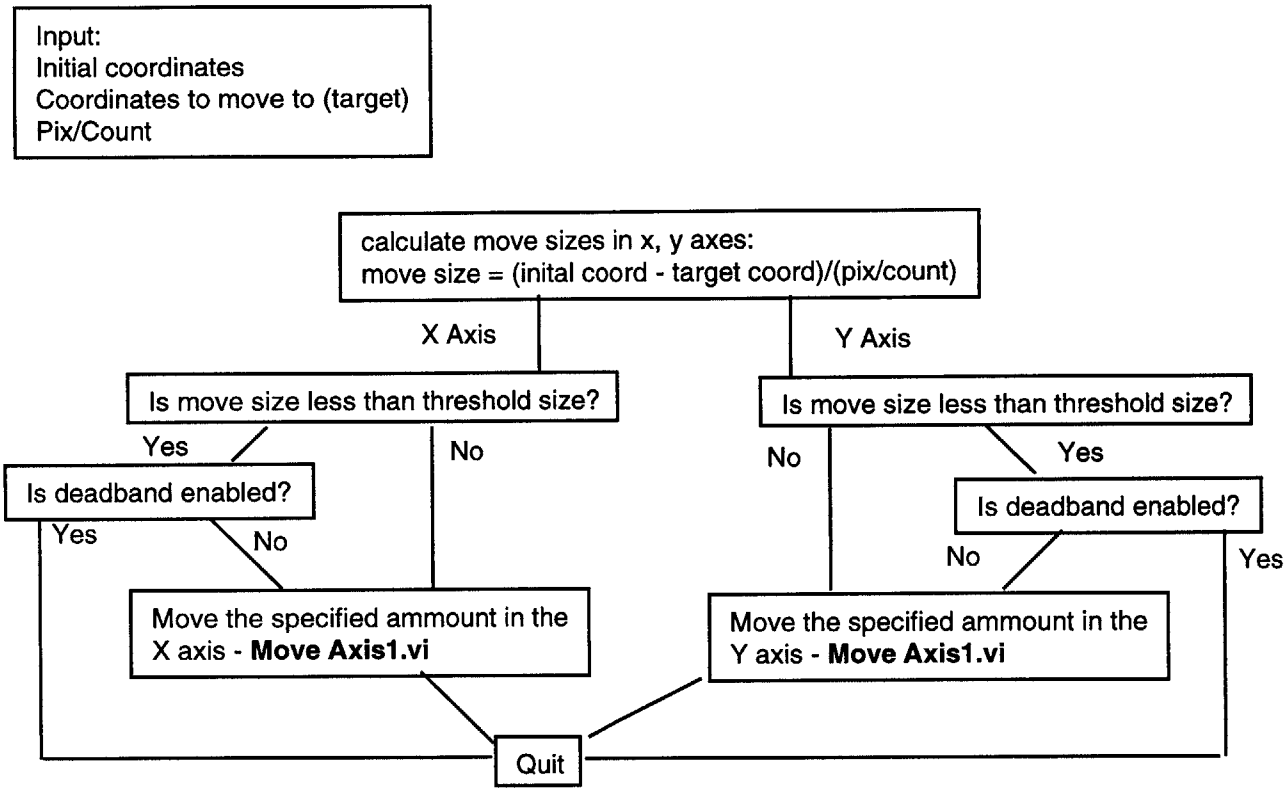
Input:
Initial coordinates
Coordinates to move to (target)
Pix/Count
calculate move sizes in x, y axes:
move size = (inital coord - target coord)/(pix/count)
X Axis
Y Axis
Is move size less than threshold size?
Is move size less than threshold size?
Yes
No
No
Yes
Is deadband enabled?
Is deadband enabled?
Yes
No
No
Yes
Move the specified ammount in the
X axis - Move Axis1.vi
Move the specified ammount in the
Y axis - Move Axis1.vi
Quit

Nozzle Finder 11

Input:
Edge Criteria
Display

Output:
Low Mag in/pix
Med Mag in/pix
High Mag in/pix

Set LED pulse width to 0.2 μs and delay to 1 μs

Request Users to Set Zoom to Zero Zoom.

Initialize motion control board

Move axis 1 to rear limit then forward 6445 counts

Move axis 3 to rear limit then right 240 counts

Move axis 4 to rear limit then up 1000 counts

Find top edge of fiber. **Particle Measure.vi**.
Move fiber 600 counts. **Move Axis.vi**

Find top edge of fiber again **Particle Measure.vi**

(motor counts)*(in/count)/(difference in pixels) = in/pixels at low mag

Zoom in 4000 counts **Move Axis.vi**

(motor counts)*(in/count)/(difference in pixels) = in/pixels at med mag

Find top edge of fiber again

Zoom in 4000 counts **Move Axis.vi**

Find top edge of fiber. Move fiber 90 counts. **Move Axis.vi**

Find top edge of fiber again

(motor counts)*(in/count)/(difference in pixels) = in/pixels at high mag

Reset to low level zoom and move to nozzle **Move Axis.vi**

Nozzle Loc 1

Input:
Display on/off
Initial nozzle X-Y position (pix)

Output:
Distance from center of image to end of nozzle in inches

Move so that the end of the nozzle is in the center of the frame
Move Center.vi

↓

Create horizontal ROI at the top of the screen and get x-coord of end of nozzle (in pixels)
ROI Edge 3.iv

↓

Determine distance from center of image to the x-coordinate of the end of the nozzle

Nozzle Test Algorithm

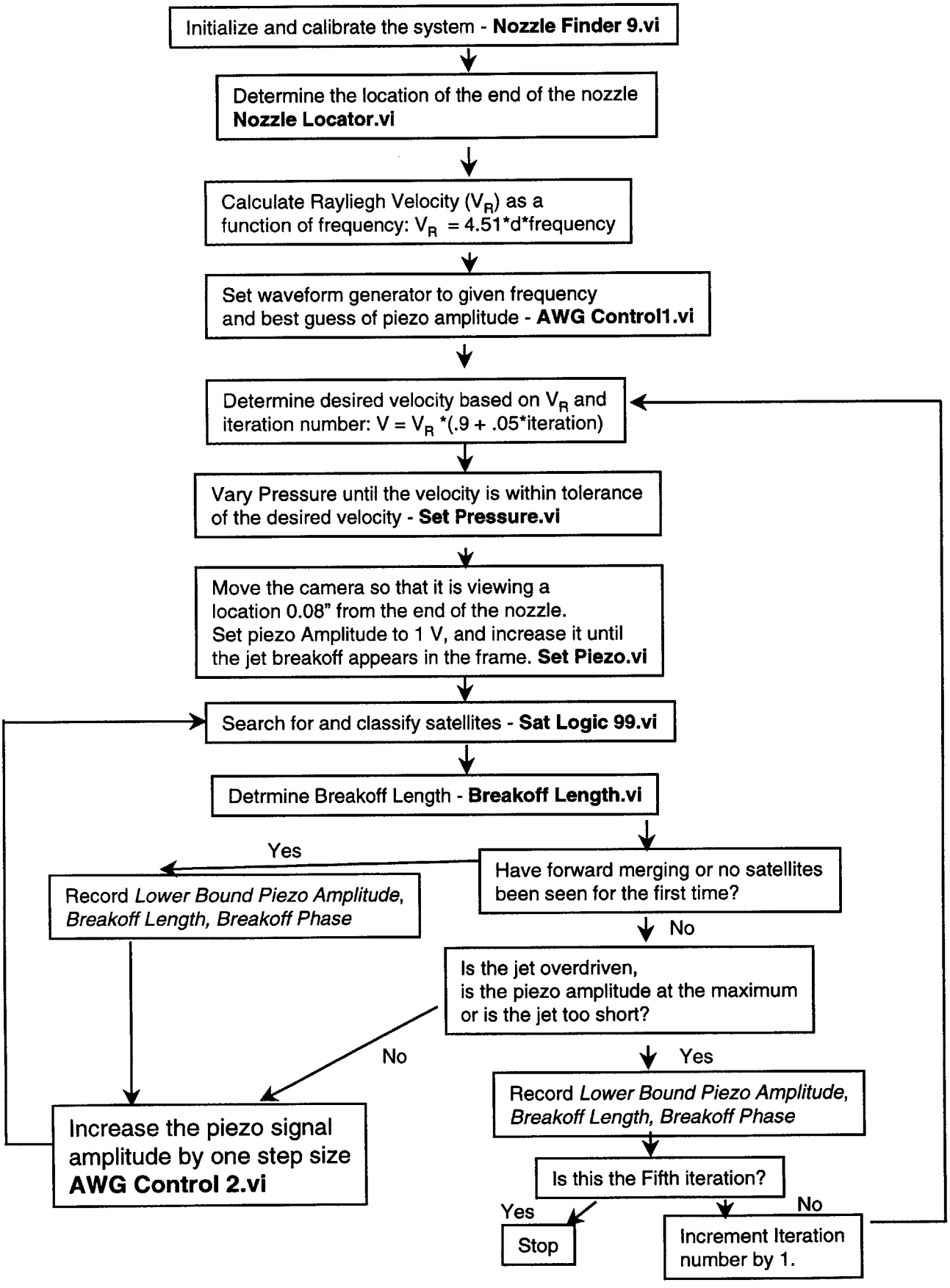

Particle Measure

Input:
Range
# of Erosions
Display on/off
Reject Border on/off

Output:
Coefficient Array
largest drop height
drop spacing
last drop position

Coefficient Array:
0 drop center x coord
1 drop center y coord
2 drop height (pixels)
3 left edge of drop x coord
4 right edge of drop x coord
5 drop circularity
6 drop width (pixels)
7 drop area (pixels^2)

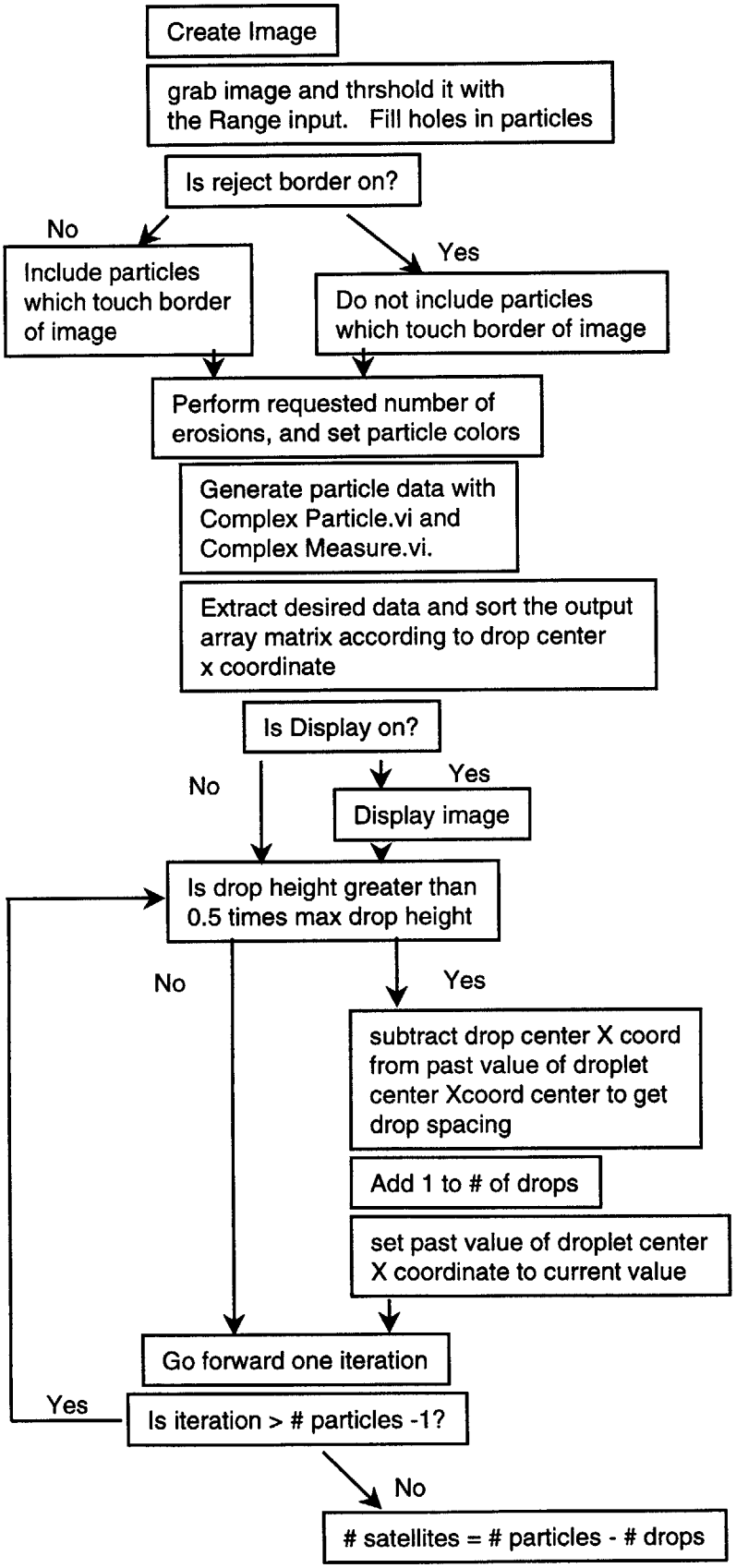

Pressure Setting Algorithm

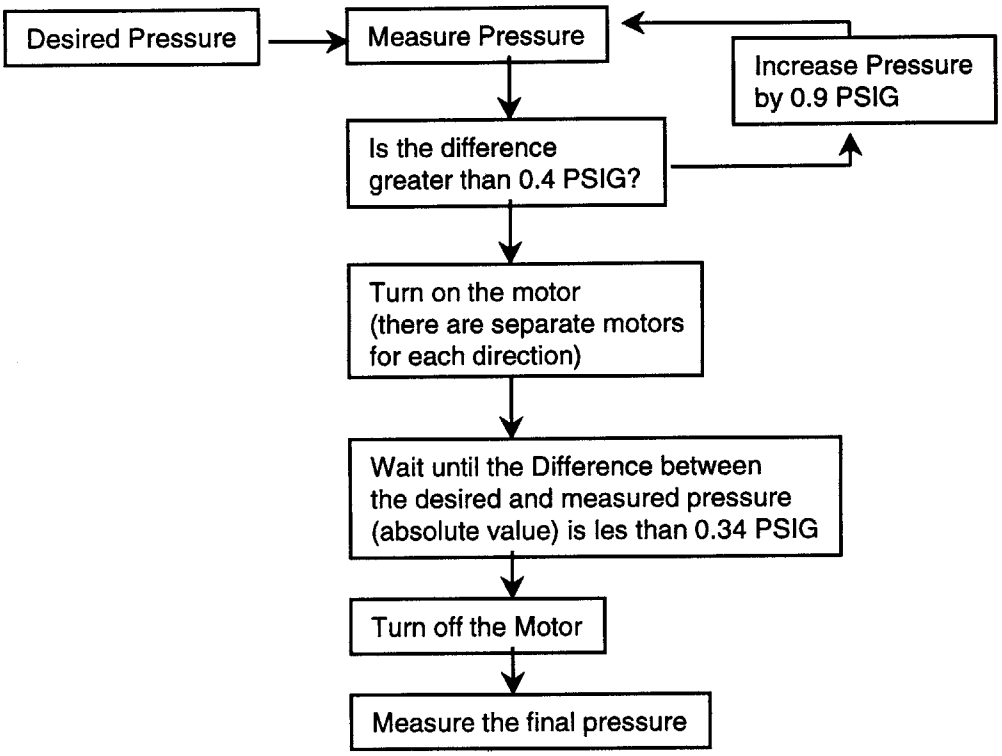

ROI Edge

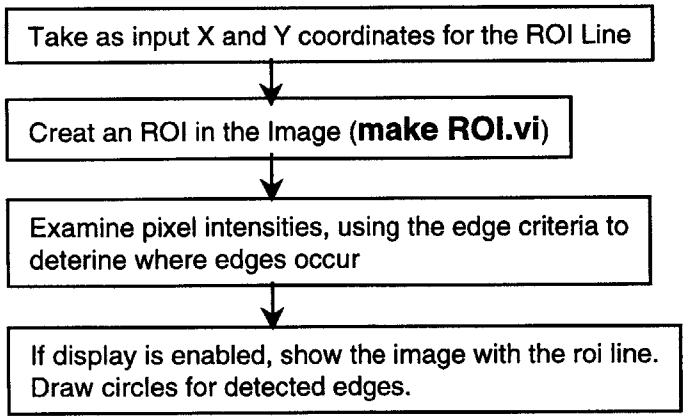

Set Piezo

Input:
Display on/off
In/Count
In/Pixel
Starting Piezo Amplitude
Nozzle Location (counts)
Piezo Step Size
Input Freq (kHz)

Output:
Piezo Amplitude which causes breakoff to occur within charging cell dimensions.

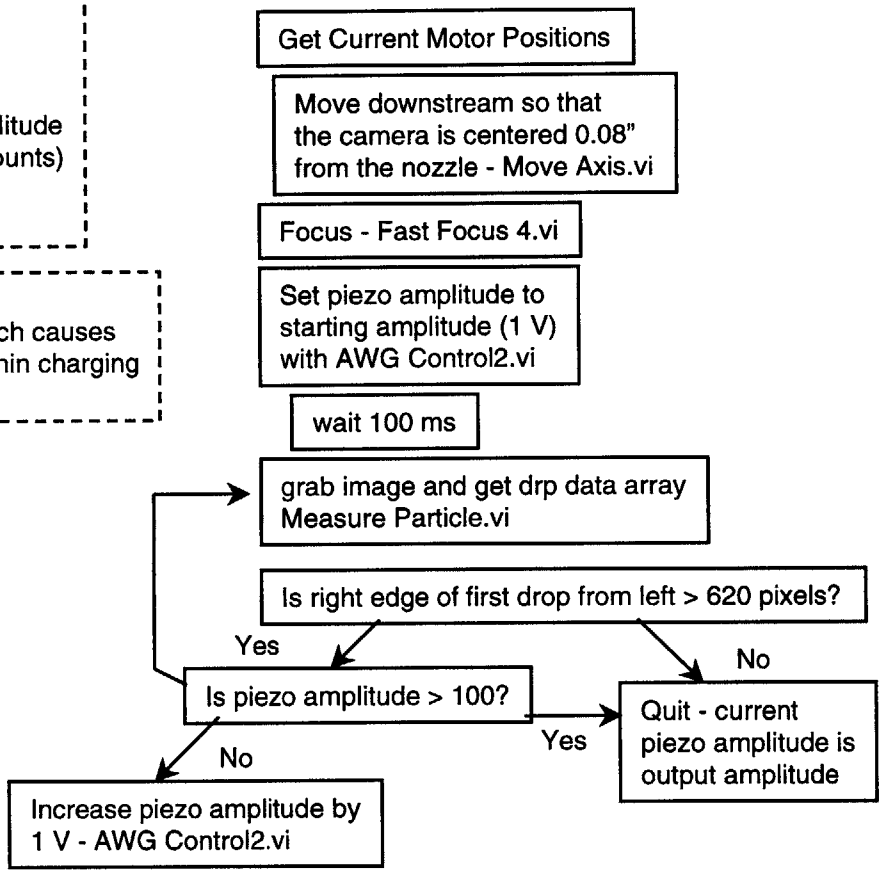

Set Velocity

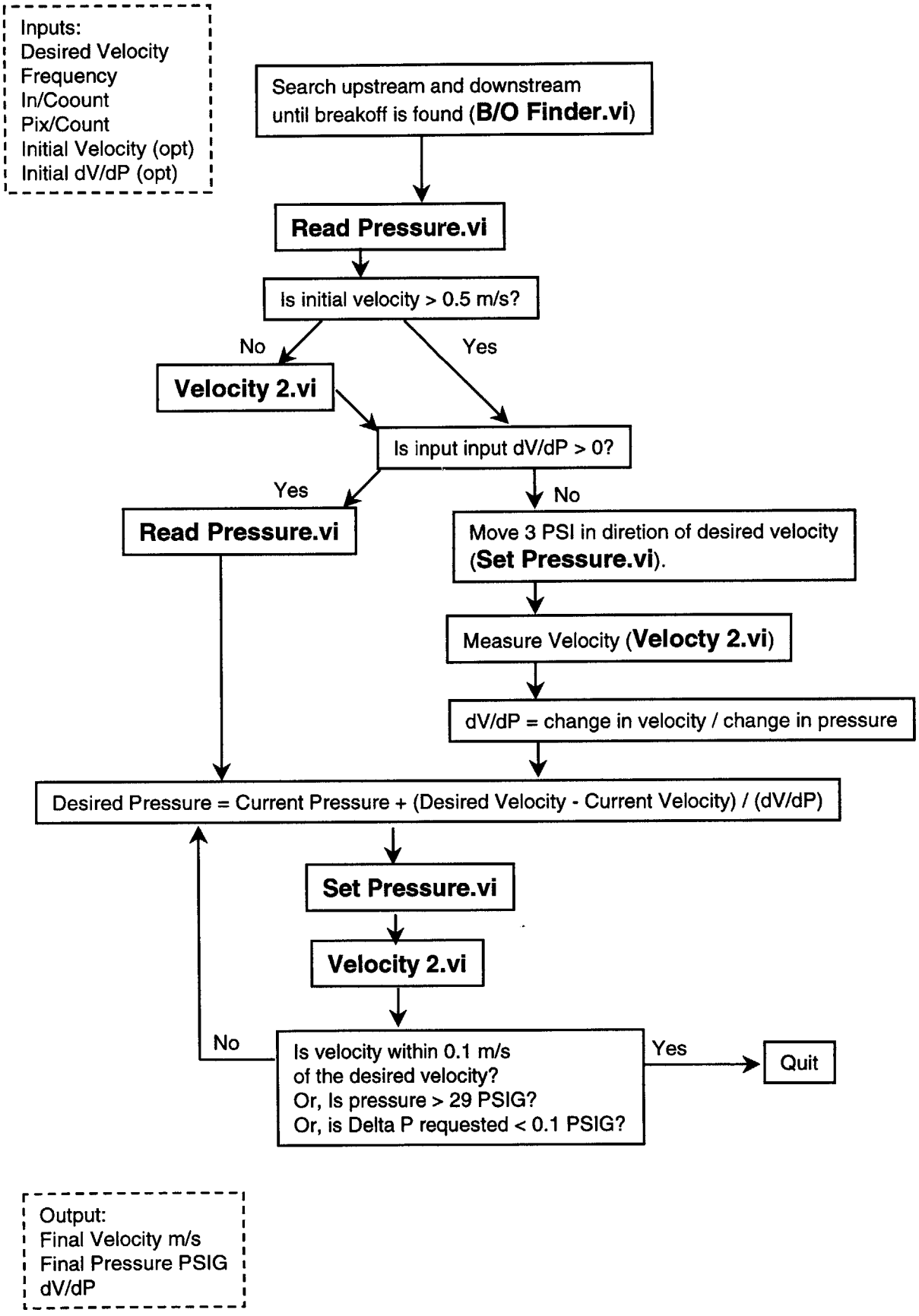

Snapshot 9

Inputs:
Range
ROI Line End Coords
# of Erosions
Edge Parameters

Create Image

Grab Frame and threshold with range, fill holes in particles, and erode the small particles the specified ammount

Create an ROI Line on the image, and return the coordinates of all edges found along that line. Edge defined as a pixel intensity derivative higher than a threshold level. Coordintes are in pixels.

Outputs:
Array with edge coords

Velocity 2

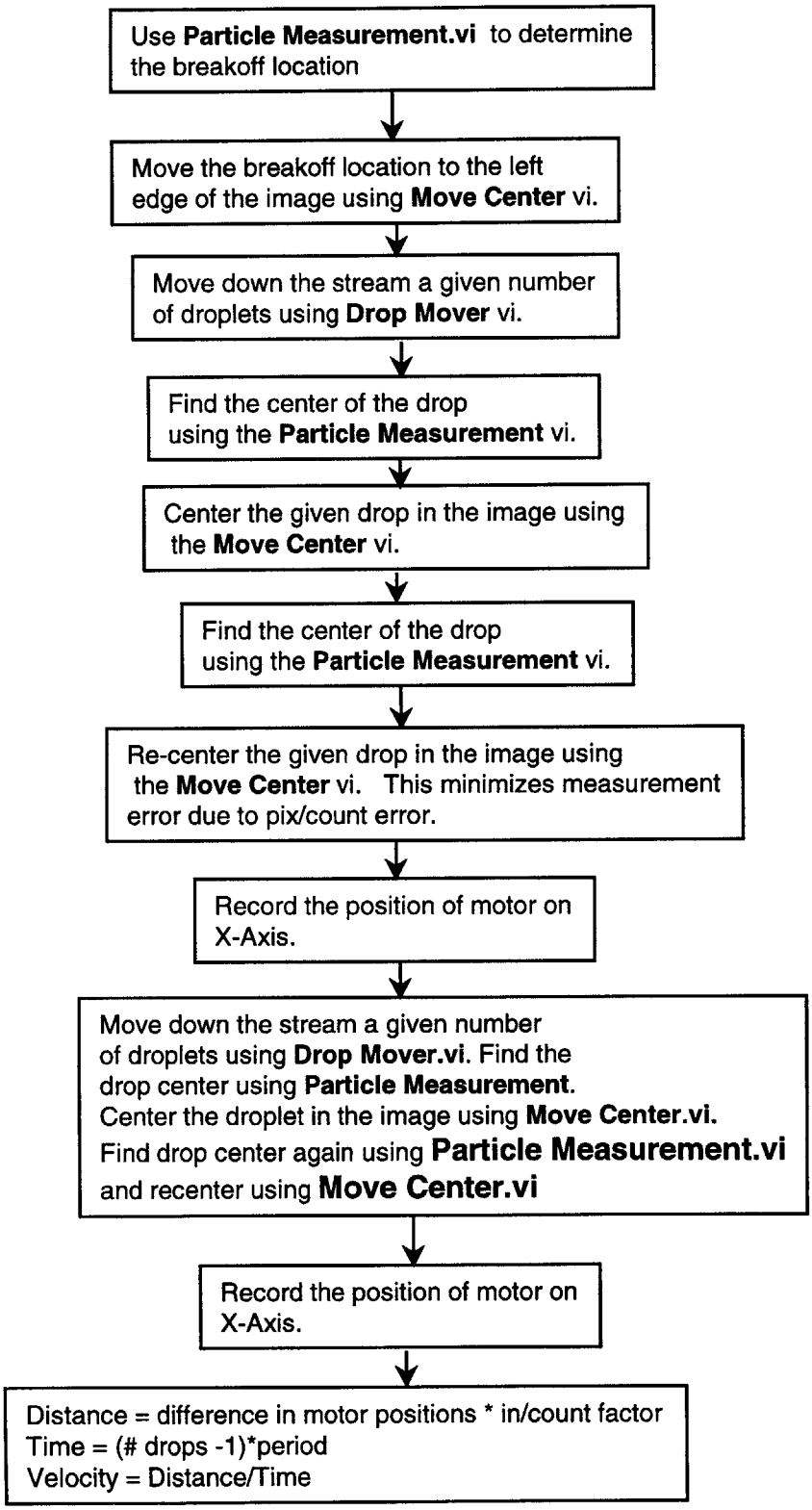
Use **Particle Measurement.vi** to determine the breakoff location
Move the breakoff location to the left edge of the image using **Move Center** vi.
Move down the stream a given number of droplets using **Drop Mover** vi.
Find the center of the drop using the **Particle Measurement** vi.
Center the given drop in the image using the **Move Center** vi.
Find the center of the drop using the **Particle Measurement** vi.
Re-center the given drop in the image using the **Move Center** vi. This minimizes measurement error due to pix/count error.
Record the position of motor on X-Axis.
Move down the stream a given number of droplets using **Drop Mover.vi**. Find the drop center using **Particle Measurement**. Center the droplet in the image using **Move Center.vi**. Find drop center again using **Particle Measurement.vi** and recenter using **Move Center.vi**
Record the position of motor on X-Axis.
Distance = difference in motor positions * in/count factor
Time = (# drops -1)*period
Velocity = Distance/Time

Zoom 1

Input:
High Mag pix/count
Display on/off
focus yes/no

Output:
Motor Positions for Drop Center

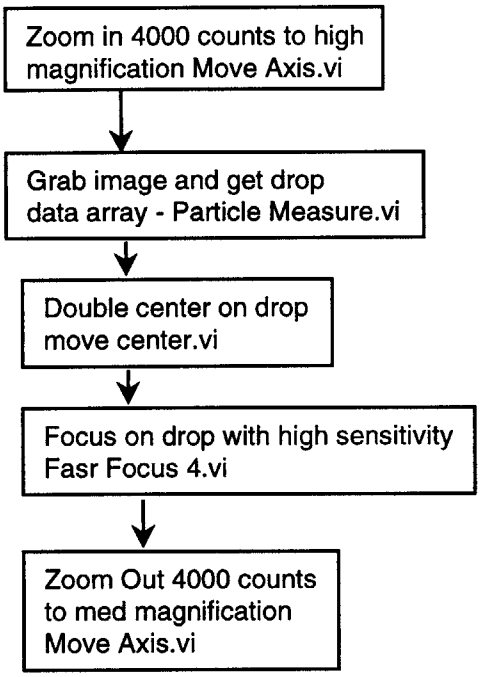

Zoomer 1

Input:
Zoom Move Size
Range
Display on/off

Output:
Pix/Count out
Total Zoom Move
Number of Droplets